

Maria Tran

Characterisation of excavation-induced soil displacement

An evaluation of prediction methods of ground surface settlement in deep excavations in soft clay

Master's thesis in Civil and Environmental Engineering

Supervisor: Steinar Nordal

Co-supervisor: Stefan Ritter, Siamak Feizi

June 2021

Maria Tran

Characterisation of excavation-induced soil displacement

An evaluation of prediction methods of ground surface settlement in deep excavations in soft clay

Master's thesis in Civil and Environmental Engineering
Supervisor: Steinar Nordal
Co-supervisor: Stefan Ritter, Siamak Feizi
June 2021

Norwegian University of Science and Technology
Faculty of Engineering
Department of Civil and Environmental Engineering



Norwegian University of
Science and Technology

Abstract

Deep excavations in soft clay may contribute to unexpected large settlement and further cause severe damage to adjacent constructions. When designing bracing system in a deep excavation, there is a certain uncertainty for predicting the surrounding ground surface settlement. Previous research acquire different prediction methods of how ground settlements adjacent to deep excavations develop. However, these existing methods indicate a lack of accurate and applicable methods for estimating the vertical and horizontal ground displacement, as well as the wall deflection. An accurate and controlled prediction of surface settlements due to a deep excavation, could ensure reliable assessments of the potential impact on the surrounding. Defining uncertain parameters to predict excavation-induced ground movements, remains a vital part of the design phase. Although complex numerical models is able to estimate quite accurate soil behaviour and are widely adopted in the design phase, challenges remains when their performance in predicting ground displacements caused by deep excavations is often not adequately evaluated. Consequently, uncertainty in how well these numerical model can predict ground displacements adjacent to deep excavations remains.

This work explored numerical modelling (i.e. PLAXIS 2D and FEM) to characterize the soil behaviour of soft clay, in order to evaluate the particular problem of ground displacement adjacent to a deep excavation. A well-described laboratory experiment based on geotechnical centrifuge testing is adopted as to achieve a replication in a numerical model. The centrifuge test provides data and results from a typical deep excavation with retaining wall and internal props in soft clay. The centrifuge experimental result is compared with the numerical model result, and provides indication of the performance and reliability of the numerical model. The validation of the numerical model considered an assessment of the soil behaviour including earth pressure, ground displacements and stress-strain performance. Relevant constitutive models is presented to explore their ability to capture the centrifuge test results, and further evaluate the unknown input parameters in a sensitivity analysis. It is found that the Hardening Soil Small model performed better than the other constitutive models (i.e. Mohr-Coulomb and Hardening Soil model). This finding was expected, due to higher complexity of the HSS model which enables to better replicate real soil behaviour. Based on this observation, the HSS model was further developed to obtain a so-called calibrated model. This calibrated model was utilised to study uncertain parameters in a parameter variation analysis, such as wall stiffness parameters. An applicable numerical model is chosen to examine how other vital parameters affects the ground displacement, for instance the bending stiffness.

The present research investigates how uncertain parameters, such as wall stiffness properties, influence the vertical and horizontal ground displacements adjacent to a deep excavation. The parameter variation of wall stiffness reveals that the bending stiffness plays a crucial role for the ground displacement, rather than the axial stiffness and specific weight. An increase in the vertical and horizontal ground displacements due to softer support systems

(i.e. reduced bending stiffness values) and a decrease of ground displacement for stiffer bending stiffness scenarios was observed. Additionally, the bending stiffness values affect the vertical and horizontal ground displacement profiles. An interesting finding is that the position of the maximum vertical displacement tends to move towards the retaining wall for more flexible retaining walls. The maximum vertical displacement adjacent to retaining wall increases when reducing the bending stiffness, while maximum horizontal displacements adjacent to wall tend to increase when the bending stiffness increases. The relations revealed in linear correlations in semi-logarithmic scale and provides a deeper understanding on how wall stiffness parameters influence the vertical and horizontal ground displacement and the wall deflection.

Overall, the calibrated model indicated agreeable estimations of vertical and horizontal displacement based on well-documented centrifuge test. The model was able to generate a sensitivity analysis and parameter variation analysis, and provided deeper knowledge of how uncertain parameters influence the ground displacement in a deep excavation. In the future, the described calibrated model can be adopted to investigate additional parameters of interest, such as the prop stiffness.

Keywords: Deep excavation, Ground displacement, Soft clay, PLAXIS 2D, Numerical model, Sensitivity analysis, Parameter variation, Centrifuge tests.

Sammendrag

Dype byggegroper i bløt leire kan bidra til uforventede store setninger, som kan danne store skader på nærliggende konstruksjoner. Under design av avstivningssystemer i dype byggegroper, forekommer det usikkerhet ved estimering av omliggende setninger. Tidligere forskningsarbeid har utviklet ulike metoder for å estimere hvordan setninger nær dype byggegroper utvikles. Disse metoder mangler imidlertid nøyaktige og anvendbare metoder for å estimere vertikal og horisontal jordforskyvning, samt avbøyningen av vegg. En nøyaktig og kontrollert prediksjon av overflatesetninger i en dyp utgravning kan sikre pålitelige vurderinger av potensielle innvirkninger på omgivelsene, samt avverge omfattende skader på menneskeliv og materielle verdier. Å definere parametere for å forutsi utgravningsinduserte jordforskyvninger er fortsatt en viktig del av designfasen. Selv om komplekse numeriske modeller tas i bruk i designfasen og kan gi nøyaktige estimater på jordoppførsel, gjenstår ofte utfordringen med å predikere en tilstrekkelig evaluering av jordforskyvninger på grunn av dype utgravninger. Dermed følger det en usikkerhet ved hvorvidt numeriske modeller kan predikere jordforskyvninger presist nok nær dype byggegroper.

I denne oppgaven er numerisk modellering (dvs. PLAXIS 2D og FEM) tatt i bruk for å karakterisere jordoppførsel i bløt leire, samt for å evaluere det spesielle problemet med jordforskyvninger ved siden av en dyp utgravning. Et velutført laboratorieeksperiment basert på geoteknisk sentrifugetesting er benyttet for å kunne gjenskape resultater i en numerisk modell. Sentrifugetesten gir data og resultater fra en typisk dyp utgravning med støttevegg og innvendige ankere i bløt leire. Resultater fra sentrifugetesten er sammenlignet med resultater fra den numeriske modellen, og har gitt indikasjoner på opptreden og påliteligheten til den numeriske modellen. Validering av den numeriske modellen vurderer jordoppførselen, inkludert jordtrykk, jordforskyvninger og spenning-tøyningstilstanden. Relevante jordmodeller evalueres etter evne til å implisere resultatene fra sentrifugetesten, og er videre tatt i bruk for å evaluere ukjente inngangsparametere i en sensitivitetsanalyse. Det er funnet at Hardening Soil Small-modellen ga bedre resultater enn de andre jordmodellene. Dette var forventet på grunn av høyere kompleksitet i HSS-modellen som gjør det mulig å replikere en reel jordoppførsel bedre. Basert på denne observasjonen ble HSS-modellen videreutviklet for å oppnå en såkalt kalibrert modell. Den kalibrerte modellen ble brukt til å studere usikre parametere i en parametervariasjonsanalyse, som stivhet av støttevegg. En anvendelig numerisk modell er valgt for å undersøke hvordan andre vitale parametere påvirker bakkenes forskyvning, for eksempel støtteveggen bøyestivhet.

Opgaven undersøker hvordan usikre parametere, som veggstivhetsegenskaper, påvirker de vertikale og horisontale forskyvninger nær en dype byggegropp. Parameter variasjonene av veggstivheten avslører at bøyestivheten spiller en avgjørende rolle i jordforskyvninger, mer betydelig enn aksialstivhet og veggens vekt. Det ble observert en økning i vertikal og horisontale jordforskyvninger ved mer fleksible støttevegger (dvs. redusert bøyestivhet) og en reduksjon i jordforskyvninger for økt bøyestivhet. I tillegg påvirker bøyestivhetsverdiene de vertikale og horisontale forskyvningsprofilene. Et interessant funn er at posisjonen til maksimal vertikal og horisontal forskyvning har en

tendens til å bevege seg mot støtteveggen for mer fleksible støttevegger. Den maksimale vertikale forskyvningen ved siden av støtteveggen øker når den bøyestivheten reduseres, mens maksimale horisontale forskyvninger ved siden av veggen har en tendens til å forbli den samme. Relasjonene avslører i lineære korrelasjoner i semilogaritmisk skala og gir en dypere forståelse av hvordan veggstivhetsegenskapene påvirker den vertikale og horisontale jordforskyvningen og veg defleksjonen .

Samlet sett indikerte den kalibrerte modellen relative korresponderende estimater av vertikal og horisontal forskyvning basert på veldokumentert sentrifuge test. Modellen var i stand til å utføre en sensitivitetsanalyse og parametervariasjon, og ga dypere kunnskap om hvordan usikre parametere påvirker jordforskyvningen i en dyp utgravning. I fremtiden kan den beskrevne kalibrerte modellen adopteres for å undersøke flere parametere av interesse, som for eksempel stivhet av anker.

Preface

This master thesis is written by Maria Tran at the Department of Civil and Environmental Engineering at the Norwegian University of Science and Technology (NTNU) in Trondheim. The work represents 30 credits of a Master in Science degree in Civil and Environmental Engineering with specializing in geotechnic, and was written during the spring of 2021. The supervision in this thesis was given by the Department of Geotechnical Engineering at NTNU. The project was written in collaboration with the Norwegian Geotechnical Institute (NGI), an international center for research and consultancy in engineering geosciences. The problem formulation has been prepared in collaboration with Stefan Ritter from NGI.

The thesis is based on my project thesis written in the fall of 2020. The focus was the estimation of the ground displacement, both vertical and horizontal, in a deep excavation in soft clay with empirical and semi-empirical methods. Due to deep excavations in an increased urbanisation, it is important with required design of retaining constructions in order to avoid construction damage adjacent to the ground settlements. The aim was to evaluate the precision of the prediction method and the reliability and applicability of the methods. An evaluation indicated a lack of consistent prediction methods for both vertical and horizontal displacement. An important aspect to the design of a required retaining construction, is to present a realistic soil model that captures the real soil behaviour. With a calibrated soil model, an investigation of retaining construction parameters can be obtained.

This master thesis will further in this paper take account for different soil models in order to provide a calibrated model, by replicate soil behaviour result from a laboratory test. The data will be conducted from a centrifuge test, and will be implemented in a numerical model, PLAXIS. A back-calculation of centrifuge test result will be provided to evaluate the performance of the model. With this, it is an aspiration through this master's thesis to get one step closer in the process of finding out how to estimate accurate ground displacement in deep excavations in soft clay, by identify the crucial parameters.

Trondheim, June 2021

Maria Tran

Maria Tran

Acknowledgments

I would first like to thank my master thesis advisor Professor Steinar Nordal of the Department of Civil and Environmental Engineering at NTNU. Professor Nordal was always just a phone call away, and was always able to provide great help and enthusiastic guidance whenever I came over challenging problems or had questions about the research and theory. He consistently accentuated that this master thesis to be my own work, yet steered me in the right direction whenever it was needed.

This master thesis is written in collaboration with NGI, and I would like to thank Stefan Ritter and Siamak Feizi from NGI for a great cooperation. With their passionate participation and input, the guidance and support sent me in the right path with the thesis. I would like to acknowledge my main advisor Stefan Ritter as a great supervisor with patient guidance and encouragement, and I am gratefully indebted for his very valuable supervision on this thesis. I would also like to send a special thanks to Siamak Feizi for great help regarding PLAXIS simulations and contribution with a lot of tips and constructive recommendations.

Finally, I wish to thank my family and my boyfriend for their support and continuous encouragement throughout my years of study and my master thesis journey. This accomplishment would not have been possible without them. Thank you.

M.T.

List of Figures

2.1	Vertical settlement profile from empirical methods and and Test 2 and Test 5. Optimized figure from Tran (2020).	10
2.2	Horizontal settlement profile with empirical methods and centrifuge tests. Optimized figure from Tran (2020).	10
3.1	Experimental setup with in-flight excavator of the centrifuge test in model scale (Lam, 2010).	13
3.2	Prop installation modelling for different excavation sequence (Lam, 2010).	14
3.3	Excavation geometry in model scale (Lam, 2010).	15
3.4	A summary of 5 centrifuge tests (Lam et al., 2014).	16
3.5	(a) Deviatoric stress and shear strain curves and (b) secant axial stiffness and shear strain with stiffness degradation curves (Lam, 2010).	17
3.6	Normalized secant shear modulus with shear strain (Lam, 2010)	18
3.7	Test 1 (SYL04) (a) Wall deflection and lateral wall displacement and (b) ground displacement with excavation sequence (Lam, 2010).	19
3.8	Active earth pressure for a total basis analysis, $r = 0$ (Emdal et al., 2019).	25
3.9	Passive earth pressure for a total basis analysis, $r = 0$ (Emdal et al., 2019).	26
4.1	Different type of constitutive models with different application (Kullingsjö, 2007).	29
4.2	Hardening soil model with hyperbolic stress-strain relation in primary loading (Locat et al., 2013).	33
4.3	Characteristic shear strain-shear modulus performance of soil with typical strain ranges. Describes the typical stiffness-strain behaviour (Sloot, 2020b).	35
4.4	Undrained shear modulus and undrained stiffness from an undrained triaxial test (Nordal, 2020).	35
4.5	Stress path for undrained condition with Mohr-Coulomb model (Brinkgreve et al., 2017).	37
4.6	PLAXIS 2D - Soil model	38
5.1	Vertical ground displacement of MC scenarios obtained from the sensitivity analysis.	45
5.2	Lateral wall deflection of MC scenarios obtained from the sensitivity analysis.	46
5.3	Vertical ground displacement of HS scenarios obtained from the sensitivity analysis.	47

5.4	Lateral wall deflection of HS scenarios obtained from the sensitivity analysis.	48
5.5	Vertical ground displacement of HSS scenarios obtained from the sensitivity analysis.	50
5.6	Lateral wall deflection of HSS scenarios obtained from the sensitivity analysis.	50
5.7	PLAXIS sensitivity analysis and parameter variation of the HSS model with scenario HSS01.	51
5.8	Horizontal ground displacement of MC07, HS08 and HSS10 from last phase.	55
5.9	Vertical ground displacement of MC07, HS08 and HSS10 from last phase.	55
5.10	Stress-strain behaviour of real soil, MC model and HS model (Teo and Wong, 2012).	57
5.11	PLAXIS Soil test showing input properties on the left and soil type test on top. The graph illustrates stress strain from the result of the input parameters.	58
5.12	Stress-strain curve of centrifuge test (Lam, 2010) and soil test result with HSS model from PLAXIS (i.e. HSS10 $K_0 = 1$).	59
5.13	Vertical ground displacement in each construction stage. Data is obtained from (Lam, 2010).	60
5.14	Lateral wall displacement in each construction stage. Data is obtained from (Lam, 2010).	60
5.15	Test 1 Vertical ground displacement - Initial phase: Install wall.	61
5.16	Test 1 Vertical ground displacement - Phase 1: Excavation 1.2m.	61
5.17	Test 1 Vertical ground displacement - Phase 2: Install prop 1.	61
5.18	Test 1 Vertical ground displacement - Phase 3: Excavation 3.36m.	61
5.19	Test 1 Vertical ground displacement - Phase 4: Install prop 2.	61
5.20	Test 1 Vertical ground displacement - Phase 5: Excavation 4.32m.	61
5.21	Test 1 Vertical ground displacement - Phase 6: Excavation 5.4m.	62
5.22	Test 1 Vertical ground displacement - Final phase: Install prop 3.	62
5.23	Test 1 Lateral wall displacement - Final phase: Install wall.	62
5.24	Test 1 Lateral wall displacement - Phase 1: Excavation 1.2m.	62
5.25	Test 1 Lateral wall displacement - Phase 2: Install prop 1.	62
5.26	Test 1 Lateral wall displacement - Phase 3: Excavation 3.36m.	62
5.27	Test 1 Lateral wall displacement - Phase 4: Install prop 2.	63
5.28	Test 1 Lateral wall displacement - Phase 5: Excavation 4.32m.	63
5.29	Test 1 Lateral wall displacement - Phase 6: Excavation 4.32m.	63
5.30	Test 1 Lateral wall displacement - Final phase: Install prop 3.	63
5.31	Lateral wall deflection and vertical ground displacement for Test 1 (SYL04) with stiff props and Test 4 (SYL03) with soft props (Lam, 2010).	64
5.32	Lateral wall displacement of Test 1, Test 4 and centrifuge Test 4.	64
5.33	Vertical ground displacement of Test 1, Test 4 and centrifuge Test 4.	64
5.34	Lateral wall and vertical ground displacement for Test 2 (SYL05) (Lam, 2010).	66
5.35	Lateral wall displacement of Test 2 with flexible wall.	66
5.36	Vertical ground displacement of Test 2 with flexible wall.	66

5.37 Apparent earth pressure of baseline Test 1 (SYL04) and Peck's maximum from estimation methods (Lam, 2010).	67
5.38 Total pressure for SYL05, (i.e Test 2 with floating, flexible wall with stiff props (Lam, 2010).	68
5.39 Position of EPC instruments in centrifuge model (Lam, 2010).	69
5.40 Test 1 (SYL04) - Total earth pressure with EPC A1, EPC A2 and EPC A4 measurement (Lam, 2010).	69
5.41 Test 1 - Total earth pressure of passive side.	70
5.42 Test 1 - Total earth pressure of active side.	70
5.43 Test 2 (SYL05) - Apparent earth pressure (Lam, 2010).	70
5.44 Test 2 - Total earth pressure on passive side before excavation.	71
5.45 Test 2 - Total earth pressure on active side before excavation.	71
5.46 Test 2 - Total earth pressure on passive side after excavation.	71
5.47 Test 2 - Total earth pressure on active side after excavation.	71
5.48 Test 1 a) Lateral wall displacement b) Vertical ground displacement	72
6.1 Lateral wall and vertical ground displacement profiles with <i>PV - Calibrated Centrifuge Test (CCT)</i> and <i>PV - 0 (Calibrated)</i> . FIKS BILDE med lateral wall	77
6.2 Parameters variation of bending stiffness <i>EI</i> .	79
6.3 Parameter variation of axial stiffness <i>EA</i> .	79
6.4 Parameter variation of bending stiffness <i>EI</i> and axial stiffness <i>EA</i> .	80
6.5 Parameter variation of bending stiffness <i>EI</i> , axial stiffness <i>EA</i> and specific weight <i>w</i> .	80
6.6 Vertical ground displacements when varying bending stiffness <i>EI</i> .	82
6.7 Horizontal ground displacements when varying bending stiffness <i>EI</i> .	82
6.8 Lateral wall deflection (i.e. horizontal ground displacements adjacent to the retaining wall) when varying bending stiffness <i>EI</i> .	83
6.9 Maximum vertical ground displacement at soil surface versus bending stiffness <i>EI</i> .	84
6.10 Maximum horizontal ground displacement versus bending stiffness <i>EI</i> .	84
6.11 Maximum lateral wall deflection versus bending stiffness <i>EI</i> .	85
6.12 Maximum vertical ground displacement adjacent to retaining wall versus bending stiffness <i>EI</i> .	85
6.13 Maximum horizontal ground displacement adjacent to retaining wall versus bending stiffness <i>EI</i> .	86
6.14 Maximum lateral wall deflection (i.e. horizontal ground displacement adjacent to the retaining wall) versus bending stiffness <i>EI</i> .	87
6.15 Position of maximum vertical ground displacement when varying bending stiffness <i>EI</i> .	87
6.16 Position of maximum horizontal ground displacement at surface when varying bending stiffness <i>EI</i> .	88
7.1 Illustration of total net active loads on flexible retaining structure (Boone and Westland, 2006).	93
B.1 PLAXIS Test 1 - Final phase: Deformed mesh u .	100
B.2 PLAXIS Test 1 - Final phase: Total displacement u .	101

B.3	PLAXIS Test 1 - Final phase: Total deviatoric strain γ_s .	101
B.4	PLAXIS Test 1 - Final phase: Total wall displacement $ u $.	102
B.5	PLAXIS Test 1 - Final phase: Total shear forces.	102
B.6	PLAXIS Test 1 - Final phase: Total bending moment.	103
D.1	PLAXIS Test 1 - Passive earth pressure before excavation.	108
D.2	PLAXIS Test 1 - Active earth pressure before excavation.	108
D.3	PLAXIS Test 1 - Passive earth pressure after excavation.	109
D.4	PLAXIS Test 1 - Active earth pressure after excavation.	109
D.5	PLAXIS Test 2 - Passive earth pressure before excavation.	110
D.6	PLAXIS Test 2 - Active earth pressure before excavation.	110
D.7	PLAXIS Test 2 - Passive earth pressure after excavation.	111
D.8	PLAXIS Test 2 - Active earth pressure after excavation.	111

List of Tables

2.1	Vertical settlement curves from empirical methods (Tran, 2020).	8
2.2	Horizontal settlement curves from empirical methods (Tran, 2020).	9
3.1	Centrifuge scaling law (Meng et al., 2020).	20
3.2	Prototype scale values calculation with model scale values for retaining wall parameters.	22
3.3	Prototype scale values calculation with model scale values for prop parameters.	23
3.4	Summary of parameters from centrifuge test in prototype scale.	27
4.1	Mohr-Coulomb model input parameters in PLAXIS (Sloot, 2020b).	31
4.2	Hardening soil model input parameters (Surarak et al., 2012).	34
4.3	Hardening Soil Small model input parameters in PLAXIS (Surarak et al., 2012).	36
4.4	Construction stages for Test 1 (SYL04) in PLAXIS model.	39
4.5	Input parameters for Mohr-Coulomb Soil model in PLAXIS.	40
4.6	Input parameters for Hardening Soil model in PLAXIS.	41
4.7	Input parameters for Hardening Soil Small model in PLAXIS.	42
5.1	Unknown input parameters for sensitivity analysis of Mohr-Coulomb Soil model in PLAXIS.	45
5.2	Sensitivity analysis for Mohr-Coulomb model.	45
5.3	Unknown input parameters for sensitivity analysis of Hardening Soil model in PLAXIS.	46
5.4	Sensitivity analysis for Hardening Soil model.	47
5.5	Unknown input parameters for Hardening Soil Small model in PLAXIS.	49
5.6	Sensitivity analysis for Hardening Soil Small model.	49
5.7	Criterion in PLAXIS Sensitivity Analysis-application.	52
5.8	PLAXIS Sensitivity analysis for Mohr-Coulomb model.	52
5.9	PLAXIS Sensitivity analysis for Hardening Soil model.	53
5.10	PLAXIS Sensitivity analysis for Hardening Soil Small model.	53
5.11	Prototype scale values calculation with model scale values for retaining wall parameters for Test 2.	65
5.12	Calibrated model: Input parameters for Test 1 with HSS10 model in PLAXIS.	74

6.1	PV Calibrated CT and PV calibrated	76
6.2	Parametric variation analysis.	76
6.3	Parameter variation for bending stiffness <i>EI</i>	81
C.1	Sensitivity analysis for Hardening Soil Small model.	105
C.2	PLAXIS Sensitivity analysis for Hardening Soil Small model.	106

List of Symbols

The List of symbols presents symbols that will be adopted in this research.

B	Width	
D	Soil thickness	
E	Young's modulus	
EA	Axial stiffness	
EI	Flexural/bending stiffness eller Inertial stiffness	
E_{50}^{ref}	Secant stiffness in standard drained triaxial test	
E_{oed}^{ref}	Tangent stiffness for primary oedometer loading	$E_{oed}^{ref} \approx E_{50}^{ref}$
E_{ur}^{ref}	Unloading/reloading stiffness from drained triaxial test	$E_{ur}^{ref} \approx 3E_{50}^{ref}$
F	Factor of safety	
F	Force	
G	Shear modulus	
G_0	Shear modulus for small strain	
G_0^{ref}	Reference shear modulus at very small strains	
G_s	Secant modulus	
G_s	Specific gravity	
G_u	Undrained shear modulus	
G_0	Small strain stiffness	
G_{max}	Maximum shear modulus	
G_{ur}	Unloading/reloading stiffness	

H	Excavation depth	
H_{wall}	Wall length	
I	Second moment of area	
K_0	Earth pressure coefficient at rest	
L	Length	
L_m	Prop length	
$L_{equivalent}$	Equivalent length	
$L_{spacing}$	Length of spacing	
L_{tt}	Travel time of wave	
M	Bending moment	
OCR	Overconsolidation ratio	
P_A	Active earth pressure	
P_P	Passive earth pressure	
R_f	Failure ratio (q_f / q_a)	Default: $R_f = 0.9$
R_{inter}	Interface strength factor (Roughness)	
S_h	Horizontal ground displacement	
S_u	Undrained shear strength	
S_v	Vertical ground displacement	
$S_{u,inc}$	Increased undrained shear strength	
V_s	Shear velocity	
a	Attraction	
c	(Effective) Cohesion	
e_0	Void ratio	
f	Mobilized friction	
g	Gravitational acceleration	
h	Average support spacing	
k	Prop stiffness	

m	Power for stress-level dependency of stiffness	
m_p	Mass weight prototype	
p_{ref}	Reference stress for stiffnesses	Default: $p_{ref} = 100kN/m^3$
q	Deviatoric stress	
r	Roughness ratio	
t	Thickness	
u_x	Lateral displacement	
u_y	Vertical displacement	
w	Specific weight	
z	Depth	
δ	Settlement	
δ_w	Lateral wall deflection	
ϵ	Strain	
ϵ_{yy}	Axial strain	
η	System stiffness	
γ	Material/Unit weight	
γ	Shear strain	$\gamma = \frac{2}{2}\epsilon_{yy}$
γ_w	Material/Unit weight of water	Default: $9,81kN/m^3$
$\gamma_{0.7}$	Threshold shear strain	$G_s = 0.772G_0$
γ_{ref}	Reference shear strain	
γ_{sat}	Unit weight for saturated material	
γ_{unsat}	Unit weight for unsaturated material	
κ	Earth pressure coefficient	
κ_A	Active earth pressure coefficient	
κ_P	Passive earth pressure coefficient	
ν	Poisson's ratio	
ν_u	Poisson ratio for undrained condition	$0.495 \approx 0.5$

ν_{ur}	Poisson's ratio for unloading-reloading	Default: $\nu_{ur} = 0.2$
ϕ	(Effective) Internal friction angle	$\psi = 30^\circ - \phi$
ψ	Dilatancy angle	
ρ	Density	
σ	Stress	
σ_1	Major principal stress	
σ_3	Minor principal stress	
σ_h	Horizontal stress	
σ_v	Vertical stress	
τ	Shear stress	

Contents

Abstract	i
Sammendrag	iii
Preface	v
Acknowledgments	vi
List of Figures	vii
List of Tables	x
List of Symbols	xiii
1 Introduction	1
1.1 Background	2
1.2 Research objectives	4
1.2.1 Sub-objectives	4
1.3 Outline of thesis	5
2 Literature review	6
2.1 Empirical methods	6
2.2 Laboratory test - Centrifuge experiments	11
3 Centrifuge test - Deep excavation in soft clay	12
3.1 General	12
3.1.1 Model set-up	13
3.1.2 Model support system	13
3.1.3 Model ground	14
3.1.4 Excavation test procedure	15
3.1.5 Test program	15
3.1.6 Undrained compression triaxial testing of core samples	16
3.1.7 Small strain stiffness	16
3.1.8 Ground displacement	18
3.1.9 Summary	18

3.2	Scaling up from model scale to prototype scale	19
3.2.1	Soil ground parameters	20
3.2.2	Retaining wall parameters	21
3.2.3	Prop parameters	22
3.2.4	System stiffness parameters	24
3.3	Soil model input	24
3.3.1	Input parameters for undrained condition	24
3.3.2	Earth pressure coefficient	25
3.4	Parameters from centrifuge test in prototype scale	26
4	Numerical modelling for simulation of deep excavation in soft clay	28
4.1	Introduction	28
4.2	Soil models	29
4.2.1	Mohr-Coulomb, <i>MC</i>	30
4.2.2	Hardening Soil, <i>HS</i>	31
4.2.3	Hardening Soil Small, <i>HSS</i>	33
4.3	Model validation	35
4.3.1	Selection of stiffness parameters	35
4.3.2	Undrained condition in soil models	37
4.3.3	Summary	37
4.4	PLAXIS model	38
4.4.1	Input parameters - Mohr-Coulomb model	39
4.4.2	Input parameters - Hardening Soil model	40
4.4.3	Input parameters - Hardening Soil Small model	40
4.4.4	Summary	41
5	Effect of input parameters in soft clay	43
5.1	Introduction	43
5.2	Sensitivity analysis of parameters	44
5.2.1	Sensitivity analysis - Mohr-Coulomb model	44
5.2.2	Sensitivity analysis - Hardening Soil model	46
5.2.3	Sensitivity analysis - Hardening Soil Small model	48
5.3	PLAXIS Sensitivity analysis and Parameter variation	50
5.4	Evaluation of sensitivity analysis	54
5.4.1	Summary	56
5.5	Replicate test result from centrifuge test	56
5.5.1	Soil test	57

5.5.2	Construction stages	59
5.5.3	Vertical ground displacement due to construction stages	61
5.5.4	Lateral wall displacement due to construction stages	62
5.5.5	Test 4 with soft props	63
5.5.6	Test 2 with flexible wall	65
5.5.7	Earth pressure	67
5.6	Validation of calibrated model	72
5.6.1	PLAXIS model outputs	73
5.7	Summary	74
6	Effect of wall stiffness	75
6.1	Parameter variation analysis of wall stiffness	75
6.1.1	Vary only bending stiffness EI	78
6.1.2	Vary only the axial stiffness EA	79
6.1.3	Vary bending stiffness EI and axial stiffness EA	79
6.1.4	Vary bending stiffness EI , axial stiffness EA and specific weight w	80
6.2	Parameter variation analysis of bending stiffness EI	81
6.2.1	Vertical ground displacement	81
6.2.2	Horizontal ground displacement	82
6.2.3	Lateral wall deflection	83
6.2.4	Maximum vertical ground displacement	83
6.2.5	Maximum horizontal ground displacement	84
6.2.6	Maximum lateral wall deflection	85
6.2.7	Maximum vertical ground displacement adjacent to wall	85
6.2.8	Maximum horizontal ground displacement adjacent to wall	86
6.2.9	Maximum lateral wall deflection at ground surface	86
6.2.10	Position of maximum vertical ground displacement	86
6.2.11	Position of maximum horizontal ground displacement	87
6.3	Summary	88
7	Discussion	89
8	Conclusion and Further Research	95
8.1	Summary of main findings	95
8.2	Conclusion	96
8.3	Recommendations for further research	97
A	Acronyms	98

<i>CONTENTS</i>	0
B PLAXIS Calculations	100
C Sensitivity Analysis	104
D PLAXIS Earth pressure	107
Bibliography	112

Chapter 1

Introduction

Due to an increase in population and urbanisation, underground space is exploited in order to counteract the high land cost in urban areas. Generally, excavation works are carried out in order to construct various types of underground infrastructure, such as deep basements, tunnels and subways. When the excavation depth is small, and enough space is available for the constructions works, an unsupported open cutting may be adopted. However, when the excavation depth is large and space of construction is limited a so-called deep excavation, which is generally supported by a retaining wall, is typically adopted. The majority of excavation works in urban areas utilize the latter technique. Since the retaining walls in an open cutting are generally considered as temporary structure, ground deformations may be acceptable as long as failure is prevented, and the stability of the wall is then the main interest in the design phase. However, excessive soil deformation near the wall may causes severe damage to adjacent structures, even for the condition with a sufficient factor of safety against failure. Therefore the wall deflection and the ground displacement due to a deep excavation in soft clay, is one of the most important design concerns in urban settings. The evaluation of ground movements is an essential factor in the design phase of these urban excavation works (Takemura et al., 1999).

There are two common techniques to predict the wall deflection and ground displacement, either by utilising empirical data or by numerical analysis based on finite element methods (FEM). Empirical methods are a valuable and important tool to estimate of ground movement induced by excavation works. However, for a detailed and reliable analysis, numerical methods are often explored. The wall deflection is generally reasonably well predicted by FEM analysis. However, the prediction of ground movement is usually not as accurate when using FEM models (Kung et al., 2007). The prediction of soil movements requires an understanding of the triggering mechanisms and of the parameters influencing them.

Soil displacements play a critical role in the construction of deep excavations with temporary retaining structures. To meet the demands on cost-effective construction without affecting the surrounding, different methods have

been proposed to classify excavation-induced ground movements. There is, however, an urgent need to quantify differences between these prediction methods to better understand their reliability and practical applicability (Tran, 2020).

The execution of excavation works requires the use of appropriate retaining wall and bracing systems. Inadequate support systems are a major concern, as an excessive ground movement induced during an excavation process could cause severe damage to adjacent constructions, cost and budget overruns, progress challenges and delays. An efficient, safe and appropriate design of support system for deep excavation is crucial.

Sophisticated constitutive models have been employed to consider the complex interactions between the soil and the structure in a deep excavation. However, such models contain large numbers of constitutive parameters where some are difficult to obtain due to complex and expensive field investigations and laboratory tests. Hence, input parameters are often affected by uncertainty. Moreover, the constitutive models have different assumptions and limitations. In other words, there are uncertainties in the models as well as in the measured data. In order to verify that a reliable and correct model is used, it is necessary to conduct model validation (Zhao et al., 2015).

This research focuses on how uncertain parameters influence the the ground displacement in a deep excavation in soft clay. A numerical model is first developed and calibrated by utilising the results of a centrifuge test series (Lam, 2010). After validation, the impact of wall stiffness on the excavation-induced ground displacement is explored in further detail.

1.1 Background

Urban deep excavations are often close to existing engineered structures and excavation-induced soil displacement may affect adjacent buildings and infrastructure. Primary concerns associated to deep excavations in soft clay are:

1. The design of a temporary or permanent support system that satisfy requirements and safety demands.
2. Reduce and avoid significant soil displacement and ground settlement.
3. Prevent damage to adjacent infrastructure and constructions.

The prediction of ground movement induced by deep excavation is a complex geotechnical problem. Typical factors with a frequent influence on the ground movement are the ground conditions (e.g. soil type and behaviour, pore water pressure, ground water level, consolidation degree etc.), depth to stiff stratum, excavation geometry (e.g. width, length, depth etc.), excavation process (e.g. sequence and quality), installation of support system and support system characteristics (e.g. stiffness, roughness etc.). Among these determining factors, the soil response

is often the most complex behaviour to capture.

Despite a number of important factors causing the behaviour of deep excavation, not all factors can be considered or reliably determined when designing retaining support system. The design of excavation support systems needs to avoid large displacement to achieve safety demands. In most cases, the design considers both empirical design charts and numerical analysis. To ensure that the rough predictions meets the observational field method, the excavation is usually performed simultaneously. Design charts may be used to compare to the monitored soil response in the ground (Kullingsjö, 2007).

Although excavation-induced ground displacement can often reasonably well be estimated by empirical and semi-empirical methods, numerical modeling provides possibilities to consider local conditions in more detail. However, despite the existence of advanced constitutive models, the numerical models often cannot fully capture the complex soil-structure mechanisms governing deep excavations and often result in unreliable estimates of excavation-induced ground displacements. For this reason, analytical methods, which generally have several limitations such as laboratory tests, are more widely adopted in practice to estimate the ground displacement due to a deep excavation (Meng et al., 2020). Excavations induce significant changes in the stress and strain fields in the soil and leads to ground displacement (Castaldo et al., 2013). As a reliable method to recreate the non-linear behaviour of soil, centrifuge modeling has been frequently employed in geotechnical engineering to realistically capture the stress-strain response of soil (Meng et al., 2020).

Problem formulation

Although a notable number of extensive methods to describe ground movements next to deep excavation exist, these studies are limited by various shortcomings, which likely affect their accuracy and reliability. Many methods often neglect, for instance, details about the ground conditions (e.g. stiffness, strength parameters), the excavation process and the type of retaining wall, and limit their predictions on only vertical surface displacement. These shortcomings result in uncertainties and different predictions, which may have detrimental impact when calculating the effects of ground displacement. There is a lack of methods for predicting and characterizing both vertical and horizontal ground displacement caused by deep excavation (Tran, 2020). Numerous studies have been carried out, but there is a big difference and relative scatter from the different methods for capturing the change of ground displacement when uncertain parameters is involved. Although some methods developed similar ground settlement profile, the difference is evident.

The following specific shortcomings were identified and will be addressed in this research:

- Empirical and semi-empirical methods to predict ground displacements caused by deep excavations are often limited to vertical displacements. Horizontal ground displacements are often neglected.

- There is a lack of calibrated numerical models for estimating ground movement of deep excavations.
- The effect of uncertain parameters such as the retaining wall stiffness on the shape and magnitude of vertical and horizontal ground displacements due to a deep excavation received scant attention in literature.
- The change of vertical and horizontal ground displacements in a deep excavation with different wall stiffness (e.g. the bending stiffness) has not been studied in detail.

A calibrated numerical model could provide guidance on the characteristics of vertical and horizontal soil displacements. With a calibrated model, an estimation of ground movement is possible to provide, even with uncertain parameters.

1.2 Research objectives

The main research question of this master thesis is:

How are short-term vertical and horizontal ground displacements adjacent to deep excavation in soft clay affected by uncertain parameters (for instance soil strength and stiffness, wall stiffness, prop stiffness etc.), and how can a calibrated model verify the sensitivity and variation of these parameters?

This dissertation aims to develop a calibrated numerical model that can be used to better understand the impact of uncertainties on ground displacements caused by deep excavations in soft clay. The method to tackle the main objective is to develop a reliable PLAXIS model that is first validated through comparison with experimental data (i.e. centrifuge test from (Lam, 2010)). After validation, a sensitivity analysis will be conducted by varying different parameters (e.g. soil stiffness and earth pressure coefficient at rest) to study their effect on ground displacements. The secondary objectives of this work were to provide new insight into the effect of the retaining wall stiffness on the vertical and horizontal soil displacements at soil surface. This will hopefully provide interesting insights that can be important for practice.

1.2.1 Sub-objectives

The sub-objectives of this master thesis are:

1. The first objective is to examine a well-performed case study of a deep excavation, and to identify relevant constitutive models that are able to capture the documented soil response.
2. The second objective is to replicate the case study in a numerical model, in order to compare and evaluate its performance to provide guidance on limitations, reliability and practicability. The aim is to develop a calibrated model that provides realistic estimations of vertical and horizontal ground displacement.
3. The final objective is to utilise the calibrated model to investigate how vital parameters (e.g. wall stiffness, soil stiffness, prop stiffness etc.) influence the excavation-induced ground displacements.

In order to accomplish these objectives, this thesis will carry out the following work:

- A relevant centrifuge test of a deep excavation in soft clay will be evaluated and replicated in a numerical model.
- A parametric analysis of uncertain input parameter for the constitutive models will be conducted, and uncertain parameters will be identified.
- A sensitivity analysis of crucial parameters (e.g. soil stiffness, earth pressure coefficient) is examined in order to determine a calibrated model.
- A calibrated model is verified by evaluate the numerical output and comparing with centrifuge test result in order to examine the influence of uncertain parameters (e.g. wall stiffness) with a parametric variation.

1.3 Outline of thesis

Chapter 1 represents this introduction, which provides the motivation, a brief background, the problem statement and the research objectives. The remaining parts of the thesis will be divided into the following chapters:

- Chapter 2 - A short review of previous research with focus on existing theory of empirical methods and an introduction to laboratory tests, such as centrifuge modelling.
- Chapter 3 - A review of the centrifuge tests conducted by (Lam, 2010). The chapter describes the development of the centrifuge tests and its outcome. It further contains calculations to derive input parameters for the numerical model by translating parameters from model scale to prototype scale.
- Chapter 4 - A numerical modelling chapter of relevant constitutive models and examines input parameters of the different constitutive models. The chapter includes the application of a numerical model to replicate centrifuge test results, and examines PLAXIS input parameters for the different constitutive models.
- Chapter 5 - The chapter examines the effect of input parameters in soft clay. A sensitivity analysis of unknown parameters in the constitutive models is compiled and a replication method of soil behaviour by investigate different approach for capturing the soil performance. Further a validation of a calibrated model based on the presented constitutive models.
- Chapter 6 - A parametric variation of uncertain parameters is presented in order to identify its influence on ground displacement.
- Chapter 7 - Discussions of different aspects based on results from the parametric study, and if the calibrated model is reliable and the influence of uncertain parameters. Additionally, avenues of future research will be presented.
- Chapter 8 - A summary and conclusion of the master thesis, and recommendations for further work.

Chapter 2

Literature review

This chapter contains of a brief review of existing work on empirical and semiempirical methods for estimating ground settlements in soft clay induced by a deep excavation. The different methods accentuate the objectives of this thesis and new techniques may be presented.

A traditional method for estimating the ground displacement due to a deep excavation in soft clay, is by empirical methods. A more detailed review of existing empirical methods is presented in the project thesis of Tran (2020). The purpose of this chapter is to have an overview of existing prediction methods and their limitations and challenges, and further identify refinements. The intention is not to give a complete description of soil displacement caused by excavation works, but rather to distinguish the potential differences in order to identify state of the art.

2.1 Empirical methods

Through the years, several empirical methods for prediction of ground displacement and wall deflection have been developed and proposed based on collecting and analyzing data from case studies. Tran (2020) compared several of these methods for both vertical and horizontal ground displacement. This previous research focused on evaluating different methods according to their relevance for ground surface settlement adjacent to a deep excavation in soft clay, and further classify which methods are accessible for particular situations.

Table 2.1 and Table 2.2 summarizes estimation methods for predicting ground displacement from different authors using different approaches. The empirical methods for vertical and horizontal ground movement predictions are presented in Figure 2.1 and Figure 2.2. As mentioned earlier, this paper will conduct centrifuge tests provided by Lam (2010), and two of these tests are represented in the figures as Test 2 and Test 5. A comparison of a laboratory test with well-defined data and empirical approaches was evaluated in earlier work (Tran, 2020).

From Table 2.1 and Table 2.2, an overview of the required input parameters for each empirical method is given. The methods shows a variation of input parameters and determining factors such as, for instance, the excavation depth and influence zone. Several methods consider the maximum vertical displacement based on a ratio with the maximum horizontal displacement (i.e. maximum lateral wall displacement). However, other methods have divided the soil volume into different influence zones. These zones define variations in the shape of the ground displacements. Additionally, some methods were developed for different support systems, such as a multi-propped sheet pile wall (SPW) in soft clay, whereas other methods consider a diaphragm wall (DW) without props.

By normalizing the vertical and horizontal ground displacement curves, as seen in Figure 2.1 and Figure 2.2, the different methods can be compared. The results show a variation of vertical and horizontal ground settlement curve when consider following aspects:

- Maximum vertical soil displacements: magnitude and location (i.e. distance from the retaining wall)
- Magnitude of vertical soil displacements directly adjacent to retaining wall
- Influence zone (i.e. extent of the soil displacements from the retaining wall)
- Maximum horizontal ground displacement: magnitude and location (i.e. distance from the retaining wall)
- Shape of the ground displacement profile (e.g. spandrel or concave)

Summary of ground surface settlement equations

Table 2.1: Vertical settlement curves from empirical methods (Tran, 2020).

Empirical methods	Equation of vertical ground settlement	Additional details
Peck (1969)	$S_v(x) = S_{max} * exp\left(-\frac{x^2}{2*i^2}\right)$ $i = W/2$	(For tunnels) S_{max} - max vertical settlement x - distance from wall W - influence zone i - notional center point
O'Rourke (1981)	$S_W = C_D * (S_W + S'_W)$ $C_D = \frac{S_W}{S_W + S'_W}$	S_W - cantilever movement S'_W - inward bulging C_D - deformation coefficient
Bowles and Caspe (1966/1988)	$\delta_v = \delta_{vm} * \left(\frac{D-x}{D}\right)^2$ $\delta_{vm} = \frac{4*V_s}{D}$ $D = H_w + B$	δ_{vm} - max vertical settlement D - influence zone x - distance from wall V_s - lateral soil volume H_w - excavation depth B - excavation width
Clough and O'Rourke (1990) (Clough et al. (1989))	$\delta_v = \delta_{hm} * R$ $\delta_v = \delta_{vm} \text{ for Zone 1}$ $\delta_v = \delta_{vm} * (1 - 0.8 * (\frac{d}{H} - 0.75)) \text{ for Zone 2}$	δ_{vm} - max vertical settlement Zone 1: $d/H \leq 0.75$ Zone 2: $d/H > 0.75$ d/H - distance from wall
Hsieh and Ou (1993/1998)	<p style="text-align: center;">Spandrel:</p> $\delta_v = \left(-0,636 * \sqrt{\frac{d}{H_e}} + 1\right) * \delta_{vm} \text{ for PIZ}$ $\delta_v = \left(-0,171 * \sqrt{\frac{d}{H_e}} + 0,342\right) * \delta_{vm} \text{ for SIZ}$ <p style="text-align: center;">Concave:</p> $\delta_v = \delta_{vm} * (0.5 + 1.5 * \frac{d}{H_e}) \text{ for PIZ 1}$ $\delta_v = \delta_{vm} * (1 - 1.25 * (\frac{d}{H_e} - \frac{1}{3})) \text{ for PIZ 2}$ $\delta_v = \delta_{vm} * (\frac{1}{6} - \frac{1}{6} * (\frac{d}{H_e} - 1)) \text{ for SIZ}$ $AIR = H_e + H_p$	δ_{vm} - max vertical settlement PIZ: $d/H_e \leq 2$ SIZ: $d/H_e > 2$ d/H_e - distance from wall PIZ 1: $d/PIZ \leq 1/3$ PIZ 2: $1/3 < d/PIZ \leq 1$ SIZ: $1 < d/PIZ \leq 2$ AIR - apparent influence range H_e - excavation depth H_p - wall penetration depth
Karlsrud (1998)	$\delta_{hm} = 0.01 * H$ $\delta_v = RF * \delta_{hm} * LB \text{ for LB}$ $\delta_v = RF * \delta_{hm} * UB \text{ for UB}$	δ_{hm} - max horizontal settlement H - excavation depth Lower bound (LB)= 0.7 Upper bound (UB)= 1.0 $RF = \delta_{vm} / \delta_{hm} = [0.5, 1.0, 0.2, 0]$
Aye et al. (2006)	$S_{i0} = S_{W0} * \left(\frac{x}{D_0}\right)^2$ $S_{W0} = \frac{4*V_0}{D_0}$	S_{W0} - max vertical settlement D_0 - influence zone V_0 - wall deflection shape x - distance from wall
Lee et al. (2007)	$s(x) = s_{max} * exp\left(0.5 - 0.5\left(1 + \frac{2x}{W}\right)^2\right)$ $s_{max} = \delta_{hm} = 0.01 * H$	s_{max} - max vertical settlement x - distance from wall W - influence zone
Kung et al. KJHH (2007) (Schuster et al. KSJH (2009))	$\delta_{hm} = 0.01 * H$ $\delta_{vm} = R * \delta_{hm}$ $\delta_v = \delta_{vm} * (1.6 * d/H_e + 0.2) \text{ for Zone 1}$ $\delta_v = \delta_{vm} * (-0.6 * d/H_e + 1.3) \text{ for Zone 2}$ $\delta_v = \delta_{vm} * (-0.05 * d/H_e + 0.2) \text{ for Zone 3}$	δ_{vm} - max vertical settlement d/H_e - distance from wall Zone 1: $0 \leq d/H_e \leq 0.5$ Zone 2: $0.5 \leq d/H_e \leq 2$ Zone 3: $2 \leq d/H_e \leq 4$ Sagging: $d/H_e < 1.4$ Hogging: $d/H_e > 1.4$

Table 2.2: Horizontal settlement curves from empirical methods (Tran, 2020).

Empirical methods	Equation of vertical ground settlement	Additional details
Aye et al. (2006)	$S_{hi} = S_{hwi} * \frac{D_{oi} - X_i}{D_{oi}}$	S_{hwi} - max horizontal settlement D_{oi} - influence zone X_i - distance from wall
Lee et al. (2007)	$h(x) = \beta^* \left(1 + \frac{2x}{W}\right) * s(x)$ $s(x) = s_{max} * \exp\left(0.5 - 0.5 \left(1 + \frac{2x}{W}\right)^2\right)$	x - distance from wall β^* - ratio of horizontal settlement W - influence zone $s(x)$ - vertical settlement at distance x
Schuster et al. KSJH (2009) (Kung et al. KJHH (2007))	$\delta_{lm} = R_l * \delta_{hm}$ Spandrel: (include adjacent constructions) $\delta_l = \delta_{lm} * \left(1 - 0.2 * \frac{d}{H_e}\right)$ for Zone 1 $\delta_l = \delta_{lm} * \left(0.8 + \frac{1}{3} * \left(1 - \frac{d}{H_e}\right)\right)$ for Zone 2 $\delta_l = \delta_{lm} * \left(0.3 + 0.12 * \left(2.5 - \frac{d}{H_e}\right)\right)$ for Zone 3 Concave: $\delta_l = \delta_{lm} * \left(0.2 + 0.8 * \frac{d}{H_e}\right)$ for Zone 1 $\delta_l = \delta_{lm} * \left(1 + 0.4 * \left(1 - \frac{d}{H_e}\right)\right)$ for Zone 2 $\delta_l = \delta_{lm} * \left(0.4 + 0.16 * \left(2.5 - \frac{d}{H_e}\right)\right)$ for Zone 3	δ_{hm} - max horizontal settlement δ_{lm} - max lateral settlement d/H_e - distance from wall Zone 1: $0 \leq d/H_e < 1$ Zone 2: $1 \leq d/H_e < 2.5$ Zone 3: $2.5 \leq d/H_e < 5$ Zone 1: $0 \leq d/H_e < 1$ Zone 2: $1 \leq d/H_e < 2.5$ Zone 3: $2.5 \leq d/H_e < 5$

Observed data with centrifuge Test 2 and Test 5 in the Figure 2.1 and Figure 2.2 differ from the other empirical methods, but is expected because of assumptions that have been made for the empirical prediction may differ from the assumptions for the centrifuge tests. This is for instance the excavation depth and the wall height. Further details are provided in Tran (2020).

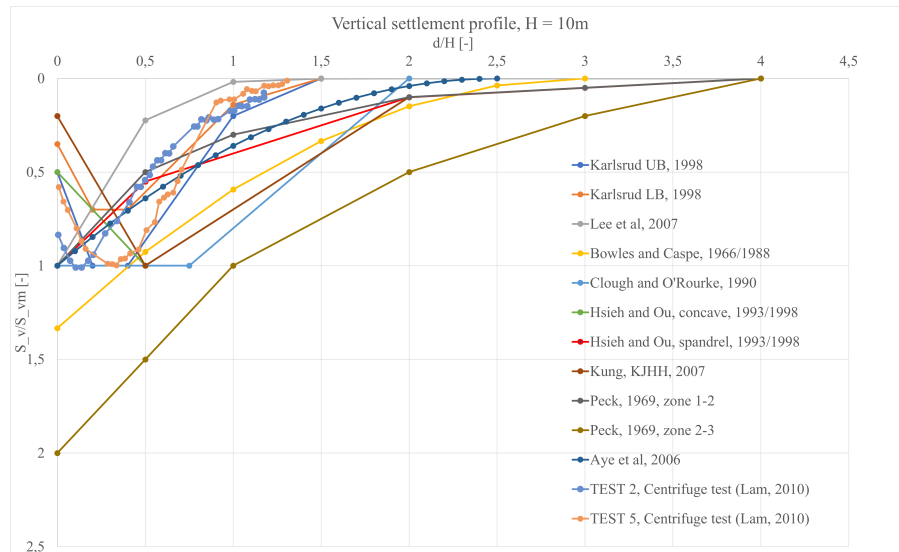


Figure 2.1: Vertical settlement profile from empirical methods and and Test 2 and Test 5. Optimized figure from Tran (2020).

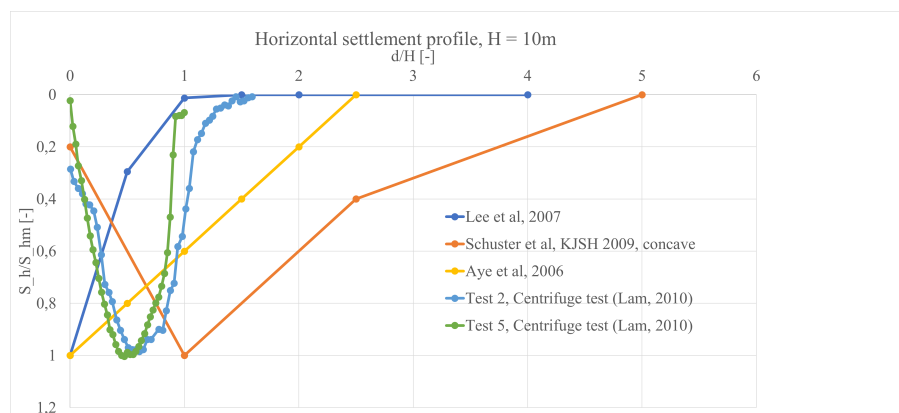


Figure 2.2: Horizontal settlement profile with empirical methods and centrifuge tests. Optimized figure from Tran (2020).

The provided tables with the empirical methods in this chapter, indicate an extensive and wide knowledge, and describe different approaches for estimating ground surface settlement. However, the methods use different input parameters which result in different predictions of ground displacement. A few methods only provide some data points and no equations describing the settlement profiles. Limited methods provide guidance on prediction of horizontal soil displacements and on potential changes of the displacement profiles with depth. The comparison shows notable differences in the existing methods for predicting ground displacements adjacent to deep excavations.

Although a considerable scatter between the different methods was observed, it was found that some methods seem to perform better than others. For multi-propped deep excavations in soft clay, the methods of KJHH (Kung et al., 2007) and KSJH (Schuster et al., 2009), (Lee et al., 2007) and (Aye et al., 2006) showed a good fit with experimental data of vertical ground displacement profiles. All these methods provide both vertical and horizontal settlement profile. For the vertical settlement profile, the method of (Karlsrud, 1998) and (Hsieh and Ou, 1998) indicate good estimations. A more detailed review of existing methods to predict deep excavation-induced ground displacements is provided in Tran (2020).

2.2 Laboratory test - Centrifuge experiments

In order to understand and evaluate the performance of deep excavations, an fundamental factor is to obtain reliable and controlled data from the field or using laboratory investigations. Common complications with field measurements is the lack of repeatably, which includes the variation of soil condition and construction sequences from one excavation to another. This often results in an uncertain comparisons between different datesets. An additional method to study deep excavations is to adopt geotechnical centrifuge modelling, which is designed as a small-scale model with the purpose to realistically replicate the respective prototype. A centrifuge model is designed to create an artificial acceleration in order to simulate realistic self-weight stresses in the soil. The generated stress will ensure to imitate a correct model of an excavation in small-scale. An advantageous of using centrifuge tests is that the different scenarios can be tested in a controlled manner. A well-defined centrifuge experiment will provide documented data to calibrate a numerical model, which will further be explored in this work.

Chapter 3

Centrifuge test - Deep excavation in soft clay

This chapter describes a well-defined laboratory test based on a centrifuge test (CT) conducted by Lam (2010), and contains a description of how to replicate input parameters from laboratory test in a numerical model by scaling laws. Further, a calculations of important soil model input is presented.

The aim of this chapter is to introduce a centrifuge test series (Lam, 2010; Lam et al., 2012) which is used in this master thesis as benchmark data to calibrate a numerical model, and present how it is modelled and conducted. In the following, this chapter will provide a brief overview of these centrifuge tests, and emphasize how these laboratory tests are used in this work. A detailed description of these centrifuge tests are provided elsewhere (Lam, 2010; Lam et al., 2012). Further, model scale parameters presented from the centrifuge test will be scaled to prototype scale parameters based on scaling laws principles.

3.1 General

The methodology of the centrifuge test, is to simulate an ideal excavation process has to be carried out in-flight, which means under gravitational acceleration. A centrifugal acceleration field of 60g was obtain, in order to replicate the stress induced by gravity in the prototype model. The in-flight excavator centrifuge method satisfy the requirements of a correct simulated model that excavate the soil. However, note that the method do not simulate a realistic construction sequence process of the excavation progress with installation of retaining wall and prop (Lam, 2010).

3.1.1 Model set-up

The experimental set-up of the model scale with an in-flight excavator is illustrated in Figure 3.1. The geometry is designed as a rectangular container made of aluminium alloy with internal dimensions 790mm in length, 180mm in width and 470mm in depth. The thickness of clay is presented as 295mm on the right side of the symmetry line. Instruments were installed for measurement of pore pressure, pore pressure transducers (PPT), earth pressure cells (EPC) on the retaining wall, bending moment strain gauges on the wall, load cells on the props, and linear variable transformers for displacement measurement (Lam et al., 2014).

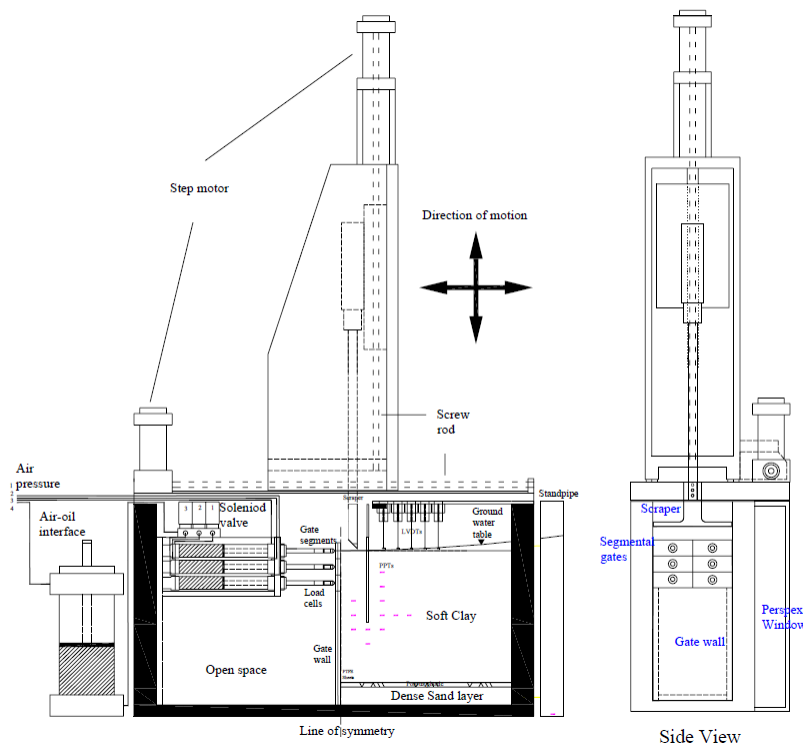


Figure 3.1: Experimental setup with in-flight excavator of the centrifuge test in model scale (Lam, 2010).

3.1.2 Model support system

The retaining wall have a length of 160mm in model scale which is equivalent to $9,6\text{m}$ in prototype scale. Lam (2010) presented two type of retaining wall, a rigid diaphragm wall and flexible wall sheet pile wall. The diaphragm retaining wall in model scale was made of a 6mm thick aluminium alloy plate, with the purpose to implicate/be equivalent to a $0,9\text{m}$ thick diaphragm wall with a stiffness EI of $280,8\text{MNm}^2/\text{m}$ in prototype scale. The test was also conducted with a sheet pile retaining wall in model scale with a 2mm thick aluminium alloy plate to implicate a sheet pile wall (US steel, PDA-27) with stiffness EI of $10,4\text{MNm}^2/\text{m}$ in prototype scale.

A prop installation sub-system to the retaining wall was designed to provide in-flight support during the experi-

ment. The propping and gate system of six props for the excavation sequence is illustrated in side view in Figure 3.1 and in Figure 3.2. The propping system have a width of 180mm , and the distance between the two-pair of props is 90mm . The cylinder support system and the gate system is designed with rigid props positioned at 0mm , 36mm and 72mm depth in model scale.

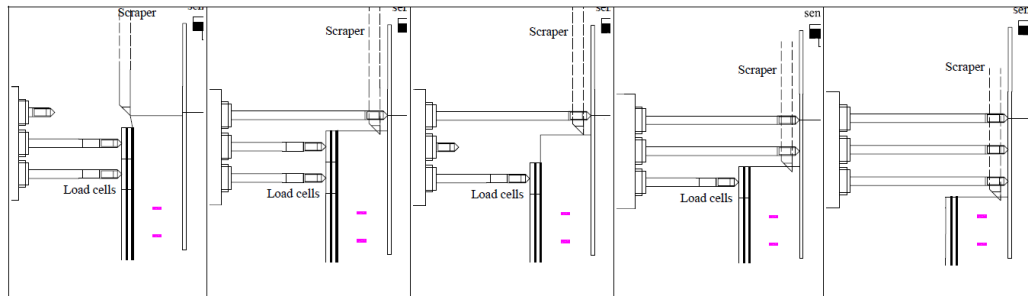


Figure 3.2: Prop installation modelling for different excavation sequence (Lam, 2010).

The model system have a hydraulic control system and is saturated with hydraulic oil before conducting the experiment. Props are driven by pistons in the cylinders through this control system. Forward pressure inlets are connected to the oil pressure reservoir in order to provide a similar propping force system at each excavation level. This prop stiffness is controlled by air pressure that compresses the oil reservoir and the air-oil interface system. The stiffness of a fully-saturated prop is further constructed with 1.66kN/mm in model scale and 100kN/mm in prototype model (Lam, 2010). The propping force can be controlled by adapt the air pressure at the air-oil interface and the associated props remain stiff by the incompressibility of hydraulic oil.

3.1.3 Model ground

The well-known lightly over-consolidated Speswhite Kaolin clay was used in the model scale. A standard procedure was further adopted in the test to ensure repetitive reproduction of the model ground with similar strength profiles in each test. Pressure was installed to achieve an estimated S_u at the mid-depth of the centrifuge model. The undrained shear strength S_u is assumed to be an average of 27kPa with a Poisson's ratio of $\nu = 0.5$ (Lam, 2010). The model scale represented in Figure 3.1 is represented in prototype scale model in Figure 3.3. The model ground have two layers of soil, a bottom layer of dense sand and a depth D of 295mm upper layer of soft clay. The ground model itself have a length dimension half the model length, which is 395mm .

Normally consolidated clay have usually an earth pressure coefficient $K_0 < 1$ and for heavily overconsolidated $K_0 > 1$. For an OC clay, it is expected that K_0 will approach 1, and it is reasonable approximation of excavation in such soil. However, it is recognized that during the excavation, the K_0 will be between active K_A and passive K_P (Lam, 2010). Additionally, it is consistent to assume that K_0 will approach K_p during an excavation. The model ground was consolidated and placed with a vertical piston as a vertical load to 160kPa and then unloaded and swelled to 26kPa . This consequently result in $\sigma_3 > \sigma_1$, and gives a $K_0 > 1$.

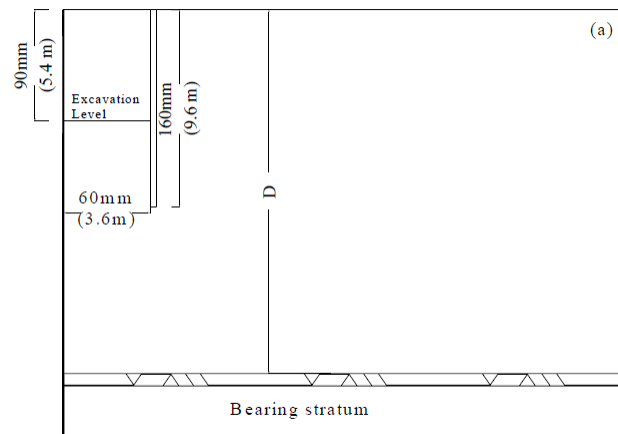


Figure 3.3: Excavation geometry in model scale (Lam, 2010).

3.1.4 Excavation test procedure

The construction stages was based on an artificial excavation process, where the sequences was divided into three levels of excavations. The initial stage was installation of retaining wall, with following first excavation and then dewatering. Then installation of first prop was set in this level at surface ground with position 0mm in model scale. Further, the next excavation level was proceeded and second prop was installed at position 36mm . Same procedure were accomplished with third prop at position 72mm . As mentioned earlier, the centrifuge test is not able to simulate a realistic construction sequence process of the excavation progress with installation of wall and prop. Therefore, a small scale robotic excavator is developed in order to remove the soil in an in-flight centrifuge test as an excavation process.

3.1.5 Test program

Five centrifuge models tests were carried out to study the undrained short-term behaviour of soft clay in an excavation, as presented with model scale values in Figure 3.4. Test 1 (SYL04), the baseline test, investigate the behaviour of a floating rigid wall installed with stiff props. Test 2 (SYL05) simulated the effect of wall flexibility and stiffness on the deformation mechanism, while Test 4 (SYL03) simulated a rigid wall supported by soft props and studied the effect of soft propping on the changes in the deformation pattern. Test 3 (SYL06) studied a fixed wall toe condition for both moving in bending and shear mode, while Test 5 (SYL07) studied the deformation in an excavation with a shallow clay thickness by using a flexible wall. Test 1 and Test 4 is designed with a diaphragm wall, while Test 2 and Test 3 is a sheet pile wall. For further assumptions, Test 1 (baseline) will mainly be in focus and referred to regarding the centrifuge test.

Centrifuge tests	1	2	3	4	5
	Floating rigid wall with stiff props	Floating flexible wall with stiff props	Fixed-base flexible wall with base grout	Floating rigid wall with soft props	Fixed-base flexible wall in shallow clay
Objectives	Baseline test	Wall stiffness	Fixed-wall toe condition	Prop stiffness	Clay thickness
Depth of clay stratum, D (mm)	300	300	300	300	160
Prop stiffness (kN/mm)	1.66	1.66	1.66	0.55	1.66
System stiffness $EH\gamma_w s^4$	2860	106	106	2860	106
Toe fixity	Free	Free	Fixed	Free	Free

Note: Numbers are in model scale.

Figure 3.4: A summary of 5 centrifuge tests (Lam et al., 2014).

3.1.6 Undrained compression triaxial testing of core samples

Triaxial testing are the most general testing equipment in the laboratory when investigating the stress strain behaviour of soil. Good agreement have been proved between the model predictions and published laboratory results for triaxial compression tests (Sivasithamparam and Castro, 2015). The stiffness of soil varies in a wide range of different strain levels. For accurate measurement of stress strain stiffness, instrumentation capable of measuring strain to an accuracy at the degree of $10^{-3}\%$ is ideally required. This level of accuracy can only be achieved by internal measurement within the triaxial cell (Lam, 2010).

The laboratory experiment was conducted in an undrained compression triaxial test with an isotropic consolidation. The first step of the undrained compression triaxial procedure was saturation. The second step included consolidation and swelling, where consolidation process brought the isotropic means effective stress p' to the stress level as in the centrifuge test with $K_0 = 1$. The sample swelled from $160kPa$ and back to a means stress level of $26kPa$. Further, the compression process represents a strain rate of 1% per hour in order to replicate the the soil behaviour in the centrifuge test.

3.1.7 Small strain stiffness

Lam (2010) presented local strain measurement by examine small strain axial stiffness during the triaxial compression test. The secant Young's modulus E was calculated as a ratio of the deviatoric stress q and the locally measured axial strain ϵ_{yy} . Undrained shear modulus G_u was derived by assuming a Poisson's ratio $\nu = 0,5$.

$$G = \frac{E}{2(1 + \nu)} = \frac{E}{2(1 + 0.5)} = \frac{E}{3} \quad (3.1)$$

An power-law idealization is used to present the stress strain curve of the Kaolin clay, and is illustrated in Figure 3.5. Further, the realistic ground displacements causes shear strains between 0.0001% and 1%. The shear modulus (i.e. small strain stiffness) G_0 of $22MPa$ that occurs at a very low level of strain was extracted from Figure 3.5. p_r is the reference pressure of $1kPa$ and is plotted against the mean effective stress p' , where both G_0 and p' values

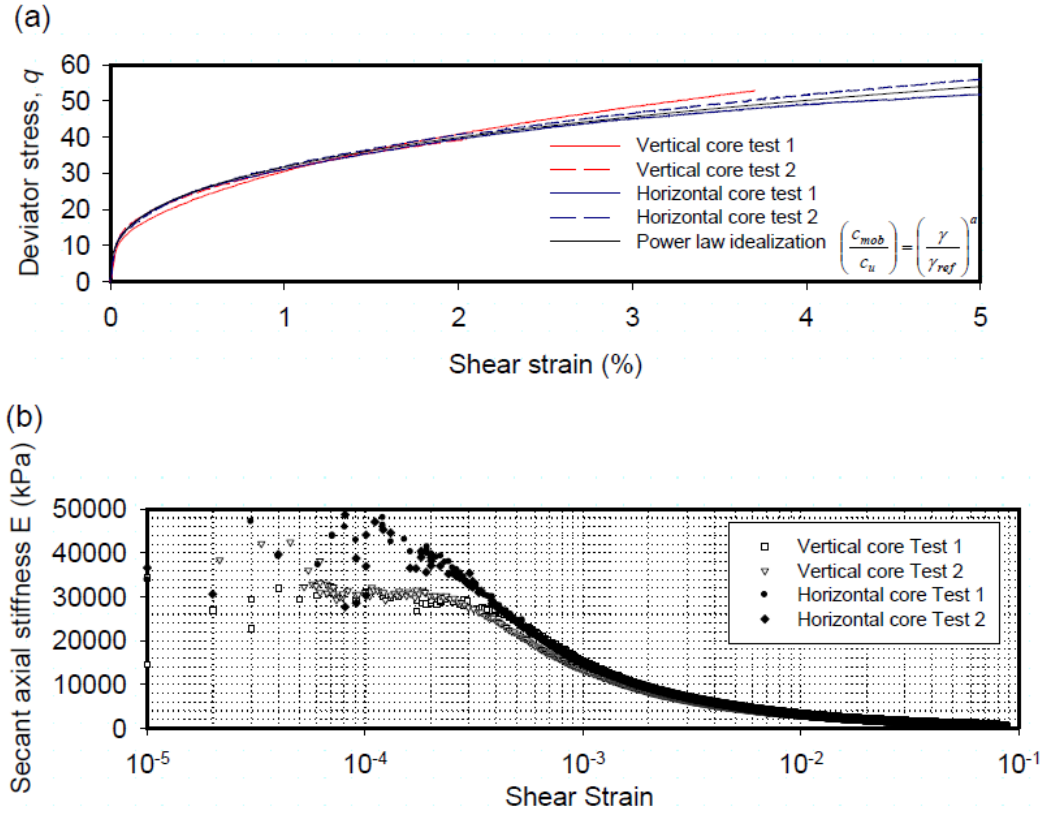


Figure 3.5: (a) Deviatoric stress and shear strain curves and (b) secant axial stiffness and shear strain with stiffness degradation curves (Lam, 2010).

was normalized by reference pressure p_r . The correlation is plotted in Figure 3.6, where a and b is constants of respectively value of 0.69 and 2.3, and where e_0 is the void ratio assumed for Kaolin clay by (Takemura et al., 1999). This γ_{ref} represents the threshold shear strain $\gamma_{0.7}$ by the definition of "about 70%" should be interpreted, more accurately as 72.2%. This gives a $G_s/G_o = 0.722$, and shear strain γ can be calculated by:

$$\gamma_{ref} = b * e_0 * 10^{-3} = 2.3 * 1.66 * 10^{-3} = 3.818 * 10^{-3} \quad (3.2)$$

$$\frac{G_s}{G_o} = 0.722 \quad (3.3)$$

$$0.722 = \frac{1}{1 + \left(\frac{\gamma}{\gamma_{ref}}\right)^a} = \frac{1}{1 + \left(\frac{\gamma}{3.818 * 10^{-3}}\right)^{0.69}} \quad (3.4)$$

$$\gamma = 9.53 * 10^{-4}, \quad (3.5)$$

which gives a relative good estimation with the normalized secant shear modulus G/G_o curve in Figure 3.6.

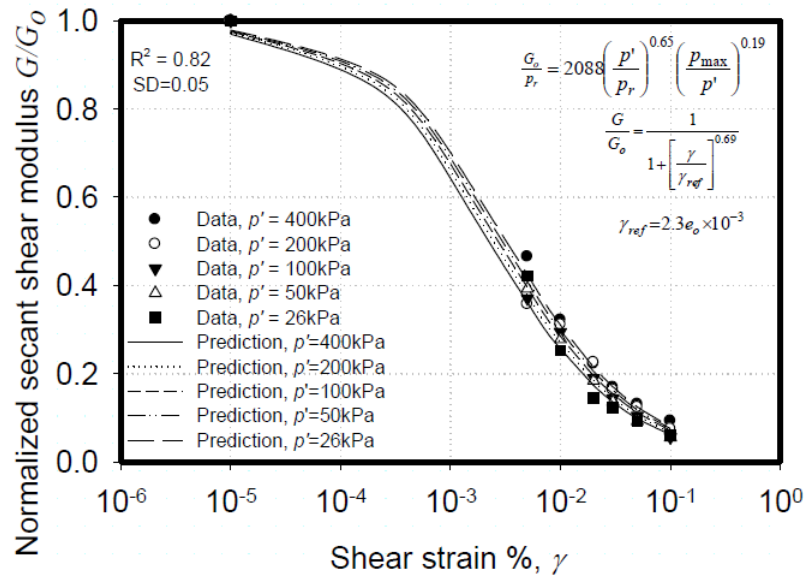


Figure 3.6: Normalized secant shear modulus with shear strain (Lam, 2010)

3.1.8 Ground displacement

The vertical ground displacement and lateral wall displacement of Test 1 is presented in the centrifuge test by Lam (2010), and is illustrated in Figure 3.7. Further in this research, the ground displacement will be an aspect when evaluating the performance of different soil models and the influence of important parameters. The outcome of vertical ground displacement S_v and horizontal ground displacement S_h behind the retaining wall will be presented and evaluated, as well as the lateral wall deflection δ_w . Note that the lateral wall deflection also represents horizontal displacement, and therefore may provide similar values.

3.1.9 Summary

Centrifuge model tests of a multi-propped deep excavation in lightly over-consolidated clay were carried out using a newly developed system, where the construction sequence of propping was precisely modelled. The method provides the realistic initial ground conditions before excavation. Additionally, the actual removal of soils provides an appropriate method of simulating passive resistance on the excavation side.

Undrained triaxial compression tests were carried out to characterize the stiffness of soil obtained from the mid depth of the deformation mechanism. With local strain measurements on the sample and geophysical soil characterization techniques, reliable stress-strain curves with a strain level below 0.1% can be obtained. A hyperbolic function is conducted to represent the actual stiffness data with a reasonable coefficient of correlation. The use of simple stress strain power law relationship is further used as a mean for a simple representation of the non-linear small strain behaviour of the Kaolin clay (Lam, 2010).

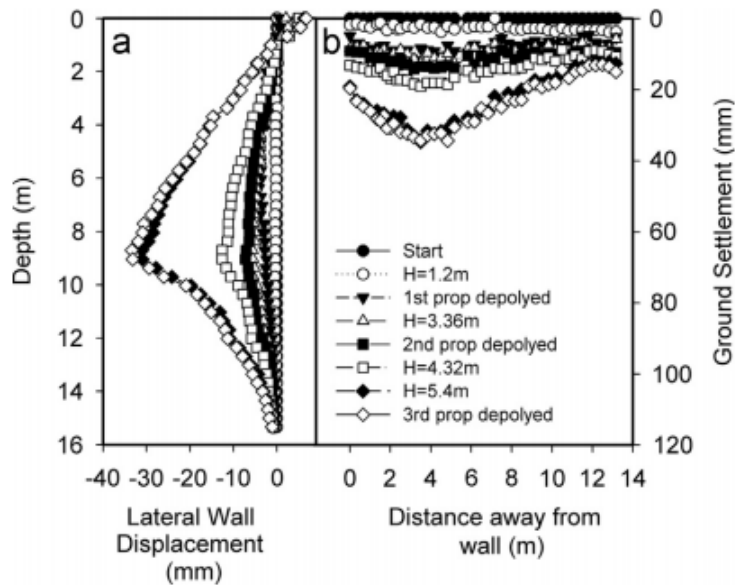


Figure 3.7: Test 1 (SYL04) (a) Wall deflection and lateral wall displacement and (b) ground displacement with excavation sequence (Lam, 2010).

In order to evaluate a prediction method of ground displacement, a calibrated model is required to be able to present reliable and comprehensive result. Generally, a model is based on a number of different parameters, which makes the analysis complex. However, when estimating and calculating with several unknown parameters or when doing a sensitivity analysis, a variation of parameters is tested, such as in Lam (2010) centrifuge tests.

3.2 Scaling up from model scale to prototype scale

In order to reproduce the soil behaviour during an excavation in soft clay, an advanced soil constitutive model is adopted. The intend is to reproduce the centrifuge test results in a numerical model in order to evaluate if the numerical model can replicate the same soil behaviour as observed in the centrifuge test. The replication is based on scaling up from centrifuge test result to prototype field dimension result, and requires input data from the centrifuge test and is gathered from Lam (2010). The centrifuge test is modelled with a gravitational acceleration of $60g$ in order to replicate a 60 times larger prototype. This means that parameters needs to be scaled from model to prototype scale using so called scaling laws. A respective scaling factor, n , is used to calculate between model, m , and prototype, p , values.

Scaling laws for geotechnical centrifuge modelling are given in Table 3.1, which indicates that different parameters have different scaling factor. The following sections describes how the prototype values for the soil model and support system are determined. Five centrifuge tests are presented, but this paper will primarily consider Test 1 (i.e. baseline test) from Table 3.4. If other tests by Lam (2010) are considered, consequently a notation will be

conducted and presented. Test 1 represents a floating rigid wall with stiff props.

Table 3.1: Centrifuge scaling law (Meng et al., 2020).

Physical quantity parameter	Unit	Scaling factor (Model/Prototype)
Gravitational acceleration g	[m/s ²]	n
Gravity ρ	[m/s ²]	n
Unit weight γ	[kN/m ³]	n
Poisson ratio ν	[-]	1
Earth pressure coefficient K_0	[-]	1
Undrained shear strength S_u	[kPa]	1
Length/width/height/depht $l/b/h/d$	[m]	$1/n$
Area A	[m ²]	$1/n^2$
Volume V	[m ³]	$1/n^3$
Settlement δ	[m]	$1/n$
Stress σ	[kPa]	1
Strain ϵ	[-]	1
Force F	[kN]	$1/n^2$
Density ρ	[kg/m ³]	1
Bending moment M	[kNm]	$1/n^3$
Bending moment pr. meter M	[kNm/m]	$1/n^2$
Flexural/bending stiffness EI	[kNm ² /m]	$1/n^4$
Flexural/bending stiffness pr. meter EI	[kNm ² /m/m]	$1/n^3$
Axial stiffness EA	[kN/m]	$1/n$
Specific weight pr. meter, w	[kN/m/m]	1
System stiffness η	[EI/ $\gamma_w s^4$]	1

* Gravitational acceleration 60g. $n = 60$.

3.2.1 Soil ground parameters

The density ρ of soil is calculated by the specific gravity G_s , where the Chinese Speswhite Kaolin clay have a specific gravity of 2.6.

$$\rho = 2.6 * 1000 \text{ kg/m}^3 = 2600 \text{ kg/m}^3 \quad (3.6)$$

Further, unit weight γ of soil is computed from:

$$\gamma_t = \rho * g = 2600 \text{ kg/m}^3 * 9.81 \text{ m/s}^2 = 25500 \text{ kg/m}^2 \text{ s}^2 = 25.5 \text{ kN/m}^3 \quad (3.7)$$

$$\gamma_s = \gamma_t - \gamma_w = 25.5 \text{ kN/m}^3 - 9.81 \text{ kN/m}^3 = 15.7 \text{ kN/m}^3, \quad (3.8)$$

where gravitational acceleration g is 9.81 m/s^2 , γ_t is total unit weight, γ_s is unit weight of soil and γ_w is unit weight of water. According to calculations from Lam (2010), the unit weight is assumed to be 16 kN/m^3 and is thus set for further calculations. Generally, the undrained shear strength increases with the depth, but is in this paper assumed constant (Lam et al., 2012). The undrained shear strength S_u is further determined as 27 kPa (Lam, 2010). Input parameters such as Young's modulus E , Poisson ratio ν , undrained shear strength S_u and earth pressure coefficient at rest K_0 have a scaling factor 1. While, the geometry parameter of the soil model have scaling factor $\frac{1}{n}$, which results in the following prototype values:

$$l_p = l_m * n = \frac{790\text{ mm}}{2} * 60 = 395\text{ mm} * 60 = 23.7\text{ m} \quad (3.9)$$

$$w_p = w_m * n = 180\text{ mm} * 60 = 10.8\text{ m} \quad (3.10)$$

$$h_p = h_m * n = 300\text{ mm} * 60 = 18\text{ m}, \quad (3.11)$$

where l_p is the length of the prototype model dimensions, w_p is the width and h_p is the height.

3.2.2 Retaining wall parameters

The geometrical input parameters of the retaining wall for the prototype model scale are calculated from Table 3.1. The geometry (i.e. the length, height and thickness) of the wall is computed with scaling factor $\frac{1}{n}$, and the area is computed with scaling factor $\frac{1}{n^2}$.

The main input parameters to model the mechanical behaviour of a retaining wall are the flexural or bending stiffness EI and axial stiffness EA , as presented in Table 3.1. Lam (2010) investigated a sheet pile wall and a diaphragm wall. The centrifuge model tests was modelled with a 2 mm and 6 mm thick aluminium alloy plate which represents a sheet pile wall with stiffness EI of $10.4\text{ MNm}^2/\text{m}$ and a 0.9 m thick diaphragm wall with stiffness EI of $280.8\text{ MNm}^2/\text{m}$. Lam (2010) presented the centrifuge Test 1 results by using the diaphragm wall, and further calculation will be carried out by assuming a diaphragm wall.

Further calculations will address the estimation of Young's modulus of retaining wall EA_{rw} and axial stiffness in prototype scale EA_p . The bending stiffness in model scale EI_m is determined by:

$$EI_m = \frac{EI_p}{n^3} = \frac{280.8\text{ MNm}^2/\text{m}}{60^3} = 1.3\text{ kNm}^2/\text{m}, \quad (3.12)$$

where EI_p is stiffness in prototype scale and n is the scaling factor (i.e. 60). The stiffness EI is given in per unit meter width as described in Table 3.2. In order to calculate the axial stiffness EA , the Young's modulus E needs to be found.

$$E_{rw} = \frac{EI_m}{I_{rw}} = \frac{1.3\text{ kNm}^2/\text{m}}{\frac{(6\text{ mm}/1000)^3}{12} * \frac{1}{1\text{ m}}} = 72.2\text{ E6 kN/m}^2 = 72.222\text{ E3 MPa}, \quad (3.13)$$

where E_{rw} is stiffness of retaining wall and I_{rw} is the second moment of area in the plane of bending (i.e. the plane where the earth pressures acts on the retaining wall). The axial stiffness EA_m of the retaining wall in model scale can thereby be computed by:

$$EA_m = E_{rw} * A_{rw} = 72.2E6kN/m^2 * \frac{6mm}{1000} * 1m * \frac{1}{1m} = 4.33E5kN/m, \quad (3.14)$$

where A_{rw} is the area of cross-section of the retaining wall per unit length meter. Further, the axial stiffness EA_p of the retaining wall in prototype scale can be determined:

$$EA_p = EA_m * n = 4.33E5kN/m * 60 = 2.60E7kN/m \quad (3.15)$$

The thickness t_m of retaining wall in model scale is $6mm$, and prototype scale thickness is calculated to be:

$$t_p = t_m * n = 6mm * 60 = 0.36m, \quad (3.16)$$

and unit length of wall L_p is $1m$ and unit height of wall H_p is $1m$ in prototype scale. The Poisson ratio ν for aluminium alloy is 0.32 and the density is found to be $2.7g/cm^3$ (Stojanovic et al., 2018), which can define the mass weight:

$$m_p = \rho * V = 2700kg/m^3 * 0.36m * 1m * 1m = 972kg/(m * m) \quad (3.17)$$

Further, the specific weight w can be calculated from the force F :

$$F = m_p * g = 972kg/(m * m) * 9.81m/s^2 = 9532.2N/(m * m) = 9.53kN/(m * m) \quad (3.18)$$

where F is equivalent to the specific weight w , which is weight per unit volume. Table 3.2 summarizes the model and prototype input parameters by using scaling laws.

Table 3.2: Prototype scale values calculation with model scale values for retaining wall parameters.

Physical quantity parameter	Scaling factor	Model value	Prototype value
Flexural/bending stiffness pr. meter, EI	$1/n^3$	$1.3kNm^2/m$	$280.8E3kNm^2/m$
Axial stiffness, EA	$1/n$	$4.33E5kN/m$	$2.60E7kN/m$
Specific weight pr. meter, w	1	$9.53kN/m/m$	$9.53kN/m/m$
Poisson ratio, ν , [-]	1	0.32	0.2

3.2.3 Prop parameters

The cylinder support system and the gate system is designed with rigid props positioned at $0mm$, $36mm$ and $72mm$ depth in model scale, which results in $0m$, $2.16m$ and $4.32m$ in prototype scale.

The distance between the props pair is determined to be 90mm in model scale from Figure 3.1, which is half the width of 180mm of the excavation model. This length represents the out-of-plane spacing $L_{spacing}$, which is the spacing of the embedded beams in the out-of-plane direction (Sloot, 2020a). Therefore, $L_{spacing,m}$ is 90mm in model scale and $L_{spacing,p}$ is 5.4m in prototype scale. The equivalent length $L_{equivalent}$ is a prop property and is the distance between the two geometry points to which the anchor is connected. In this case, half an excavation is normally considered, so the $L_{equivalent}$ will be the excavation width 60mm in model scale and 3.6m in prototype scale.

$$L_{spacing,p} = L_{spacing,m} * n = 90\text{mm} * 60 = 5.4\text{m} \quad (3.19)$$

$$L_{equivalent,p} = L_{equivalent,m} * n = 60\text{mm} * 60 = 3.6\text{m} \quad (3.20)$$

However, as mentioned earlier in Chapter 3, the equivalent stiffness $\frac{EA}{L_{equivalent}}$ is defined and controlled by air pressure that compresses the oil reservoir in the air-oil interface, and indicates that it is not the length that controls the props. The prop stiffness from Table 3.4 represented 1.66kN/mm in model scale and 100kN/mm (i.e. verified in Equation 3.21) in prototype scale represents $\left(\frac{EA_p}{L_{equivalent}}\right)_p$.

$$\left(\frac{EA}{L_{equivalent}}\right)_p = \left(\frac{EA}{L_{equivalent}}\right)_m * n = 1.66\text{kN/mm} * 60 = 99.6\text{kN/mm} \quad (3.21)$$

which is approximate 100kN/mm . The axial stiffness of prop is therefore calculated with:

$$\left(\frac{EA_p}{L_{equivalent}}\right)_p = 100\text{kN/mm} \quad (3.22)$$

$$EA_p = \left(\frac{EA_p}{L_{equivalent}}\right)_p * L_{equivalent} = \frac{100\text{kN} * 1\text{m}}{10^{-3}\text{m}} = 10\text{E}4\text{kN} \quad (3.23)$$

where the $L_{spacing} = 5.4\text{m}$ and $L_{equivalent} = 1\text{m}$. Axial stiffness EA is presented in Table 3.3.

Table 3.3: Prototype scale values calculation with model scale values for prop parameters.

Physical quantity parameter	Scaling factor	Model value	Prototype value
Prop stiffness $\frac{EA}{L_{equivalent}}$	$1/n$	1.66kN/mm	100kN/mm
Axial stiffness EA	$1/n$	1660kN	$10\text{E}4\text{kN}$
Length of spacing $L_{spacing}$	n	90mm	5.4m
Length of equivalent $L_{equivalent}$	n	60mm	1m

3.2.4 System stiffness parameters

The system stiffness η can be expressed as presented in (Tran, 2020):

$$\eta = \frac{EI}{\gamma_w * h^4} \quad (3.24)$$

where EI is the bending stiffness per unit width of the retaining wall, γ_w (i.e. 9.81 kN/m^3) is the unit weight of water and h is the average support spacing. The average support spacing h_m in model scale is 36 mm , which gives a h_p of 2.16 m in prototype scale. The system stiffness of the prototype model is calculated to be:

$$\eta_p = \frac{EI_p}{\gamma_w * h_p^4} = \frac{280.8 \text{ E}3 \text{ kNm}^2 / \text{m}}{9.81 \text{ kN/m}^3 * (2.16 \text{ m})^4} = 1315 \quad (\neq 2860, \text{ see Table 3.4}) \quad (3.25)$$

which is not similar to system stiffness $\eta = 2860$ provided from Lam (2010) in Table 3.4. The system stiffness is not a direct input for a constitutive model in PLAXIS, and is therefore determined as a minor parameters and a negligible factor.

3.3 Soil model input

This section will determine additional input parameters that is not provided directly from centrifuge test by Lam (2010).

3.3.1 Input parameters for undrained condition

Clay have a very low permeability, and during rapid loading/unloading of saturated clay the pore water does not dissipate and no drainage occurs. This results in an undrained condition, despite effective properties. Note that clay in an undrained condition will perform different regarding strength and stiffness compared to a drained condition. A deep excavation is usually not a permanent construction, and is therefore often assumed short term and undrained condition for clay when evaluating the soil behaviour in an excavation. The following input parameters for the different soil models is therefore based on an undrained condition.

The unit weight γ_s for an undrained soft clay is determined as 16 kN/m^3 , as mentioned in previous section. Further, there is assumed no friction angle $\phi = 0^\circ$ and consequently no dilatancy angle $\psi = \phi - 30^\circ = 0^\circ$. The cohesion c is set to 0 kPa due to no attraction $a = 0 \text{ kPa}$ and friction angle $\phi = 0^\circ$. The undrained shear strength S_u is defined with 27 kPa , but no increase in undrained shear strength is assumed $S_{u,inc} = 0 \text{ kPa}$. The Poisson's ratio ν is set to 0.5 based on undrained condition. As for the interface strength factor, the roughness R_{inter} of clay, it is assumed 1, while 0.5 for interfaces between soil and structures. The earth pressure coefficient at rest K_0 is assumed anisotropic with vertically unloaded and consequently $K_0 > 1$.

3.3.2 Earth pressure coefficient

The centrifuge test provided by (Lam, 2010), installed earth pressure cells for capturing the soil performance under the excavation construction. By assuming fully mobilized shear strength $f = 1$, the earth pressure coefficient at rest K_0 can be determined. The maximum shear stress is limited by the soil strength, but more dominantly by the roughness of the wall. Further, the roughness ratio r can be described as for an undrained analysis:

$$r = \frac{\tau}{\tau_c} = \frac{\tau}{\frac{S_u}{F}}, \quad (3.26)$$

where $r = 0$ is assumed when no upward or downward forces are transferred from soil to wall (i.e. frictionless wall). The earth pressure coefficient κ is further calculated by:

$$w = \frac{1}{2} * \arcsin r = 0 \quad (3.27)$$

$$\kappa = 1 + 2w + \cos 2w = 2 \quad (3.28)$$

Earth pressure can be determined by certain assumptions (i.e. full mobilization $f = 1$ and $F = \frac{1}{f} = 1$):

$$P_{A/P} = p_v \mp \kappa_{A/P} * \frac{S_u}{F} = \gamma * z \mp \kappa_{A/P} * S_u \quad (3.29)$$

Active earth pressure, as illustrated in Figure 3.8, can be calculated:

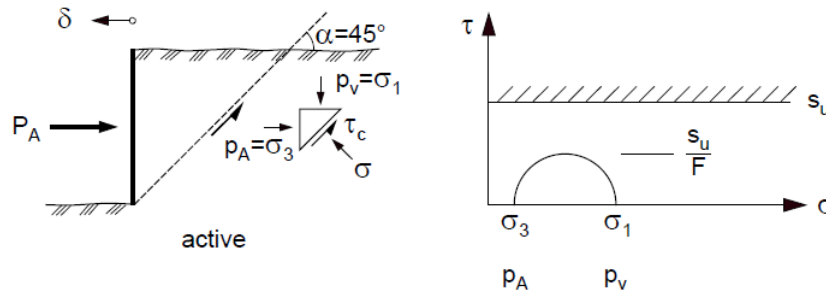


Figure 3.8: Active earth pressure for a total basis analysis, $r = 0$ (Emdal et al., 2019).

$$p_v = \gamma * z = 16 \text{ kN/m}^3 * 9.6 \text{ m} = 153.6 \text{ kPa} \quad (3.30)$$

$$P_A = p_v - \kappa_A * \frac{S_u}{F} = 153.6 \text{ kPa} - 2 * \frac{27 \text{ kPa}}{1} = 99.6 \text{ kPa} \quad (3.31)$$

Note that P_A is σ_3 and p_v is σ_1 . Consequently, earth pressure coefficient at rest K_0 can be determined as:

$$K_0 = \frac{\sigma_3}{\sigma_1} = \frac{99.6 \text{ kPa}}{153.6 \text{ kPa}} = 0.65, \quad (3.32)$$

which is the active earth pressure coefficient κ_A on the active side in a total basis analysis. For the passive side is illustrated in Figure 3.9, can be calculated as:

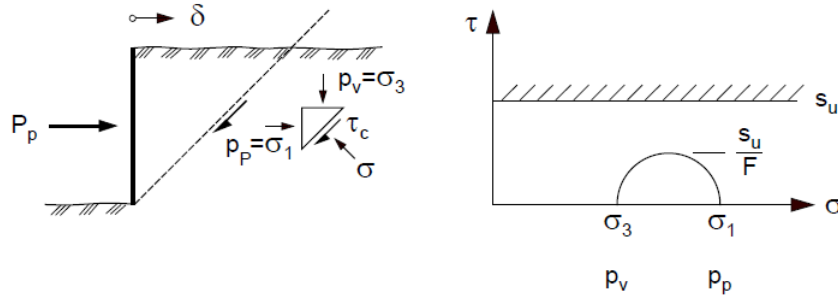


Figure 3.9: Passive earth pressure for a total basis analysis, $r = 0$ (Emdal et al., 2019).

$$p_v = \gamma * z = 16 \text{ kN/m}^3 * (9.6 - 5.4) \text{ m} = 67.2 \text{ kPa} \quad (3.33)$$

$$P_p = p_v + \kappa_p * \frac{S_u}{F} = 67.2 \text{ kPa} + 2 * \frac{27 \text{ kPa}}{1} = 121.2 \text{ kPa}, \quad (3.34)$$

where P_p is σ_1 and p_v is σ_3 .

$$K_0 = \frac{\sigma_1}{\sigma_3} = \frac{121.2 \text{ kPa}}{67.2 \text{ kPa}} = 1.804, \quad (3.35)$$

which is the passive earth pressure coefficient κ_p in a total basis analysis. The κ_A and κ_p value develops the lower and upper limit of the earth pressure coefficient at rest, K_0 . The K_0 will have a value between κ_A and κ_p , which is approximate 0.65 – 1.8. According to Lam (2010), the centrifuge sample was unloaded vertically under consolidation and was swelled back from 160 kPa to 26 kPa, it is then appropriate to suggest that $K_0 > 1$. K_0 will therefore be considered as an unknown parameter in this paper, but will be in the range between κ_A and κ_p and larger than 1.

3.4 Parameters from centrifuge test in prototype scale

For the numerical model, it is chosen to use prototype values for the input parameters in PLAXIS. Additionally, most output result carried out from Lam (2010) is presented in prototype values. Therefore, scaling laws were used to transform the obtained experimental results into prototype scale values. Additionally, a validation of input parameters have been conducted in this chapter.

A summary of parameters provided based on centrifuge test from Lam (2010) and by scaling law calculations. For further calculations, Table 3.4 will be the parameter properties for baseline Test 1 and be the main input parameters in numerical models. The identified unknown parameters that is not provided from Lam (2010) centrifuge

test, nor identified by scaling law or relevant research, will be further be determined under the term *unknown* parameters.

Table 3.4: Summary of parameters from centrifuge test in prototype scale.

Parameters	Description	Prototype value	Additional details
<i>Soil properties</i>			
G_s	Specific gravity	2.6	(Lam, 2010)
γ_s	Unit weight	16kPa	(Lam, 2010)
E	Young's modulus	**	(Lam, 2010) 1 – 50MPa
ν_u	Poisson's ratio	0.5	(Lam, 2010)
S_u	Undrained shear strength	27kPa	(Lam, 2010)
c'	Effective cohesion	0kPa	Undrained condition
ϕ	Angle of internal friction	0°	Undrained condition
ψ	Angle of dilatancy	0°	Undrained condition
G_o	Shear stiffness	22MPa	(Lam, 2010)
K_0	Earth pressure coefficient at rest	**	
<i>Retaining wall properties</i>			
EI	Flexural/bending stiffness	280.8E3kNm ² /m	Scaling law (Lam, 2010)
EA	Axial stiffness	2.60E7kN/m	Scaling law (Lam, 2010)
w	Specific weight pr. meter	9.53kN/m/m	Scaling law (Lam, 2010)
ν	Poisson's ratio	0.32	(Stojanovic et al., 2018)
<i>Prop system properties</i>			
$\frac{EA}{L_{equivalent}}$	Prop stiffness	100kN/mm	Scaling law (Lam, 2010)
EA	Axial stiffness	10E4kN	Scaling law (Lam, 2010)
$L_{spacing}$	Length of spacing	5.4m	Scaling law (Lam, 2010)
$L_{equivalent}$	Equivalent length of prop	1m	Scaling law (Lam, 2010)
<i>Bracing system properties</i>			
η	System stiffness	1315	Scaling law \neq 2860 (Lam, 2010)

* Note: Additional parameters in PLAXIS are not considered and default settings is used. *Unknown* parameters is marked with **.

Chapter 4

Numerical modelling for simulation of deep excavation in soft clay

This paper is carried out using plain strain finite element PLAXIS 2D and aims to describe three constitutive models from the numerical software. Firstly, the chapter will introduce the general theory of soil models and secondly describe relevant soil models and its input parameters. Further, the PLAXIS model will be presented.

4.1 Introduction

Constitutive models have been carried out in terms of their ability to describe the soil behavior. Constitutive relations represent mathematically models of soil behavior, for instance how stresses and strain will interact. These relations may be complex and requires refined constitutive models. A number of different constitutive models have been developed as an attempt for a sufficient representation of how soil acts. The most suitable model for a specific situation depends on estimating the value of a complex model and the value of finding the input parameters. Figure 4.1 shows a number of constitutive models that have been proposed earlier. The different models vary with the number of parameters and the possibility to describe a real soil behavior. On the other hand, some models are easier to adopt and analyse, but may provide a more simple description of the soil behavior.

The Finite Element Method (FEM or FE method) is a numerical method for approximations of different engineering problems and has become a common practice in order to analyse and optimize calculations of soil behaviour. It is able to illustrate a relative relation between stress-strain behaviour of soil. However, soil behaviour is complex and is based on a multi-phase material that exhibits in both elastic and non-linear plastic range. The deformations includes recoverable elastic strains defined by isotropic behaviour and irreversible plastic strains controlled by the yield criterion, the flow rule and the hardening rule (Kullingsjö, 2007). Soil behaves non-linearly and shows typically heterogeneous, anisotropic and time dependant behaviour when subjected to stresses. Generally, soil be-

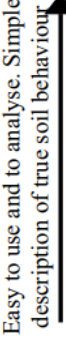
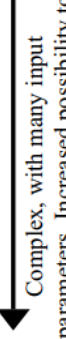
	Type of constitutive relation	Example of models
Easy to use and to analyse. Simple description of true soil behaviour 	Linear elastic	Hook's law
	Non-linear elastic	Duncan and Chang (1970)
	Elastic perfectly plastic, Hardening models	Drucker and Prager (1951) Druckers's Cap (Drucker <i>et al.</i> , 1957) <i>e-ADP</i> (Grimstad <i>et al.</i> , 2006)
	Bounding surface models	<i>MIT-E3</i> (Whittle, 1987) <i>MIT-S1</i> (Pestana, 1994)
	Multi surface models	Bubble model (Al-Tabbaa and Wood, 1989)
		 Complex, with many input parameters. Increased possibility to describe true soil behaviour

Figure 4.1: Different type of constitutive models with different application (Kullingsjö, 2007).

haves differently in primary loading, unloading and reloading (Huat *et al.*, 2009). Further, soil experiences small strain stiffness at very low strains and at stress reversal situations.

Although, the FEM gives a good estimate for the geotechnical calculations and solutions, the FEM is not an exact method. Note that this level of inaccuracy should not effect the computed results, but rather combine the proper result from the numerical methods with engineering knowledge. The different soil models implemented in PLAXIS have different levels of accuracy and are not always suitable for all types of soil materials. It is therefore important to have a good understanding of the different soil models. Furthermore, the theory behind some of the relevant soil models will be reviewed.

4.2 Soil models

Due to different soil behaviour and the challenge of capturing it, a number of complex soil models have been developed with associated parameters. A simple constitutive model is the linear or non-linear elastic soil models. The soil behaviour is described as elastic with one stiffness parameters. The model is associated with a lack of replicating the soil behaviour, and is recommended to not be adopted in practice.

A further developed model, the elastic-perfectly plastic model, such as the Mohr-Coulomb (MC) model, is based on the theory of perfect linear elasto-plastic (PLEP) or ideal elasto-plastic. It is a relatively simple model, and is considered as the most widely used model among geotechnical constitutive models. The models seems to be sufficient for some areas of geotechnical problems. However, a lack of representing the real soil behaviour have to be taken into account because of the stress path predicted is misleading and indicates an over-estimated soil strength in the case of soft clay (Surarak *et al.*, 2012).

An additional model, is an isotropic hardening single surface plasticity model. The isotropic hardening surface plasticity models, such as the Modified Cam clay (MCC) model, have one plastic yield surface, the so-called *cap*, which is controlled by the preconsolidation stress. The model is able to replicate a relatively real soil behaviour. The models is based on an elliptic yield surface which separates the elastic behaviour from the plastic behaviour (Surarak et al., 2012).

Further, an isotropic hardening double surface plasticity models, such as the Hardening Soil (HS), have two plastic yield surface, a *cap* and a so-called *cone*, which is a hyperbola used to describe how elastic and plastic strains increase gradually. The hyperbola will gradually expand when loading toward failure and gives plastic strains controlled by the increase in mobilized friction (Nordal, 2020). The model gives a more realistic displacement patterns for the working load conditions, especially in an excavation in soft clay. The predicted movement patterns induced by excavation are realistic and have no influence on the finite element boundary conditions (Surarak et al., 2012).. The Hardening Soil Small (HSS) model is an optimized model of the HS model, but takes account for the small strain behaviour.

For replicating of the centrifuge tests, three constitutive models is taken into account: Mohr-Coulomb (MC), Hardening Soil (HS) and Hardening Soil Small (HSS). For the following chapter, an evaluation of the soil models will be presented. These particular soil models have been chosen to be carried out in this thesis because of its characteristics, performance, function and ability to predict ground movement and wall deflection in a deep excavation in soft clay. The input parameters for each model vary, and will be presented in the following sections.

Note that the NGI-ADP soil model is not considered in this research. NGI-ADP is an elasto-plastic constitutive model which is based on the undrained shear strength approach with direct input from shear strengths (Grimstad et al., 2011). Although, the NGI-ADP soil model can realistically simulate the anisotropic undrained stress strain responses and undrained shear strengths of clay, and is suited for estimation of soil behaviour in an deep excavation in soft clay (Ukritchon and Boonyatee, 2015), the aspire in this research is to investigate other possibilities in additional soil models, such as the MC, HS and HSS model.

4.2.1 Mohr-Coulomb, *MC*

Mohr-Coulomb model, the classic Linear Elastic Perfectly Plastic model, is a simple elastic-perfectly plastic model which is generally used to model soil behaviour and is considered as a first-order model (Huat et al., 2009). The model describes a linearly stress-strain behaviour in the elastic range by taking to account Hooke's law with Young's modulus E and Poisson's ratio ν and is considered to be the most prominent failure criterion model for calculating soil strength. The failure criteria is defined by the friction angle ϕ and cohesion c , and the flow rule is defined by dilatancy angle ψ , as presented in Table 4.1. The yield surface is a function described with friction angle ϕ' and

attraction a . While the dilatancy angle ψ' describes the potential function, which means for an associated flow rule, ψ' is equal to ϕ' (Kullingsjö, 2007).

Mohr-Coulomb model represents the yield criterion with failure surface cone. For linear elasto perfectly plastic model (PLEP), there are no hardening parameters and the yield surface correspond to failure surface. Since no hardening parameters are defined, such as mobilized friction, no plastic strains occur within the stress state reaches failure. If an hardening parameter is defined and the yield cone is within the failure cone, plastic behaviour will occur without reaching failure (Kullingsjö, 2007).

In reality, soils behave non-linearly when expose to changes of stress or strain. The stiffness of soil depends on the stress and strain level, and the stress path. However, simpler advanced models, such as Mohr-Coulomb, is used as a first approximation of soil behaviour.

Table 4.1: Mohr-Coulomb model input parameters in PLAXIS (Sloot, 2020b).

Parameters	Description
<i>Basic parameters for soil stiffness</i>	
E	Young's modulus
ν	Poisson's ratio
K_0	Earth pressure coefficient at rest
<i>Failure and strength parameters</i>	
ϕ	(Effective) angle of internal friction
ψ	Angle of dilatancy
c'	(Effective) cohesion
S_u^{ref}	Undrained shear strength

Note: Additional parameters in PLAXIS is not considered and default settings is used.

4.2.2 Hardening Soil, HS

The Hardening Soil model, also called the isotropic hardening model, is an advanced model for simulating the behaviour of different types of soil, both soft and stiff soils (Sloot, 2020b). Unlike Mohr Coulomb, the yield surface of a hardening plasticity model is not fixed in principal stress space, but rather expands due to plastic straining. The HS model is based firstly on the theory of plastic rather than elastic, it includes soil dilatancy and introduce the yield cap. The HS model characteristics are:

- Plastic straining due to primary deviatoric loading: E_{50}^{ref}
- Plastic straining due to primary compression: E_{oed}^{ref}

- Elastic unloading-reloading: E_{ur}^{ref} , ν_{ur}
- Stress dependent stiffness according to a power law: m
- Failure according to the Mohr-Coulomb failure criterion: c , ϕ and ψ

A basic characterisation of the Hardening soil model is the stress dependency of soil stress. The stress-strain behaviour for primary loading is non-linear, and E_{50} is the corresponding stress independent stiffness modulus:

$$E_{50} = E_{50}^{ref} \left(\frac{c' \cos \phi' - \sigma'_3 \sin \phi'}{c' \cos \phi' + p^{ref} \sin \phi'} \right)^m, \quad (4.1)$$

where E_{50}^{ref} is a reference stiffness modulus corresponding to the reference stress p^{ref} , which is set as default value 100 kN/m^2 in PLAXIS. The minor effective principal stress σ'_3 defines the actual stiffness, and power m defines the amount of stress dependency, which is $0.9 - 1$ for soft clay (Surarak et al., 2012). The function of reference oedometer modulus E_{oed}^{ref} is to control the magnitude of the plastic strain that emerges from the yield cap.

$$E_{oed} = E_{oed}^{ref} \left(\frac{c' \cos \phi' - \sigma'_1 \sin \phi'}{c' \cos \phi' + p^{ref} \sin \phi'} \right)^m, \quad (4.2)$$

$E_{oed}^{ref} \approx E_{50}^{ref}$, and is therefore usually assumed as $E_{oed}^{ref} = E_{50}^{ref}$ (Phien-Wej et al., 2012). The stress dependent stiffness modulus for unloading and reloading stress paths is illustrated in Figure 4.2 and is calculated by:

$$E_{ur} = E_{ur}^{ref} \left(\frac{c' \cos \phi' - \sigma'_3 \sin \phi'}{c' \cos \phi' + p^{ref} \sin \phi'} \right)^m, \quad (4.3)$$

where E_{ur}^{ref} is the reference modulus for unloading and reloading, which corresponds to the reference pressure p^{ref} . For various soil type it is usually assumed $E_{50}^{ref} \approx 3E_{ur}^{ref}$, but vary from three to five times the E_{ur}^{ref} for soft clay (Brinkgreve et al., 2017).

The HS model takes account for both the stiffness from primary loading and stiffness from unloading-reloading. The model is also based on a combined failure mechanism that takes account for the hardening in both shear and compression. This makes the model capable of modelling irreversible, plasticity shear due to deviatoric stress in primary loading and irreversible plasticity shear due to compression in oedometer or isotropic loading. The failure mechanism in HS is illustrated in Figure 4.2 with a *cone* and a *cap*, where the MC criterion defines the limited failure mechanism with the shear hardening as the cone. The cap is defined by pre-consolidated p'_c , with the failure mechanism from compression hardening.

A significant characterisation of the HS is that the stiffness is stress dependent, which means that the stiffness increase with increased stress. This means that the HS do not assume a constant stiffness in the soil, but gives a

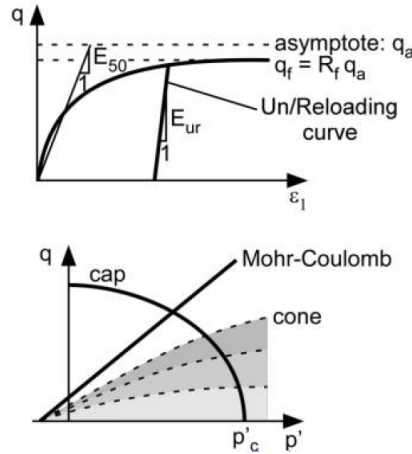


Figure 4.2: Hardening soil model with hyperbolic stress-strain relation in primary loading (Locat et al., 2013).

more realistic representation of the soil behaviour and mechanism. In PLAXIS, the model is designed with 3 stiffness parameters. The first one is E_{50}^{ref} which is the stiffness at 50% of maximum shear strength with a reference $p_{ref} = 100 kPa$, in a drained triaxial test. The second stiffness relates to the elastic stiffness when unloading-reloading E_{ur}^{ref} . Both parameters gives a non-linear stiffness modulus which depends on the stress. The third stiffness parameter, is the oedometer stiffness for one-dimensional compression E_{oed}^{ref} (Surarak et al., 2012).

According to (Sloot, 2020b), when an undrained behaviour is considered in the Hardening Soil model, it is recommended to use Undrained (A) as Drainage type. Another alternative is Undrained (B) if the effective strength properties and undrained shear strength is unidentified by Undrained (A). By using Undrained (B) the material loses its stress-dependency of stiffness. While Undrained (C) is inaccessible for an undrained condition, since the model is essentially formulated as an effective stress model.

4.2.3 Hardening Soil Small, HSS

Hardening Soil Small (HSS) model is an advanced model for simulating the soil behaviour, and is based on the Hardening Soil (HS) model including small strain specifications (Sloot, 2020b). It offers same application as the HS model, but includes calculations for the very small-strain soil stiffness, the additional characteristics of $\gamma_{0.7}$ and G_0^{ref} . The model in PLAXIS have additionally two parameters to describe the variation of stiffness with strain:

- The initial or very small-strain shear modulus: G_0^{ref}
- The shear strain level (i.e. secant shear modulus G_s have a 70% reduction of G_0): $\gamma_{0.7}$

The Hardening Soil Small model assumes elastic material behaviour during an unloading and reloading condition. The elastic range of soils is when the soil recover and is reversible from applied straining. However, this strain range where the soil is considered elastic, is very small. Figure 4.3 illustrates the typical stiffness-strain behaviour where an increase in the strain amplitude, decrease the soil stiffness non-linearly. Plotting the soil stiffness, i.e.

Table 4.2: Hardening soil model input parameters (Surarak et al., 2012).

Parameters	Description
<i>Failure parameters from Mohr-Coulomb</i>	
S_u	Undrained shear strength
ϕ	(Effective) angle of internal friction
ψ	Angle of dilatancy
c'	Cohesion
<i>Basic parameters for soil stiffness</i>	
E_{50}^{ref}	Secant stiffness in standard drained triaxial test
E_{oed}^{ref}	Tangent stiffness for primary oedometer loading
E_{ur}^{ref}	Unloading / reloading stiffness (default $E_{ur}^{ref} = 3E_{50}^{ref}$)
m	Power for stress-level dependency of stiffness
K_0	Earth pressure coefficient at rest
<i>Advanced parameters (advised to use the default setting (Sloot, 2020b)).</i>	
ν_{ur}	Poisson's ratio for unloading-reloading (default $\nu_{ur} = 0.2$)
p^{ref}	Reference stress for stiffness (default $p^{ref} = 100 \text{ kN/m}^2$)
K_0^{nc}	K0-value for normal consolidation (default $K_0^{nc} = 1 - \sin \phi$)
R_f	Failure ratio q_f/q_a (default $R_f = 0.9$)

Note: Additional parameters in PLAXIS is not considered and default settings is used.

shear modulus G/G_0 , against the shear strain γ_s in log, provides a characteristic S-shaped stiffness reduction curve (Sloot, 2020b).

The typical shear strain adjacent to geotechnical structures can be measured and the applicable strain ranges of laboratory tests can be captured. The results concludes that the minimum strain which can be reliably measured in classical laboratory tests, such as triaxial and oedometer tests, shows that the soil stiffness is generally decreased to less than half its initial value. Figure 4.3 shows that very small-strain soil stiffness and its non-linear dependency on the strain amplitude, plays a crucial role and should be taken to account when performing geotechnical analysis. The shear modulus can be determined as:

$$G_0 = G_0^{ref} \left(\frac{c' \cos \phi' - \sigma'_3 \sin \phi'}{c' \cos \phi' + p^{ref} \sin \phi'} \right)^m \quad (4.4)$$

G_0^{ref} is obtained by determined the E_0/E_{ur} ratio by assuming $E_{ur} = 3E_{50}$, where E_0 is the small strain Young's modulus (Zhang et al., 2015). This is subsequently expressed by:

$$G_0^{ref} = \frac{E_0^{ref}}{2(1 + \nu_{ur})}, \quad (4.5)$$

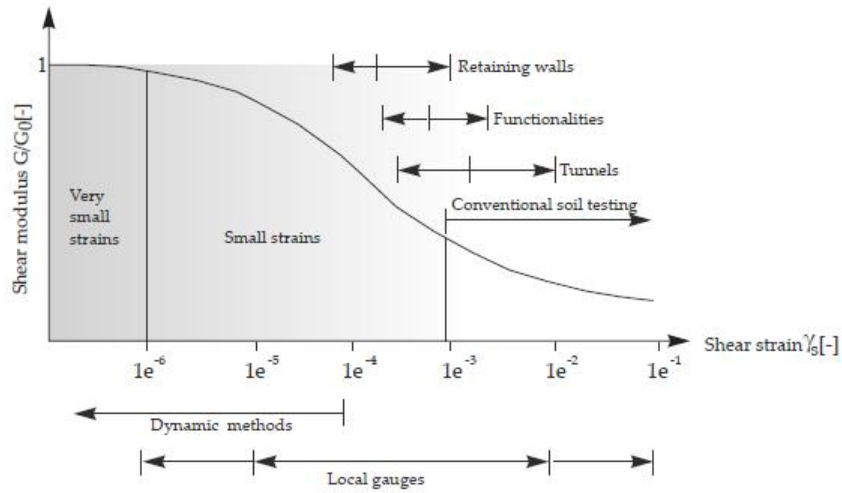


Figure 4.3: Characteristic shear strain-shear modulus performance of soil with typical strain ranges. Describes the typical stiffness-strain behaviour (Sloot, 2020b).

where ν_{ur} is set as default of 0.2. The $\gamma_{0.7}$ varies from 0.0001 – 0.0004 (Zhang et al., 2015), but is generally assumed as 0.0002 (Zhao et al., 2015).

4.3 Model validation

4.3.1 Selection of stiffness parameters

Undrained average stiffness or shear modulus G_{50}^u is usually defined from stress strain curve from an undrained triaxial test. The shear modulus is defined as seen in Figure 4.4, by the linear approximation of the shear stress and shear strain curve with the 50% failure capacity. The maximum shear strain is $\gamma = \frac{3}{2}\epsilon_y$ as shown in Figure 4.4 be-

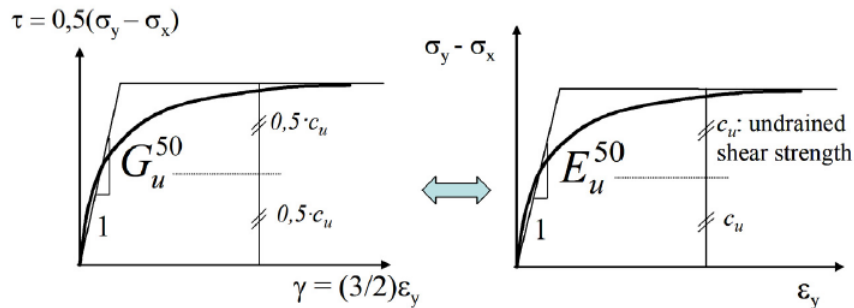


Figure 4.4: Undrained shear modulus and undrained stiffness from an undrained triaxial test (Nordal, 2020).

cause the volume change is equal to 0. Further, the undrained stiffness E_u^{50} is equal to $3G_u^{50}$, if $E_u^{50} = \frac{\delta\sigma_y}{\delta\epsilon_y}$. Undrained

Table 4.3: Hardening Soil Small model input parameters in PLAXIS (Surarak et al., 2012).

Parameters	Description
<i>Failure parameters from Mohr-Coulomb</i>	
S_u	Undrained shear strength
ϕ	(Effective) angle of internal friction
ψ	Angle of dilatancy
c	Cohesion
<i>Basic parameters for soil stiffness</i>	
E_{50}^{ref}	Secant stiffness in standard drained triaxial test
E_{oed}^{ref}	Tangent stiffness for primary oedometer loading
E_{ur}^{ref}	Unloading / reloading stiffness (default $E_{ur}^{ref} = 3E_{50}^{ref}$)
m	Power for stress-level dependency of stiffness
K_0	Earth pressure coefficient at rest
<i>Advanced parameters (advised to use the default setting (Sloot, 2020b)).</i>	
ν_{ur}	Poisson's ratio for unloading-reloading (default $\nu_{ur} = 0.2$)
p^{ref}	Reference stress for stiffness (default $p^{ref} = 100kN/m^2$)
K_0^{nc}	K0-value for normal consolidation (default $K_0^{nc} = 1 - \sin \phi$)
R_f	Failure ratio q_f/q_a (default $R_f = 0.9$)
<i>Small strain</i>	
$\nu_{0.7}$	Poisson's ratio for unloading-reloading
G_0^{ref}	Reference shear modulus at very small strains ($\epsilon < 10^{-6}$)
$\gamma_{0.7}$	Threshold shear strain at which $G_s = 0.722G_0$

Note: Additional parameters in PLAXIS is not considered and default settings is used.

stiffness relates to the undrained shear strength c_u or S_u , and is therefore necessary to determine the undrained stiffness. The difference in stiffness is related to no volume change during undrained conditions while large plastic volumetric changes may occur during drained conditions (Nordal, 2020). Simple models, such as MC model, is dominated by elasticity and can not consequently calculate just ad the constrain of no volume change.

By assuming a Poisson's ratio $\nu = 0.5$ in incompressibility, a relation of soil skeleton shear stiffness is equal to the undrained stiffness is described since the elasticity in the shear stiffness is not affected by volumetric stiffness. However, in practice for soft clay condition, drained stiffness parameters are not able to model the undrained behaviour in simple models by simply specifying undrained conditions in order to prevent volumetric deformations. The model will require an undrained stiffness parameter directly. This is preferably as shear modulus by either add the undrained zero volumetric strain requirement by $\nu = 0.5$ in a total stress analysis or a low ν in an effective stress analysis.

4.3.2 Undrained condition in soil models

For the linear elastic model Mohr-Coulomb in an undrained condition, the changes in the pore water pressure will be given directly of the changes in the total stresses for the undrained condition. This means that changes in the total stresses do not change the effective stresses in the soil, but only a certain increase in pore water pressure. This means that the shear strength in undrained condition is constant and independent from the stresses. Therefore, the failure mechanism/criterion is defined when the maximum shear stress at failure is the undrained shear strength S_u . Clay have a non-linear behaviour and will in reality not have a vertical stress path, but rather bend against the MC failure line, as illustrated in Figure 4.5. Note that the HS and HSS model is able to provide a more realistic soil behaviour and stress path than MC model, and will be represent a stress path between (1) MC model and reality (2) (Teo and Wong, 2012), as illustrated in Figure 4.5.

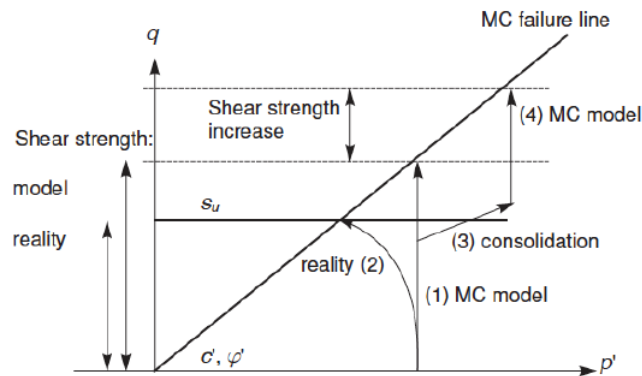


Figure 4.5: Stress path for undrained condition with Mohr-Coulomb model (Brinkgreve et al., 2017).

4.3.3 Summary

The purpose of this chapter is to summarize relevant constitutive models that is capable of simulating the soil behaviour in a deep excavation in soft clay. Likewise, an identification of the different input parameters in every soil models will clarify the differences and its variety of unknown parameters. Consequently, the most qualified and proficient models will be evaluated for their performance when estimating the ground surface displacement.

Soil behaviour and ground displacement adjacent to excavations should preferably be simulated using an advanced soil model. However, if proper parameters are selected a rough preliminary simulation, by using a simple MC model for instance, could give interesting information. Despite other constitutive models ability to produce accurate numerical results, such as the HS and HSS, the result based on a specific problem, such as a multi-propped deep excavation in soft clay, will not necessary exhibit the same accuracy level. In numerical modelling, it is significant to select a suitable model to the considered problem.

Typical challenges for geotechnical engineers is to choose the most appropriate soil model applicable in their numerical modeling. Consequently, an understanding on the concepts, advantageous and limitations is therefore important. It is significant to conduct various constitutive model comparisons along with additional full-scale centrifuge experiments to determine the degree of realism in the models, in order to adjust and refine model application.

In order to adjust constitutive models for predictions of ground settlement due to deep excavations in soft clay, relevant constitutive models is presented. Hence, the most reliable and capable models for predicting ground displacement and wall deflection is based on their ability to capture soil behaviour. The models is based on undrained conditions, short term in order to imitate soft clay. However, the models is based on different assumptions and different limitations and boundaries, which will affect the outcome of ground displacement. The aim is to use a constitutive model that allows to capture the soil behaviour affected by a deep excavation.

4.4 PLAXIS model

An idealized excavation in prototype model from the centrifuge test is presented in PLAXIS. A numerical model is modelled for MC, HS and HSS as *material model* with same soil model criteria, as illustrated in Figure 4.6. The soil

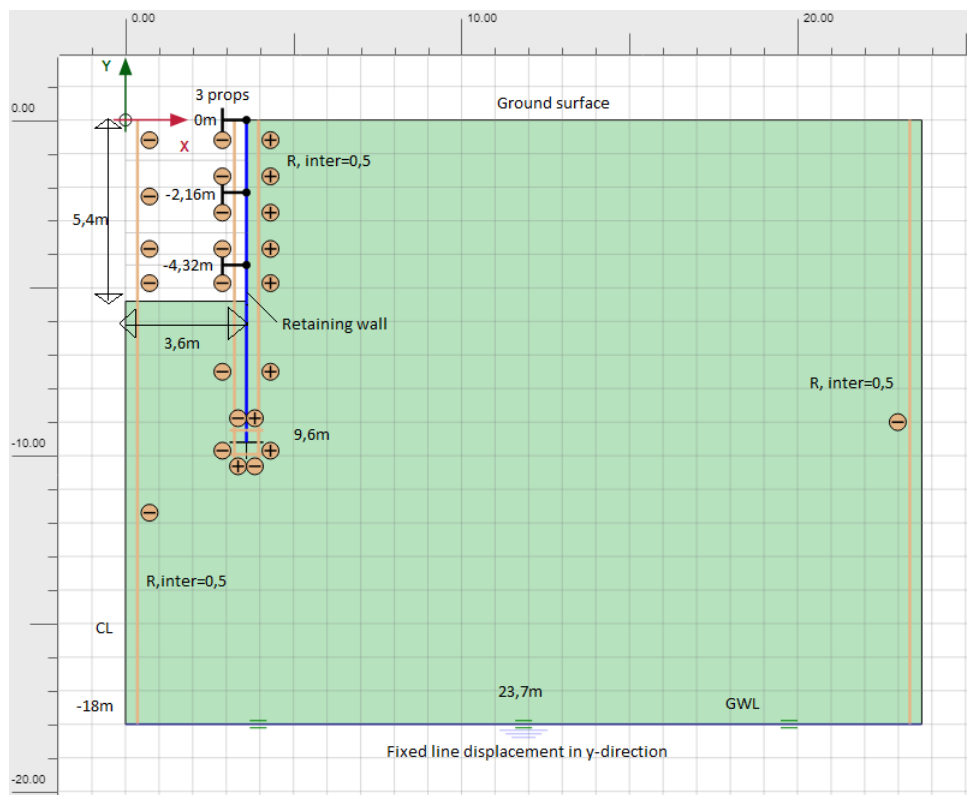


Figure 4.6: PLAXIS 2D - Soil model

model in PLAXIS is constructed in plain strain coordinate system with $x_{min} = 0m$, $x_{max} = 23.7m$, $y_{min} = -18m$ and $y_{max} = 0m$ with a $18m$ layer of soft clay in an excavation depth of $5.4m$. The line displacement in the bottom is defined as fixed in y-direction and free in x-direction. Additionally, fully fixed is determined for x_{min} , x_{max} and y_{min} -boundary deformations in *model condition*. y_{max} is set as free in order to replicate a similar experiment setup as the centrifuge test with a free surface.

The $9.6m$ long retaining wall is defined as an elastic beam element with interface elements on both side with $R_{inter} = 0.5$. The interface is extended below the wall tip in vertical and horizontal direction for numerical reasons, such as movement at failure. Additionally, the vertical boundaries is determined with $R_{inter} = 0.5$ in order to replicate the roughness from the model box in the centrifuge test. The internal bracing consists of props across the excavation and is placed with a centre to centre distance of a $5.4m$ normal to the paper plane (i.e. $L_{spacing}$). The length of the prop to the center line (CL) is $3.6m$ (i.e. $L_{equivalent}$). The construction stages is described in Table 4.4.

Table 4.4: Construction stages for Test 1 (SYL04) in PLAXIS model.

Phase procedure	Phase description
Initial phase	Initial phase
Phase 1	Dummy phase
Phase 2	Installation of retaining wall to depth $-9.6m$
Phase 3	Excavation to depth $-1.2m$
Phase 4	Installation of first prop at depth $0.0m$
Phase 5	Excavation to depth $-3.36m$
Phase 6	Installation of second prop at depth $-2.16m$
Phase 7	Excavation to depth $-4.32m$
Phase 8	Excavation to depth $-5.4m$
Phase 9	Installation of third prop at depth $-4.32m$

In order to calculate and evaluate the ground displacement in a deep excavation in soft clay, a calibrated model is required to be determined. The calibrated model is defined by investigating its reliability and performance when calculating the soil response. Further, a summary of input parameters in PLAXIS for the different soil models is presented in Table 4.5 for MC model, Table 4.6 for HS model and Table 4.7 for HSS model. The tables include parameters presented by centrifuge test from Lam (2010), default settings from PLAXIS, assumptions values based on related theory and knowledge and previous presented calculations. Unknown parameters, i.e marked with ***Unknown*, is identified and will be evaluated in the next chapter.

4.4.1 Input parameters - Mohr-Coulomb model

For the Mohr-Coulomb model, a drainage type *Undrained (C)* is chosen, because of the undrained or short-term material behaviour in which stiffness and strength are defined in terms of undrained properties. Excess pore pressures are not explicitly calculated, but are included in the effective stresses. Further, Table 4.5 summarizes the

important parameters provided from centrifuge test (Lam, 2010), assumed parameters based on earlier studies and research, default parameters based on model specifications and unknown parameters. The earth pressure coefficient at rest K_0 and Young's modulus E_u is identified as the unknown parameters for the MC model.

Table 4.5: Input parameters for Mohr-Coulomb Soil model in PLAXIS.

Parameters	Description	PLAXIS input value	Additional details
Undrained	Drainage type	Undrained (C)	Stiffness and strength are defined in terms of undrained properties
$\gamma_{sat} = \gamma_{unsat}$	Unit weight	$16kN/m^3$	From (Lam, 2010) Centrifuge test
E_u	Young's modulus	**	(1 – 50)MPa (Lam, 2010)
ν_u	Poisson ratio	0.5	From (Lam, 2010) Centrifuge test
S_u^{ref}	Undrained shear strength	$27kPa$	From (Lam, 2010) Centrifuge test
ϕ_u	Friction angle	0°	Default. Undrained condition
ψ	Dilatancy angle	0°	Default. Undrained condition
$S_{u,inc}$	Increased undrained shear strength	$0kPa$	From (Lam, 2010) Centrifuge test
$R_{inter,soil}$	Interface strength factor (roughness)	1 (Rigid)	Default
$R_{inter,wall}$	Interface strength factor (roughness)	0.5 (Manual)	(Fartaria, 2012)
K_0	Earth pressure coefficient at rest	**	Anisotropy, $K_0 > 1, 0.65 > K_0 > 1.8$

Note: Additional parameters in PLAXIS follows default settings. **Unknown input parameters.

4.4.2 Input parameters - Hardening Soil model

For the Hardening Soil model, *Undrained (B)* is chosen as drainage type because of the undrained or short-term material behaviour in which stiffness is defined in terms of effective properties and strength is defined as undrained shear strength. The unknown parameters identified for the HS model is the soil stiffness parameters E_{50}^{ref} , E_{oed}^{ref} and E_{ur}^{ref} , and the earth pressure coefficient at rest K_0 , as presented in Table 4.6.

4.4.3 Input parameters - Hardening Soil Small model

The Hardening Soil Small model follows the Hardening Soil with providing same drainage type with the ability based on undrained or short-term material behaviour in which stiffness is defined in terms of effective properties and strength is defined as undrained shear strength. The model is in this thesis conducted with *Undrained (B)* as drainage type. The identified unknown parameters for the HSS model is presented in Table 4.7, and includes the soil stiffness parameters E_{50}^{ref} , E_{oed}^{ref} and E_{ur}^{ref} , the earth pressure coefficient at rest K_0 and the threshold shear strain $\gamma_{0.7}$.

Table 4.6: Input parameters for Hardening Soil model in PLAXIS.

Parameters	Description	PLAXIS input value	Additional details
Undrained	Drainage type	Undrained (B)	Stiffness are defined in terms of effective stresses and strength are defined in terms of undrained shear strength
$\gamma_{sat} = \gamma_{unsat}$	Unit weight	$16kN/m^3$	From (Lam, 2010) Centrifuge test
E_{50}^{ref}	Secant stiffness in standard drained triaxial test	**	
E_{oed}^{ref}	Tangent stiffness for primary oedometer loading	**	$E_{oed}^{ref} \approx E_{50}^{ref}$
E_{ur}^{ref}	Unloading/reloading stiffness	**	$E_{ur}^{ref} \approx 3E_{50}^{ref}$
m	Power for stress-level dependency of stiffness	1.0	Soft clay (Sloot, 2020b).
S_u^{ref}	Undrained shear strength	$27kPa$	From (Lam, 2010) Centrifuge test
ϕ_u	Friction angle	0°	Default. Undrained condition
c	Cohesion	$0kPa$	Default. Undrained condition
ψ	Dilatancy angle	0°	Default. Undrained condition
$S_{u,inc}$	Increased undrained shear strength	$0kPa$	From (Lam, 2010) Centrifuge test
$R_{inter,soil}$	Interface strength factor (roughness)	1 (Rigid)	Default
$R_{inter,wall}$	Interface strength factor (roughness)	0.5 (Manual)	Assumed, (Fartaria, 2012)
R_f	Failure ratio, (q_f/q_a)	0.9	Default
K_0	Earth pressure coefficient at rest	**	Anisotropy, $K_0 > 1, 0.65 > K_0 > 1.8$

Note: Additional parameters in PLAXIS follows default settings. **Unknown input parameters.

4.4.4 Summary

Related constitutive models have been chosen and presented for their ability to capture and estimate the soil behaviour in a deep excavation. The aim is to provide a calibrated model that is able to calculate similar and realistic soil behaviour. As presented, a number of *unknown* parameters have been identified for the different soil models. The next chapter deals with a sensitivity analysis in order to examine the influence of the unknown parameters and the outcome of ground displacement when varying these parameters.

Table 4.7: Input parameters for Hardening Soil Small model in PLAXIS.

Parameters	Description	PLAXIS input value	Additional details
Undrained	Drainage type	Undrained (B)	Stiffness are defined in terms of effective stresses and strength are defined in terms of undrained shear strength
$\gamma_{sat} = \gamma_{unsat}$	Unit weight	$16kN/m^3$	From (Lam, 2010) Centrifuge test
E_{50}^{ref}	Secant stiffness in standard drained triaxial test	**	
E_{oed}^{ref}	Tangent stiffness for primary oedometer loading	**	$E_{oed}^{ref} \approx E_{50}^{ref}$
E_{ur}^{ref}	Unloading/reloading stiffness	**	$E_{ur}^{ref} \approx 3E_{50}^{ref}$
m	Power for stress-level dependency of stiffness	1.0	Soft clay (Sloot, 2020b).
S_u^{ref}	Undrained shear strength	$27kPa$	From (Lam, 2010) Centrifuge test
ϕ_u	Friction angle	0°	Default. Undrained condition
c	Cohesion	$0kPa$	Default. Undrained condition
ψ	Dilatancy angle	0°	Default. Undrained condition
$S_{u,inc}$	Increased undrained shear strength	$0kPa$	From (Lam, 2010) Centrifuge test
$R_{inter,soil}$	Interface strength factor (roughness)	1 (Rigid)	Default
$R_{inter,wall}$	Interface strength factor (roughness)	0.5 (Manual)	Assumed, (Fartaria, 2012)
R_f	Failure ratio, (q_f/q_a)	0.9	Default
K_0	Earth pressure coefficient at rest	**	Anisotropy, $K_0 > 1, 0.65 > K_0 > 1.8$
$\nu_{0.7}$	Poisson's ratio for unloading-reloading	0.2	Default
$\gamma_{0.7}$	Threshold shear strain ($G_s = 0.722G_0$)	**	(Zhang et al., 2015)
G_0^{ref}	Reference shear modulus at very small strains	$22MPa$	From (Lam, 2010) Centrifuge test

Note: Additional parameters in PLAXIS follows default settings. **Unknown input parameters.

Chapter 5

Effect of input parameters in soft clay

This chapter aims to develop a calibrated model by examine the effect of input parameters in a deep excavation in soft clay. The first part contains of a sensitivity analysis of the unknown parameters identified in Chapter 4, in order to examine their influence on the ground displacement. The second part is to gain a better understanding of the soil behaviour when validating the calibrated model. By examining the impact of crucial soil parameters from numerical outputs (e.g. ground displacement, stress-strain characteristics, earth pressure etc.), a better understanding of the influence of each parameter is established.

5.1 Introduction

Uncertainty and sensitivity analysis as part of the modeling process, contributes to a more well-evaluated and comprehensive analysis. This chapter focuses on a sensitivity analysis (SA), which is the computation of the effect of changes in input parameters or assumptions. Uncertainties can be categorized as:

- Input uncertainties: Variability, measurement, sampling and systematic errors.
- Parameter uncertainties: the data used to calibrate parameter values.
- Model uncertainties: simplification of real-world processes, miss-specification of the model structure, aggregation errors, application/scenario.

Sensitivity analysis is an essential step in the model-building process for a calibrated model. A SA method identifies which parameters have a significant impact on the simulation and are critical for reducing the number of parameters required in the model validation (Wesseling et al., 2020).

Sensitivity analysis and parameter identification techniques are utilized to calibrate and validate the model based on field and laboratory measurement. The mechanical behaviour of soil can be modeled in an advanced soil model

with different parameters. A sensitivity analysis evaluates the relative sensitivity of model response to each input parameter. For a complicated non-linear problem, the numerical simulation is a computationally expensive FE-model. In order to have an efficient calibrated model as well as robust, it is favorable to reduce the number of considered parameters when performing a SA (Zhao et al., 2015). The SA explores the input parameters contribution, relation and its independence compared to other unidentified parameters, and evaluates the performance.

Sensitivity analyses study the effects of the input parameters will have on the output values. In this thesis, numerical models are studied in order to better understanding the characteristics of ground displacements next to deep excavations. Note that since a model is a simplified version of real soil behaviour, it is bound to contain certain sources of uncertainty that result in a discrepancy between the output obtained from that model and the measurements obtained from the centrifuge test.

5.2 Sensitivity analysis of parameters

In the following section, a sensitivity analysis of unknown parameters will be presented. This is crucial, since perhaps the biggest challenge to PLAXIS users is the choice of input parameters. This parametric study will execute a sensitivity analysis manually in Excel by examine the outputs from PLAXIS, and will be referred to as SA or manual sensitivity analysis (MSA). For each soil model, a set of different scenarios is presented, where the unknown parameters varies in a defined range. Note that these unknown parameters is identified parameters from the previous Chapter 4. The unknown parameters have been manipulated in order to match the ground displacement and wall deflection. An interpret of the influence by the unknown parameters will be presented. Test 1 from Lam (2010) presented the lateral wall deflection δ_w (i.e. horizontal movement of retaining wall) and vertical ground displacement S_v (i.e. vertical ground movement behind retaining wall), as seen in Figure 3.7. Additionally, these values and the maximum vertical ground displacement adjacent to the retaining wall $S_{v,max}$, will be used as reference result when evaluating the SA result.

5.2.1 Sensitivity analysis - Mohr-Coulomb model

Based on the principle of the MC model, described in Section 4.2.1, a SA will be carried out from PLAXIS result based on a manual sensitivity analysis for this constitutive model. It is expected an elastic domination in the soil behaviour for the simple MC model, and a larger failure criterion as mentioned in Chapter 4. However, a rough preliminary prediction provides an interesting indication. Therefore, an estimation of the MC model is taken to account. The SA is applied with the unknown input parameters from Table 5.1, and is manually conducted in Excel. The SA procedure is simplified and summarized in Table 5.2.

The first set of analyses examined the impact of the Young's modulus E_u with $1MPa$ and the earth pressure coeffi-

Table 5.1: Unknown input parameters for sensitivity analysis of Mohr-Coulomb Soil model in PLAXIS.

Parameters	Description	Value range	Additional details
E_u	Young's modulus	1MPa – 50MPa	(Lam, 2010)
K_0	Earth pressure coefficient at rest	0.65 – 1.8	$K_0 > 1, 0.65 < K_0 < 1.8$

* Note: Additional parameters in PLAXIS follows default settings.

Table 5.2: Sensitivity analysis for Mohr-Coulomb model.

Parameter	Description	Range	Sensitivity analysis ID						
			MC01	MC02	MC03	MC04	MC05	MC06	MC07
E_u	Young's modulus	1 – 50MPa	1	50	2.5	5	5	5	5
K_0	Earth pressure coefficient	0.65 – 1.8	1.0	1.0	1.0	1.0	0.65	1.8	1.1
Results from centrifuge Test 1 [mm]			Results from PLAXIS in [mm]						
Max. lateral wall deflection, $\delta_{w,max} = 33.3$			152.4	5.8	70.1	36.3	32.3	132.8	52.2
Max. vertical ground displacement, $S_{v,max} = 34.4$			43.7	3.3	37.1	20.5	20.3	66.8	26.6
Max. vertical displacement adjacent to wall, $S_{v,max} = 19.5$			36.9	1.9	15.6	9.3	13.6	16.9	10.3

Notations: The result is from PLAXIS and based on the last construction stage: Installation of prop 3.

cient at rest K_0 to be isotropic with a value of 1.0. Table 5.2 indicates that the stiffness parameter E_u has a significant influence on the soil behaviour, and values between 2.5MPa and 5MPa gives similar magnitude of displacement and settlements as the centrifuge test. This can be seen with the MC03 and MC04, as illustrated in Figure 5.1 and Figure 5.2. However, a value of 2.5MPa indicates similar ground settlement S_v , while much higher lateral wall deflection. For a E_u value of 5MPa, a similar trend of lateral wall deflection δ_w , while much lower ground settle-

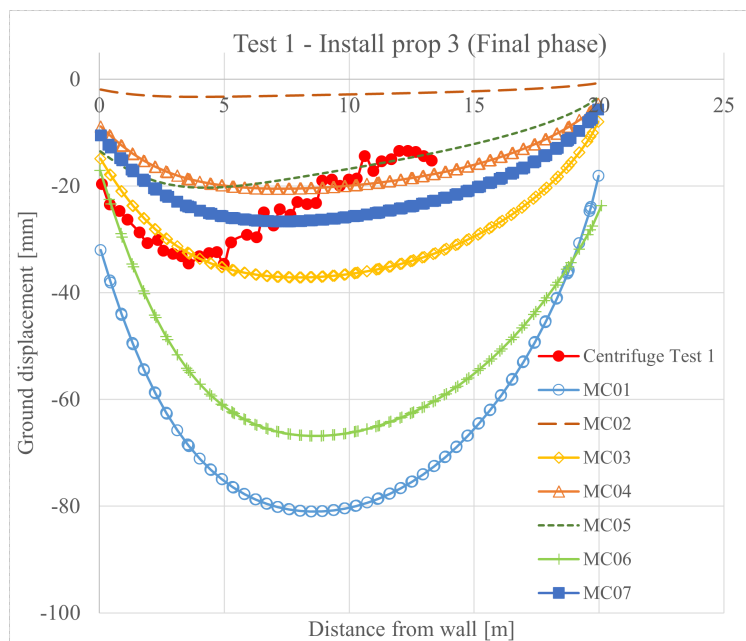


Figure 5.1: Vertical ground displacement of MC scenarios obtained from the sensitivity analysis.

ment. Further, by varying the earth pressure coefficient at rest K_0 in the MC04 to MC07, a value between 1.0 and 1.1 indicates akin as Lam's centrifuge test. Both parameters E_u and K_0 shows significant influence in the ground settlement and lateral wall deflection.

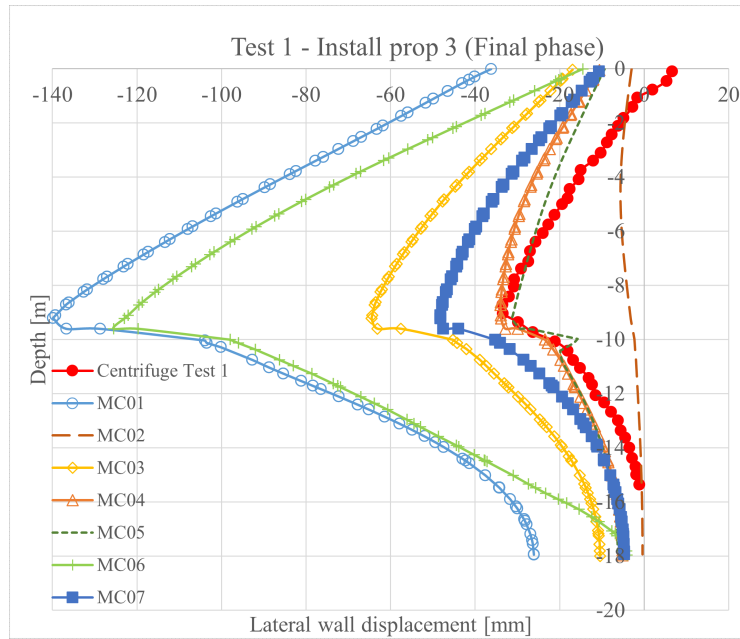


Figure 5.2: Lateral wall deflection of MC scenarios obtained from the sensitivity analysis.

5.2.2 Sensitivity analysis - Hardening Soil model

For the HS model, it is expected a more similar soil displacement profile as the centrifuge test from Lam (2010). The complex model is based on several parameters which increases its accuracy. The HS model requires three different stiffness parameters as presented in Table 5.3. A SA of the unknown parameters for a HS model is manually done in Excel. The procedure is presented in Table 5.4 with parameters from Table 5.3.

Table 5.3: Unknown input parameters for sensitivity analysis of Hardening Soil model in PLAXIS.

Parameters	Description	Value range	Additional details
E_{50}^{ref}	Secant stiffness	1 – 50 MPa	
E_{oed}^{ref}	Tangent stiffness	1 – 50 MPa	$E_{oed}^{ref} \approx E_{50}^{ref}$
E_{ur}^{ref}	Unloading/reloading stiffness	3 – 150 MPa	$E_{ur}^{ref} \approx 3E_{50}^{ref}$
K_0	Earth pressure coefficient at rest	0.65 – 1.8	$K_0 > 1, 0.65 < K_0 < 1.8$

* Note: Additional parameters in PLAXIS follows default settings.

A SA of the HS model emphasizes the importance of stiffness parameters and accentuates their dominant role for the numerical outcome. Note that E_{oed}^{ref} is assumed equal to E_{50}^{ref} and is therefore applied with same values as E_{50}^{ref} .

Table 5.4: Sensitivity analysis for Hardening Soil model.

Parameter	Description	Range	Sensitivity analysis ID							
			HS01	HS02	HS03	HS04	HS05	HS06	HS07	HS08
E_{50}^{ref}	Secant stiffness	1 – 50MPa	1	50	10	4	4	4	4	4
E_{oed}^{ref}	Tangent stiffness	1 – 50MPa	1	50	10	4	4	4	4	4
E_{ur}^{ref}	Unloading/reloading stiffness	3 – 150MPa	3	150	30	12	16	16	16	16
K_0	Earth pressure coefficient	0.65 – 1.8	1.0	1.0	1.0	1.0	1.0	0.65	1.8	1.1
Results from centrifuge Test 1 [mm]			Results from PLAXIS in [mm]							
Max. lateral wall deflection, $\delta_{w,max} = 33.3$			136.5	4.9	15.7	39	38.4	10.4	33.5	33.8
Max. vertical ground displacement, $S_{v,max} = 34.4$			67.7	3	10.3	21.9	21.7	9.4	16.3	20.8
Max. vertical displacement adj. to wall, $S_{v,max} = 19.5$			30	1.7	4.7	9.8	9.9	6.9	12	9.4

Notations: The result is from PLAXIS and based on the last construction stage: Installation of prop 3.

Different outcome may occur if other assumptions would have been made. Additionally, the unloading/reloading stiffness E_{ur}^{ref} is usually assumed as $3E_{50}^{ref}$, but for clay a three to five times the E_{50}^{ref} may be considered. From the first sets of the analysis, such as HS01 and HS02, it indicates a significant influence from the secant stiffness as revealed in Figure 5.3 and Figure 5.4. However, the last sets show that the earth pressure coefficient at rest K_0 plays an additional role in the ground displacement, for instance HS06 and HS07. Sets HS04 and HS05, indicate

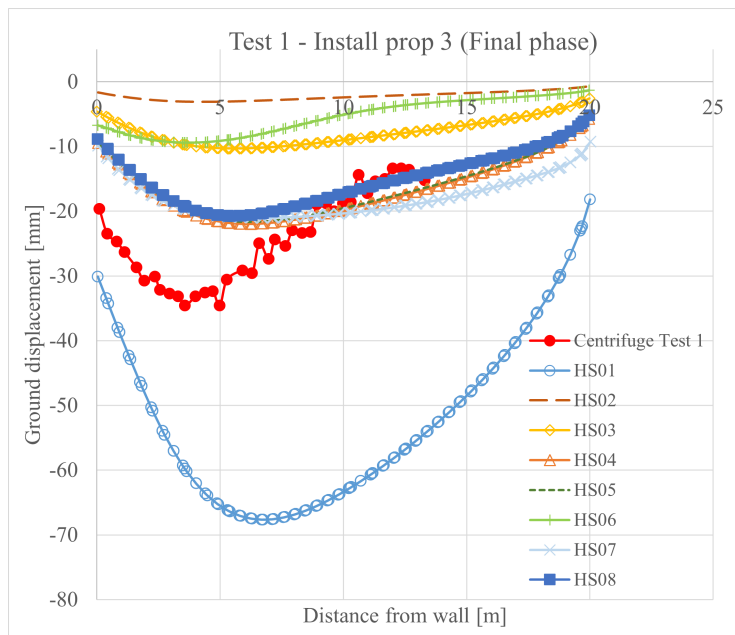


Figure 5.3: Vertical ground displacement of HS scenarios obtained from the sensitivity analysis.

less effect from the unloading/reloading stiffness when varying the parameter. The ground displacement indicates elastic and plastic deformation based on the ground displacement profile, unlike the MC model. The displacement profile tends to replicate similar shape as the centrifuge test. The HS model shows smaller variation in the ground displacement and wall deflection when varying the unknown parameters.

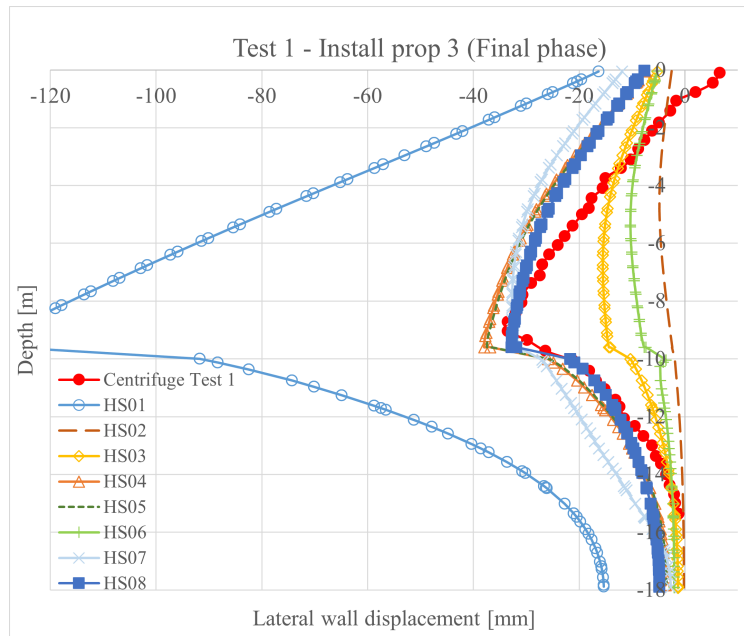


Figure 5.4: Lateral wall deflection of HS scenarios obtained from the sensitivity analysis.

5.2.3 Sensitivity analysis - Hardening Soil Small model

For the HSS model, a more accurate soil displacement profile than the HS model is expected, based on the small strain behaviour. Especially adjacent to constructions. The HSS model provides additionally more parameters compared to the HS model due to its complexity. The threshold shear strain $\gamma_{0.7}$ is added as an unknown parameter for this SA. Due to the complexity with the unknown parameters for the HSS model in the SA, a simplification of the analysis is presented in Table 5.6. Additional sensitivity analysis have been conducted and presented in Appendix C, and the ones of interest are presented in Table 5.6.

The HSS model differs from the HS model by including the small strain parameters: G_0 and $\gamma_{0.7}$. The uncertain threshold shear strain $\gamma_{0.7}$ shows a negligible influence factor on the ground displacement and wall deflection. $\gamma_{0.7}$ shows a low influence level in HSS06 and HSS07. The parameter is therefore chosen to have a value of the average $\gamma_{0.7} = 0.0002$. Additionally, the displacement increases if the earth pressure coefficient at rest K_0 increase and the parameter shows its importance, as presented in Figure 5.5 and Figure 5.6. With regard to the stiffness parameters, they clearly show a significant dominance on the influence level. The shear modulus G_0 was given from the centrifuge test with value 22MPa , which limits the stiffness range compared to the HS model. With a defined

Table 5.5: Unknown input parameters for Hardening Soil Small model in PLAXIS.

Parameters	Description	PLAXIS input settings/value	Additional details
E_{50}^{ref}	Secant stiffness	1 – 25MPa	
E_{oed}^{ref}	Tangent stiffness	1 – 25MPa	$E_{oed}^{ref} \approx E_{50}^{ref}$
E_{ur}^{ref}	Unloading/reloading stiffness	3 – 50MPa	$E_{ur}^{ref} \approx 3E_{50}^{ref}$
$\gamma_{0.7}$	Threshold shear strain, ($G_s = 0.722G_0$)	0.00015 – 0.00025	(Zhao et al., 2015)
K_0	Earth pressure coefficient at rest	0.65 – 1.8	$K_0 > 1, 0.65 < K_0 < 1.8$

* Note: Additional parameters in PLAXIS follows default settings.

Table 5.6: Sensitivity analysis for Hardening Soil Small model.

Parameter	Description	Range	Sensitivity analysis ID							
			HSS01	HSS04	HSS05	HSS06	HSS07	HSS08	HSS09	HSS10
E_{50}^{ref}	Secant stiffness	1 – 25MPa	1	4	4	4	4	4	4	4
E_{oed}^{ref}	Tangent stiffness	1 – 25MPa	1	4	4	4	4	4	4	4
E_{ur}^{ref}	Unloading /reloading stiffness	3 – 50MPa	3	12	16	16	16	16	16	16
$\gamma_{0.7}$	Threshold shear strain, ($G_s = 0.722G_0$)	0.00015–0.00025	0.0002	0.0002	0.0002	0.00015	0.00025	0.0002	0.0002	0.0002
K_0	Earth pressure coefficient	0.65 – 1.8	1.0	1.0	1.0	1.0	1.0	0.65	1.8	1.1
Results from centrifuge Test 1 [mm]			Results from PLAXIS in [mm]							
Max. lateral wall deflection, $\delta_{w,max} = 33.3$			44.4	26	32	34	30	7.9	26.6	27.4
Max. vertical ground displacement, $S_{v,max} = 34.4$			27.9	17.1	18.9	20	18.3	7.1	17.8	18.3
Max. vertical displacement adj. to wall, $S_{v,max} = 19.5$			18.3	8.5	7.8	5	7.4	7.7	9	7.8

Notations: The result is from PLAXIS and based on the last construction stage: Installation of prop 3.

shear modulus value, PLAXIS required $E_{ur}^{ref} \leq 2.4G_0^{ref}$ and consequently $E_{ur}^{ref} > 2E_{50}^{ref}$. Unlike the HS, the HSS shows that the unloading/reloading stiffness plays a bigger role, as presented in HSS04 and HSS05. Additionally, the result from set HSS01 and HSS10 shows an agreeable fit with centrifuge test result. Vertical ground displacement profile for the HSS01 reveals similar shape as the centrifuge test, as well as the value of the maximum vertical displacement and maximum vertical displacement adjacent to the wall. However, for the lateral wall deflection, both HSS01 and HSS10 indicates good estimations compared to the centrifuge test. The HSS10 shows lower vertical ground displacement values, but reveals similar displacement shape. Note that HSS10 will be further validated for the HSS model, due to a good fit with the stress-strain curve in the soil property estimation in a soil test that will be presented in Section 5.5. Although the HSS10 scenario is selected as a representative HSS model, the HSS01 would likely be a preferable replacement scenario with respect to the ground displacement profile.

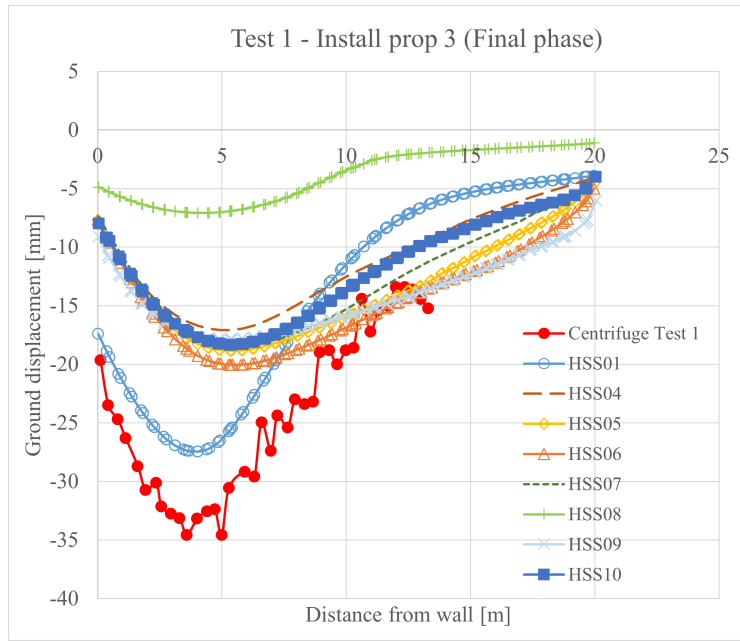


Figure 5.5: Vertical ground displacement of HSS scenarios obtained from the sensitivity analysis.

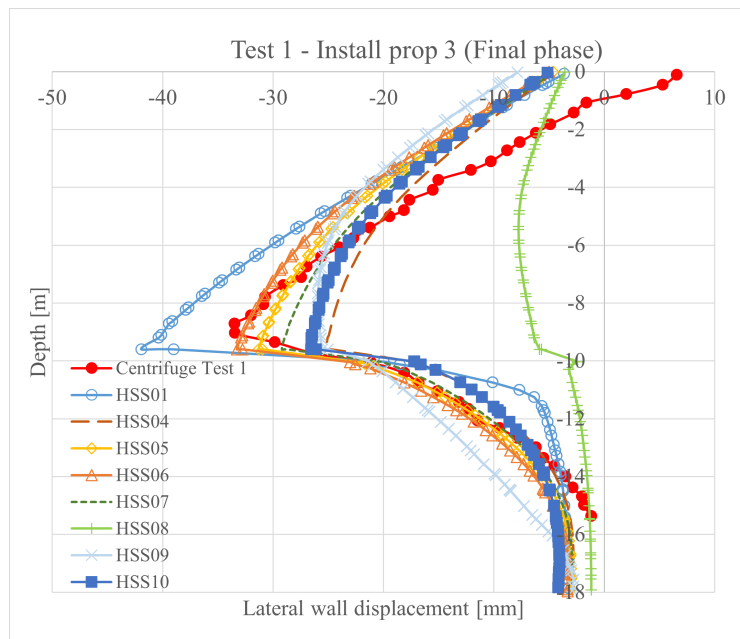


Figure 5.6: Lateral wall deflection of HSS scenarios obtained from the sensitivity analysis.

5.3 PLAXIS Sensitivity analysis and Parameter variation

A *sensitivity analysis parameter variation*-application is directly available in PLAXIS (PSA), and may be used to evaluate the influence of the individual parameters for soil and structure parameters. The user can select parameters of interests and study the sensitivity with respect to displacements, stresses or safety factors at different phases in the construction process. The theory is quite simplistic and could be carried out manually by the user, by re-

peatedly calculating the construction phases using different inputs. Additionally, using the sensitivity analysis tool is advantageous as it saves time and reduces the possibility of human error. In this paper, the sensitivity analysis application in PLAXIS is used to verify the reliability and obtained result of the manual sensitivity analysis.

The first part of the PLAXIS sensitivity analysis (PSA) is the selection parameter function, where parameters from all soil models can be examined. A PLAXIS calculation of all phases requires a certain amount of computer capacity, and is in this case only able to perform a SA for a maximum of three parameters at a time. For every parameter, a minimum, maximum and a reference value is chosen, an example is presented in Figure 5.7. The minimum and maximum value range should be approximate $\pm 10\%$ of a reference value. The relative sensitivity or *SensiScore* describes the effect of varying the input variable the overall outcome for all criteria relative to the effect of the other input variables. The criteria can be set in the application based on displacement, stress strain and reached values for chosen phase in the construction stages, as seen in Figure 5.7. The SensiScore gives a percentage value of 100%



Figure 5.7: PLAXIS sensitivity analysis and parameter variation of the HSS model with scenario HSS01.

distributed to the three parameters depends on their influence ability. The one with the highest SensiScore, have the highest level of influence. The MC model requires only two parameters, and is able to calculate in a wider range than $\pm 10\%$. A higher number of calculation analysis is required for the HS and the HSS model, due to PLAXIS calculations with value ranges that correlates. The most prominent value from MSA is selected as *Ref* value for the PSA, and is presented in Table 5.8, Table 5.9 and Table 5.10.

By selecting the parameters of interest and define a given range of uncertainty for the unknown parameter, the PSA offers to apply several criterion preferences. In the performed analysis, several criterion based on different phase, values and points in the model can be selected. The chosen criterion conducted in the sensitivity analysis is presented in Table 5.7. For *displacement* and *stress strain* criterion, a chosen node and stress point is required. There are three nodes and three stress points corresponding to the active side, passive side and wall tip. The different points gives a slightly different result in the SensiScore values, but commonly the wall tip provides the mean of the

active and passive side. In the following analysis, the wall tip node and stress point is chosen as criterion.

Table 5.7: Criterion in PLAXIS Sensitivity Analysis-application.

Criterion	Description
Criterion 1	Phase: Install prop 3 (Last phase) Criterion: Displacement Point: Node - Active, Passive or Wall tip Value type: $ u $
Criterion 2	Phase: Install prop 3 (Last phase) Criterion: Stress strain Point: Stress point - Active, Passive or Wall tip Value type: γ_{xy}
Criterion 3	Phase: Install prop 3 (Last phase) Criterion: Reached values Value type: $SumM_{sf}$

PLAXIS Sensitivity analysis - MC model

Table 5.8 presents the different set of PSA for the MC model. PSA-MC05 indicates a significant influence of the Young's modulus E_u with a SensiScore of 79%, especially regarding the displacement criterion. However, the earth pressure coefficient at rest K_0 shows a SensiScore of 21% which shows a relative relevant parameter. The unknown parameters from PSA results affirm the results from the MSA.

Table 5.8: PLAXIS Sensitivity analysis for Mohr-Coulomb model.

Parameter	Ref	Range ($\pm 10\%$)	SensiScore [%]				
			PSA-MC01	PSA-MC02	PSA-MC03	PSA-MC04	PSA-MC05
Criterion:			1	2	3	1,2	1,2,3
E_u	5MPa	1 – 50MPa	64	94	0	79	79
K_0	1.1	0.65 – 1.8	36	6	0	21	21

Notations: The result is from PLAXIS SA tool and based on the last construction stage: Installation of prop 3.

PLAXIS Sensitivity analysis - HS model

The different set of PSA for the HS model is summarized in Table 5.9. The PSA for the HS model includes additionally several stiffness parameters, which leads to a more considerable analyze. The tangent stiffness E_{oed}^{ref} shows an insignificant affect for all criterion in PSA-HS1, PSA-HS2, PSA-HS3 and PSA HS4, and is negligible for further PSA for the HS model. The secant stiffness E_{50}^{ref} and the unloading/reloading stiffness E_{ur}^{ref} shows however, a rather vital influence compared to the tangent stiffness. Compared with E_{50}^{ref} and E_{ur}^{ref} , the earth pressure coefficient at rest K_0 in PSA-HS7 plays a vital role with a SensiScore of 50% with all criterion, unlike in the PSA for the MC model.

Table 5.9: PLAXIS Sensitivity analysis for Hardening Soil model.

Parameter	Ref	Range $\pm 10\%$	SensiScore [%]						
			PSA-HS1	PSA-HS2	PSA-HS3	PSA-HS4	PSA-HS5	PSA-HS6	PSA-HS7
Criterion:			1	2	3	1,2,3	1	2	1,2,3
E_{50}^{ref}	4MPa	3.6 – 4.4MPa	81	83	0	82	29	23	26
E_{oed}^{ref}	4MPa	3.6 – 4.4MPa	0	0	0	0	–	–	–
E_{ur}^{ref}	16MPa	14.4 – 17.6MPa	19	17	0	18	29	19	24
K_0	1.1	0.99 – 1.21	–	–	–	–	42	58	50

Notations: The result is from PLAXIS SA tool and based on the last construction stage: Installation of prop 3 with $a \pm 10\%$ of the Ref-value determined from MSA.

PLAXIS Sensitivity analysis - HSS model

A complete table summarizing the PSA for the HSS model, is presented in Appendix C. The PSA sets of interest is presented in Table 5.10. The PSA for the HSS model gives similar indication of SensiScore values as with the PSA HS. Due to a more complex soil model, the HSS includes the threshold shear strain $\gamma_{0.7}$ as an unknown parameter. The input parameter, together with the E_{50}^{ref} shows an important role. However, PSA-HSS9 indicates a vital influence of the earth pressure coefficient at rest K_0 with a SensiScore of 66% with the respect to all criterion.

Table 5.10: PLAXIS Sensitivity analysis for Hardening Soil Small model.

Parameter	Ref	Range $\pm 10\%$	SensiScore [%]					
			PSA-HSS1	PSA-HSS3	PSA-HSS4	PSA-HSS6	PSA-HSS7	PSA-HSS9
Criterion:			1	1,2,3	1	1,2,3	1	1,2,3
E_{50}^{ref}	4MPa	3.6 – 4.4MPa	89	91	51	52	26	31
E_{oed}^{ref}	4MPa	3.6 – 4.4MPa	0	0	–	–	–	–
E_{ur}^{ref}	16MPa	14.4 – 17.6MPa	11	9	7	5	4	3
$\gamma_{0.7}$	0.0002	0.00018 – 0.00022	–	–	42	43	–	–
K_0	1.1	0.99 – 1.21	–	–	–	–	70	66

Notations: The result is from PLAXIS SA tool and based on the last construction stage: Installation of prop 3 with $a \pm 10\%$ of the Ref-value determined from MSA.

Table 5.8, Table 5.9 and Table 5.10 presents results from PLAXIS SA, by evaluating the influence of three chosen parameters in each analysis. For instance, the PSA of the HSS model illustrates a SensiScore of 11% for E_{ur}^{ref} , while a SensiScore of 89% for E_{50}^{ref} and 0% for E_{oed}^{ref} in set PSA-HSS1. This indicates a relative low influence from the latter, and a relative dominant influence from E_{50}^{ref} . The PSA-MC, PSA-HS, and PSA-HSS compared with the manual sensitivity analysis (MSA), indicates similar influence for the unknown parameters. Especially, the dominance of

the earth pressure coefficient at rest K_0 and the secant stiffness E_{50}^{ref} .

5.4 Evaluation of sensitivity analysis

The manual SA of the input parameters in the soil models shows a variation of how they influence and affect the vertical ground displacement and lateral wall deflection. The demonstration of the sensitivity analysis illustrates that the constitutive models have a number of well-defined parameters as well as a number of unknown parameters. The number of the unknown parameters varies, and the level of influence varies. An indication is that simple models have less unknown parameters, such as the MC model. More complex and accurate models, such as the HS and the HSS, provides a number of unknown parameters, especially the HSS model.

By applying the sensitivity analysis tool from PLAXIS, a verification of the result from the manual sensitivity analysis can be obtained. The PSA is a simple and quickly application, and is therefore used for both MC, HS and HSS model. The PSA shows that the stiffness parameter E has a significant influence on how the soil behaves and the outcome of it, and shows a crucial dominance, especially in the MC model. For the HS and HSS model, the stiffness parameter is divided into three stiffness parameters. The E_{oed}^{ref} has a minimal influence on the outcome. Meanwhile, E_{oed}^{ref} is usually assumed to be the same as E_{50}^{ref} . The E_{ur}^{ref} has a minor influence, but showed a greater impact than the E_{oed}^{ref} . However, the E_{50}^{ref} shows to be a dominant parameters and has a crucial influence on the soil behaviour. The PSA shows how one single parameter can overrule the other parameter. The earth pressure coefficient at rest K_0 and the threshold shear strain $\gamma_{0.7}$ plays an important role with respect to the PSA, but shows a rather insignificant affect on the ground displacement in the MSA.

Keep in mind that the calculation function in the PSA is limited by only being able to consider three parameters at a time and that the analyze and SensiScore is based only on the relation between the chosen three parameters of interest. Additional combinations of the parameters could be analyzed, but all parameters are mainly compared to the most dominant parameters (i.e. the E_{50}^{ref}). Other combination, such as the E_{oed}^{ref} , $\gamma_{0.7}$ and K_0 , is not considered here in order to simplify the analyze. Note that the effect of other important factors, such as retaining wall and prop system, is not considered in the sensitivity analysis. Soil properties have been in focus in the SA and PSA, in order to verify a sufficient calibrated soil model. Moreover, the calibrated model will be able to examine other uncertain parameters and analyse their influence on the ground displacement. The aim of the sensitivity analysis is to emphasize which unknown parameters have significant influence on the ground displacement, in order to be able to develop a calibrated model.

Evaluating the influence of the unknown parameters is crucial since perhaps the biggest challenge to PLAXIS model users, is the choice of input parameters. These must be selected with careful consideration, if the model is to pro-

duce accurate results. One example is the wall stiffness parameter discussed earlier. In the MC model, it is important to consider which stress state will be applicable because this will dictate the value of the stiffness parameter. In the HS and HSS models, this issue is dealt with through the use of different stiffness parameters defined for different stress states.

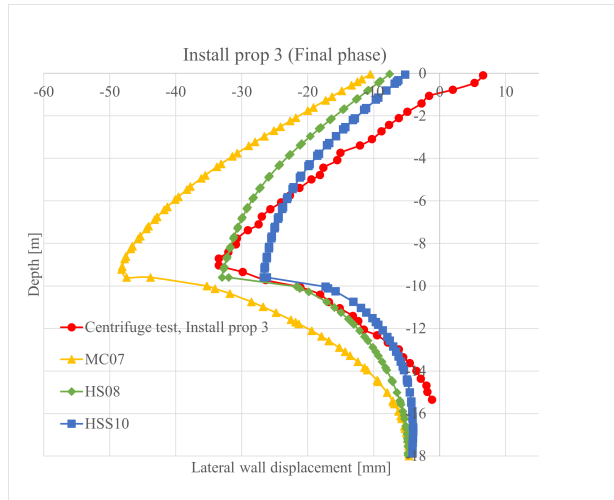


Figure 5.8: Horizontal ground displacement of MC07, HS08 and HSS10 from last phase.

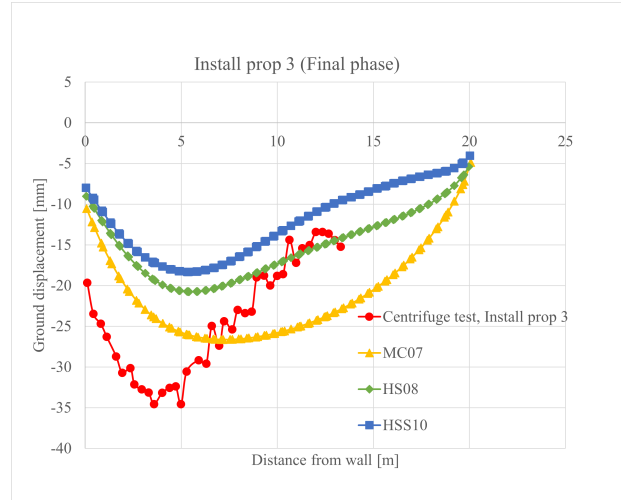


Figure 5.9: Vertical ground displacement of MC07, HS08 and HSS10 from last phase.

A comparison of the most prominent SA set from each soil models is represented in Figure 5.8 and Figure 5.9. MC07 shows rather high values for vertical and horizontal ground displacement compared with the centrifuge test. The HS08 and HSS10 gives slightly similar trends, but HSS10 shows an improved vertical displacement shape.

Based on the findings from MSA and PSA, the following conclusion may therefore be drawn: MC, HS and HSS can produce reasonable wall deflection and ground movement that compared well with measured data from the centrifuge test. The HS and HSS model produced a more realistic ground settlement profile. The consideration of non-linear and inelastic stiffness in the HS and HSS model gave a better prediction of the settlements near the excavation. The MC provides a greater vertical displacement magnitude than the HS and HSS, but HS and HSS provide similar horizontal displacement magnitude as the centrifuge test.

The SA manual and SA PLAXIS (PSA) is used to verify the sensitivity of the different parameters. Based on the SA manual and SA PLAXIS, it is to conclude that in the HSS model, the unknown stiffness parameter E_{50}^{ref} and E_{ur}^{ref} and the unknown earth pressure coefficient at rest K_0 , have a dominant impact and affect the models the most.

5.4.1 Summary

A sensitivity analysis is obtained based on the numerical calculation in PLAXIS, by investigating the unknown parameters. The objective of the SA is to get a deeper understanding for which parameters influence the ground displacement the most. The analysis is conducted by both manual sensitivity analysis and by adopting the *Sensitivity and parameter variation*-tool in PLAXIS.

For both the MSA and PSA, the different scenarios for the different soil models show a variation of ground displacement. Overall, these results indicate that the HSS model provides better agreement with the centrifuge test, despite more input parameters that could not be directly obtained from the centrifuge experiment. The HSS model is more complex than the MC and HSS model, and the computed ground displacements provides a reasonable and well replication of the characteristic soil displacement profile adjacent to a deep excavation of soft clay.

The result from PLAXIS shows similar vertical ground displacements and lateral wall deflection, but also maximum displacement adjacent to the wall. Additionally, a more similar fit with the displacement curve profile is provided from the HSS model with HSS10, as presented in Figure 5.8 and Figure 5.9. Together these results provide important insights into the influence of soil models and their input parameters on ground displacements due to a deep excavation. The next chapter, will therefore explore the numerical model based on the HSS model.

5.5 Replicate test result from centrifuge test

This section aims to replicate the soil behaviour presented in the centrifuge test. Further, a *Soil Test* application from PLAXIS is used for calculations of soil properties. Additionally, other impacts of soil performance, such as ground displacement during excavation process and earth pressure, is evaluated. Moreover, other centrifuge test from Lam (2010) is examined in order to verify a calibrated model.

A method for replicating the soil behaviour is to imitate the stress-strain response. The idea is to replicate the centrifuge experiment to derive parameters of a respective constitutive model. Soil ground displacement can be estimated based on the stress-strain characteristics. This approach is diverse from the conventional applications of plasticity theory based on the concept of stress behaviour and displacement due to mobilized soil strength. The aim is to identify the typical stress-strain data that represents a particular zone in the soil. The strain represents a plastic deformation mechanism and can be used to predict the boundary displacement (Lam, 2010).

The stress-strain behaviour in a soil model can be expressed differently than the real soil, as illustrated in Figure 5.10. The MC soil model is based on both elastic and plastic strain, but is elastic before reaches failure and is only

plastic when reached failure. In contrast, real soil response is elastic-plastic (i.e. non-linear) even before failure. The HS and HSS soil model captures this non-linear behaviour by varying the secant modulus E_{50}^{ref} during primary loading. It also captures the inelastic response during unloading-reloading by using the unloading-reloading modulus E_{ur}^{ref} . The MC model does not capture the inelastic response, and reaches failure at much higher stresses than the real soil, as seen in Figure 4.5. Under drained condition, the stiffness modulus is stress-dependent, this stress-dependency behaviour is captured by the HS and HSS but not by the MC model (Teo and Wong, 2012). Consequently, the soil behaviour is better captured by the HS and HSS model, which additionally captures the small strain behaviour. Therefore, the replication of the soil behaviour and development of a calibrated model will further only be considered with the HSS model, in order to limit and specify the calculations.

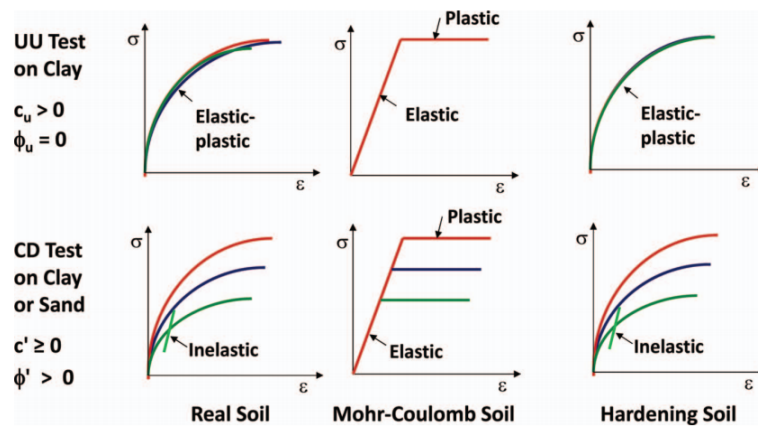


Figure 5.10: Stress-strain behaviour of real soil, MC model and HS model (Teo and Wong, 2012).

This section aims to verify a calibrated soil model based on replication of soil behaviour from centrifuge test. Additionally to Test 1, centrifuge Test 2 and Test 4 provided by Lam (2010) is also considered and examined in order to replicate the soil behaviour and distinguish the result from the centrifuge tests and the numerical model.

5.5.1 Soil test

In order to evaluate a soil behaviour from a numerical model for a particular condition, such as a deep excavation in soft clay, similar soil properties and condition is recommended. With respect to the evaluation of soil behaviour and performance, it is required a soil test. A typical approach for evaluating the soil behaviour is to replicate and/or manipulate the stress-strain curve. From Lam (2010), a shear strain and deviatoric stress curve is plotted, as seen in Figure 3.5 from Section 3.1.7. By replicating a similar shear strain-stress curve, an evaluation and comparison between the numerical calculations in PLAXIS and result from centrifuge test can be established.

An undrained triaxial compression test with an isotropic consolidation was carried out on vertically- and horizontally cut specimens presented in Chapter 3 and more detailed described by Lam (2010). The triaxial test loaded the

sample with 160 kPa in total as a vertical preconsolidation stress, and subsequently unloaded and let the sample swell back to 26 kPa , which was controlled by the initial cell pressure. The S_u from Lam (2010) is defined as 27 kPa , which result in a q of 54 kPa by using the relation: $S_u = \frac{q}{2}$. The deviatoric stress q leaves further a σ_3 , the horizontal stress as:

$$q = \sigma_1 - \sigma_3 = 160\text{ kPa} - \sigma_3 = 54\text{ kPa} \tag{5.1}$$

$$\sigma_3 = 106\text{ kPa} \tag{5.2}$$

The horizontal stress is then assumed larger than the vertical stress. This means that the soil sample shows a history of shear strain and an anisotropic preconsolidation, and mobilized relative shear strength is therefore applied with 0.2 in the *Soil Test*. The soil sample was conducted with an isotropic compression under an anisotropic consolidation process. The undrained triaxial compression test was isotropical conducted with $K_0 = 1$ due to isotropic consolidation.

The Hardening Soil Small (HSS) model has a significant ability replicate a stress-strain curve similar to real soil and to reproduce a good prediction for ground displacement in deep excavation in soft clay. Further, a *Soil Test* will therefore be presented for the HSS model. Figure 5.11 shows the *Soil Test* application in PLAXIS with HSS10.

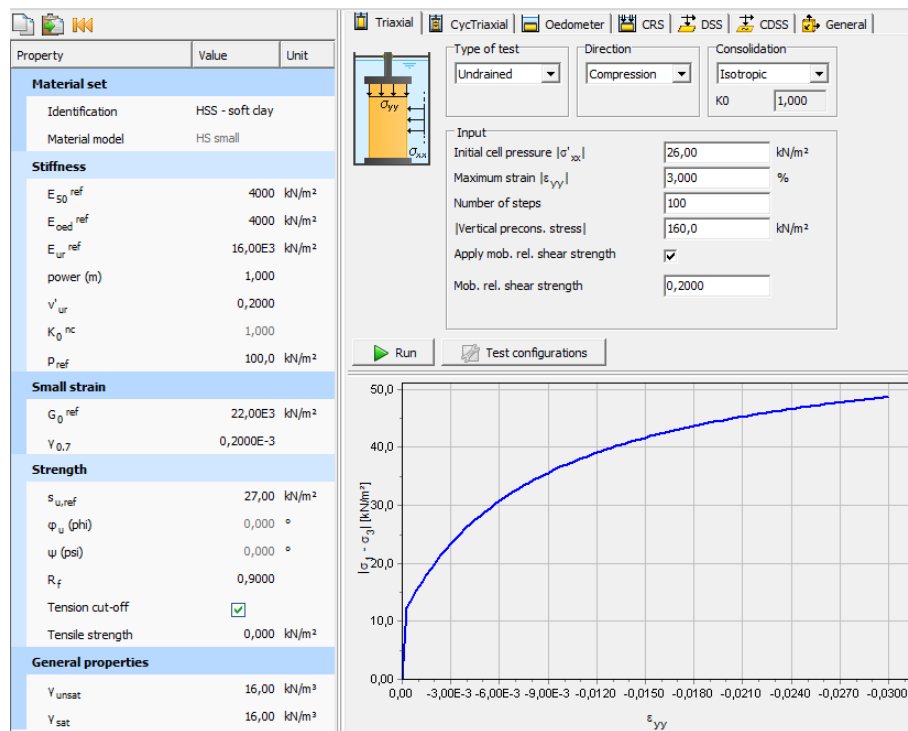


Figure 5.11: PLAXIS Soil test showing input properties on the left and soil type test on top. The graph illustrates stress strain from the result of the input parameters.

The output from the Soil Test is a curve of axial strain ϵ_{yy} and deviatoric stress $q = \sigma_1 - \sigma_3$ as presented in Figure 5.11. As mentioned, a similar shear strain and deviatoric stress curve is envisioned in order to compare the soil materials and its behaviour. This transformation is presented earlier in Section 4.3. The axial strain ϵ_{yy} from the Soil Test is further converted to shear strain γ , in order to compare with stress-strain curve from Lam (2010) in Figure 3.5. The triaxial test is for an undrained compression test, which derives in a no volume change:

$$\Delta\epsilon_v = \Delta\epsilon_1 + 2\Delta\epsilon_3 = 0 \quad (5.3)$$

$$\Delta\epsilon_3 = -\frac{1}{2}\Delta\epsilon_1 \quad (5.4)$$

The maximum shear strain γ is calculated by inserting Equation 5.4 in the following:

$$\gamma = \Delta\epsilon_1 - \Delta\epsilon_3 = \Delta\epsilon_1 - \left(-\frac{1}{2}\Delta\epsilon_1\right) = \frac{3}{2}\Delta\epsilon_1, \quad (5.5)$$

where ϵ_1 is the axial strain ϵ_{yy} in a triaxial compression test and ϵ_3 is the lateral strain. The transformation is presented in Figure 5.12. The graph shows an almost perfectly fitted shear strain stress curve for shear strain value

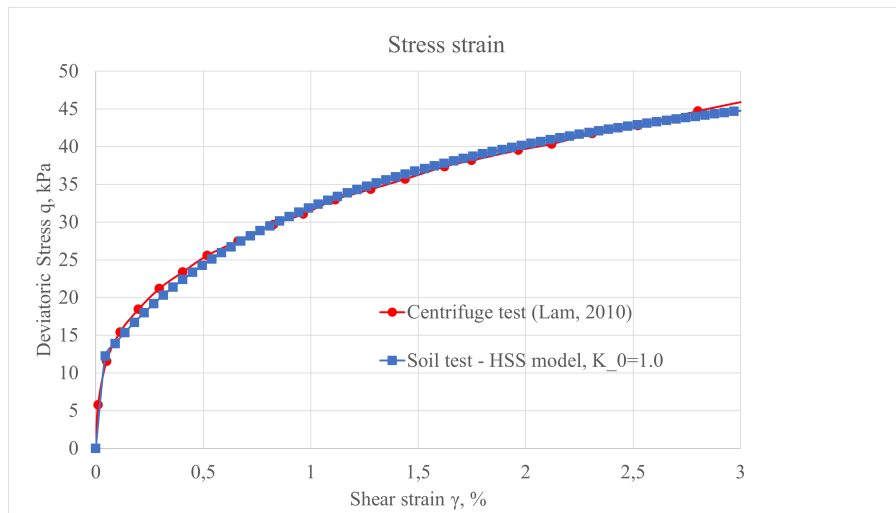


Figure 5.12: Stress-strain curve of centrifuge test (Lam, 2010) and soil test result with HSS model from PLAXIS (i.e. HSS10 $K_0 = 1$).

less than 3%, and indicates a good fit regarding replicating the soil behaviour. The replicated shear strain stress curve imitate the soil behaviour, and the used to verify the soil material in a numerical model.

5.5.2 Construction stages

An approach to evaluate if the numerical model is able to capture the real soil behaviour is to compare the computed soil response at different construction stages to the one measured in the centrifuge test. A crucial factor that have a significant influence on the ground displacement is the excavation sequences and process. An evaluation of the construction stages may give an indication of how and why the numerical model behave differently compared

to the centrifuge test. For each construction stage, vertical ground displacements and lateral wall displacement are evaluated and presented with centrifuge Test 1 results and PLAXIS output results. Centrifuge Test 1 from Lam (2010) illustrates the construction stages as in Figure 5.13 and Figure 5.14.

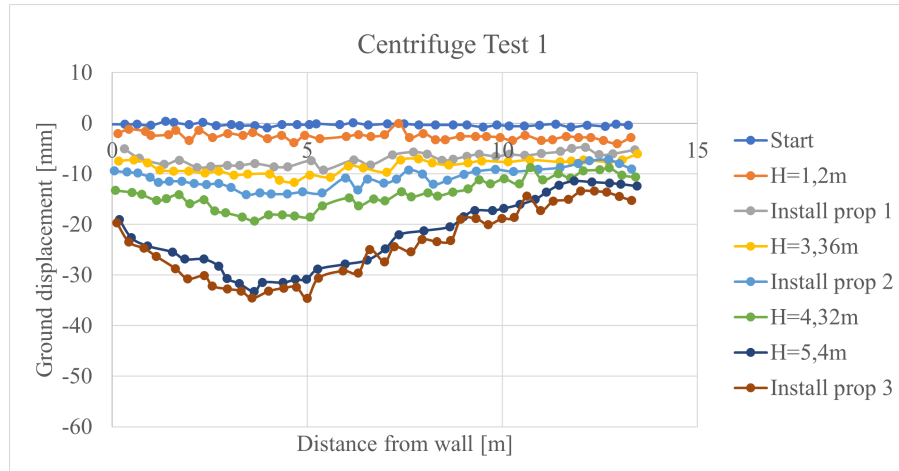


Figure 5.13: Vertical ground displacement in each construction stage. Data is obtained from (Lam, 2010).

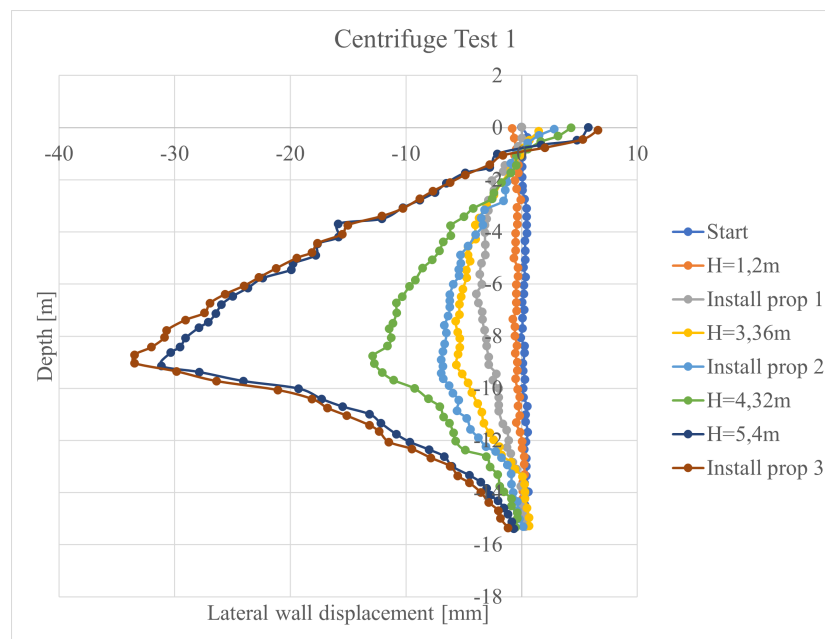


Figure 5.14: Lateral wall displacement in each construction stage. Data is obtained from (Lam, 2010).

For the following comparison with numerical model PLAXIS, the HSS10 model identified from previous chapter will be adopted for the comparison of construction stages. Input values for retaining wall and prop is based on Table 3.2 and Table 3.3.

5.5.3 Vertical ground displacement due to construction stages

The vertical ground displacement from PLAXIS shows significantly less ground displacement compared to the centrifuge test in all stages, as presented in the figures below. In Figure 5.15 *install wall phase*, the numerical and centrifuge test shows similar displacement magnitude and the influence zone differ in each stage. Figure 5.22 of *final phase* shows a concave shape of the settlement curve for centrifuge test and PLAXIS. The maximum vertical displacement differ in magnitude, but is located at approximately the same distance from the wall. However, the maximum vertical displacement adjacent to the wall for PLAXIS are approximately half of the ones from the centrifuge test. Note that the centrifuge test do not provide similar influence zone compared to what HSS10 represents. Additionally, the magnitude of the displacement shows a lack of similarity.

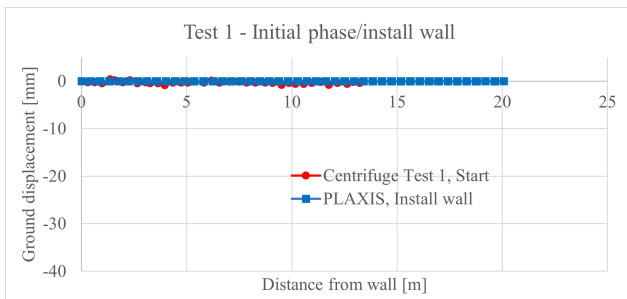


Figure 5.15: Test 1 Vertical ground displacement - Initial phase: Install wall.

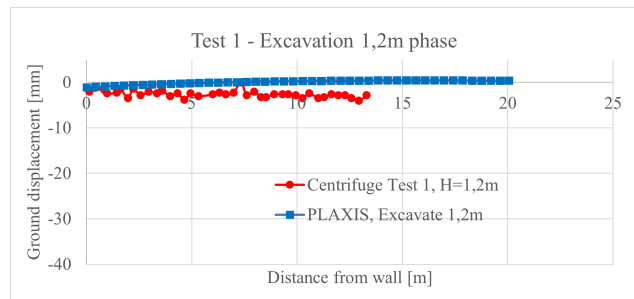


Figure 5.16: Test 1 Vertical ground displacement - Phase 1: Excavation 1.2m.

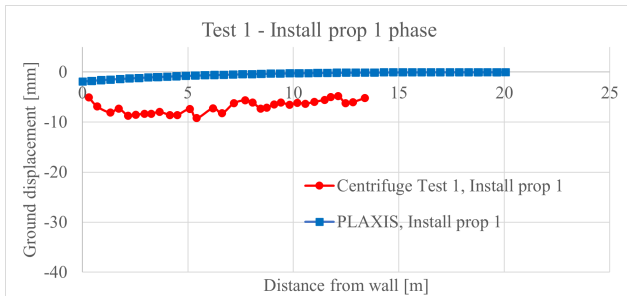


Figure 5.17: Test 1 Vertical ground displacement - Phase 2: Install prop 1.

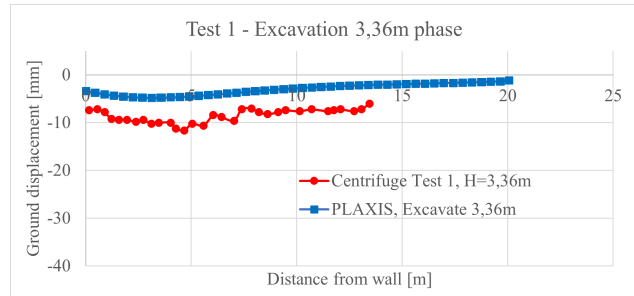


Figure 5.18: Test 1 Vertical ground displacement - Phase 3: Excavation 3.36m.

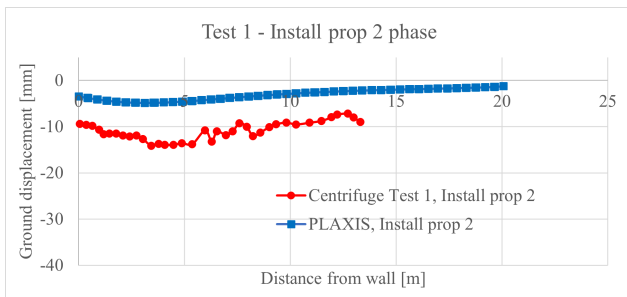


Figure 5.19: Test 1 Vertical ground displacement - Phase 4: Install prop 2.

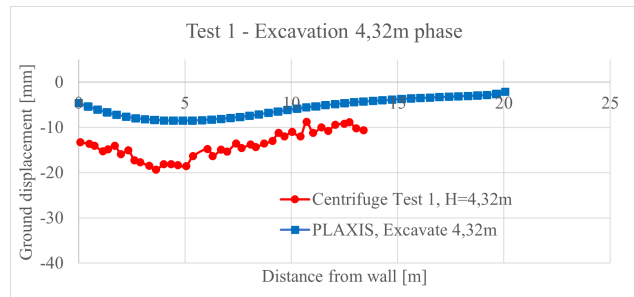


Figure 5.20: Test 1 Vertical ground displacement - Phase 5: Excavation 4.32m.

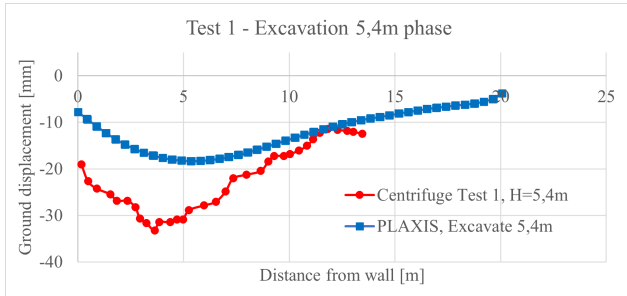


Figure 5.21: Test 1 Vertical ground displacement - Phase 6: Excavation 5.4m.

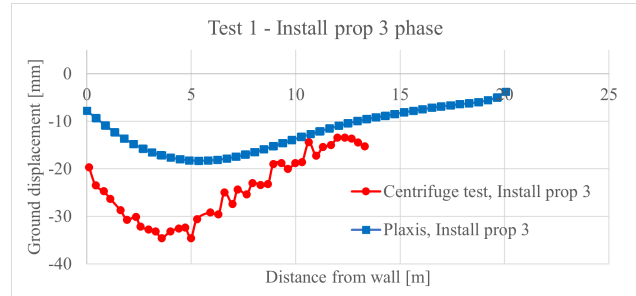


Figure 5.22: Test 1 Vertical ground displacement - Final phase: Install prop 3.

5.5.4 Lateral wall displacement due to construction stages

The lateral wall displacement for the centrifuge test and PLAXIS shows varied result for the different construction stages, as illustrated in the figures below. However, both *initial phase* in Figure 5.23 and *final phase* in Figure 5.30 shows similar trends. Under construction stages, the maximum horizontal wall displacement in PLAXIS follows similar values as the centrifuge test. Additionally, the magnitude of horizontal wall displacements obtained in the numerical model was within 20% of the one measured in the centrifuge experiment. However, the displacement profiles differ in *Install prop 1 phase*, *Excavation 3,36m phase* and *Install prop 2 phase*. The lateral wall displacement at ground surface varies for all stages, and the lateral wall displacement at the tip of the wall varies. Although the horizontal displacement in PLAXIS and in the centrifuge test indicates relatively different behaviour, the final stage shows a similar trend as seen in Figure 5.30.

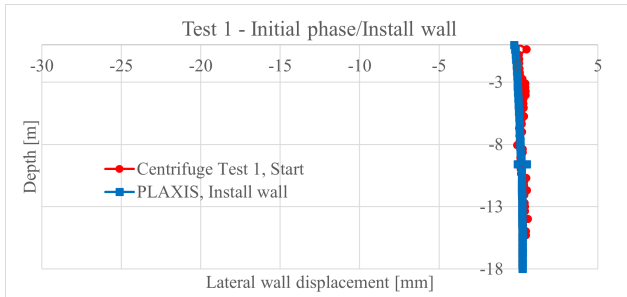


Figure 5.23: Test 1 Lateral wall displacement - Final phase: Install wall.

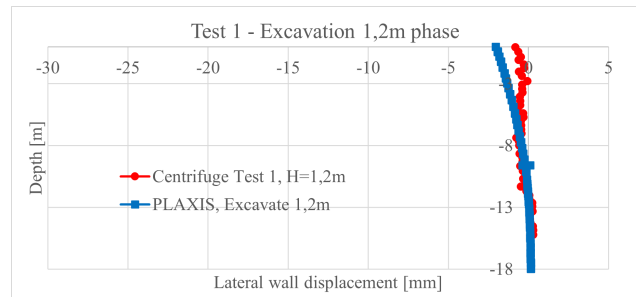


Figure 5.24: Test 1 Lateral wall displacement - Phase 1: Excavation 1.2m.

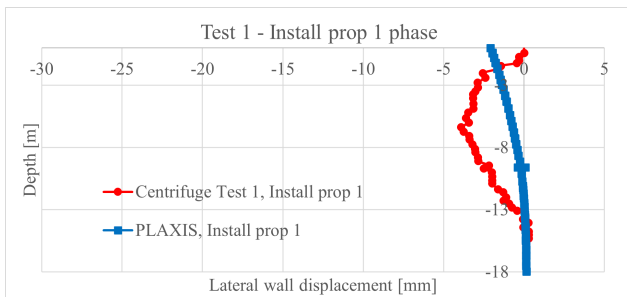


Figure 5.25: Test 1 Lateral wall displacement - Phase 2: Install prop 1.

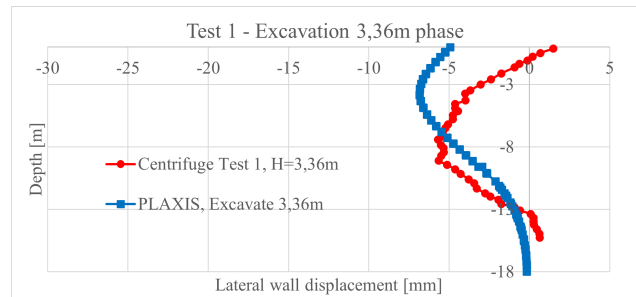


Figure 5.26: Test 1 Lateral wall displacement - Phase 3: Excavation 3.36m.

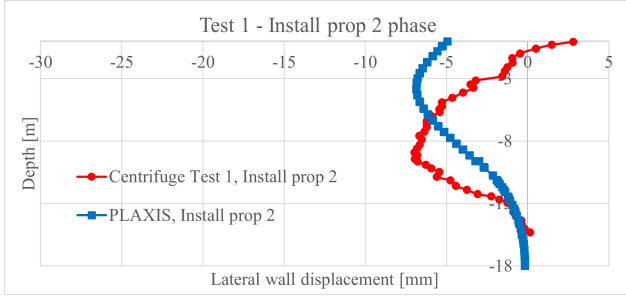


Figure 5.27: Test 1 Lateral wall displacement - Phase 4: Install prop 2.

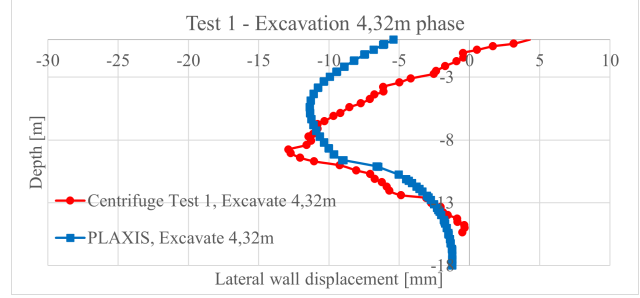


Figure 5.28: Test 1 Lateral wall displacement - Phase 5: Excavation 4.32m.

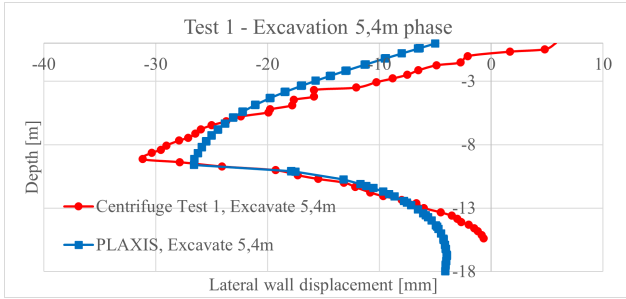


Figure 5.29: Test 1 Lateral wall displacement - Phase 6: Excavation 4.32m.

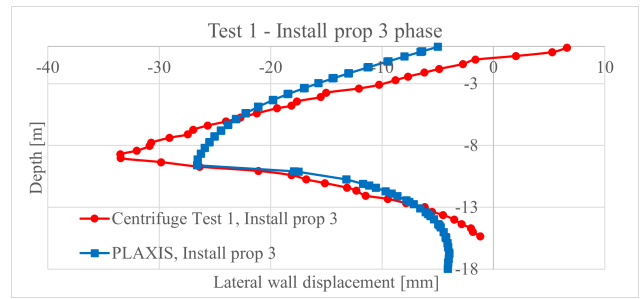


Figure 5.30: Test 1 Lateral wall displacement - Final phase: Install prop 3.

5.5.5 Test 4 with soft props

Lam (2010) presented five different centrifuge tests, and this paper has so far considered the baseline Test 1 (i.e. rigid wall with stiff props). Test 4 with a floating rigid wall and soft props aimed to investigate the influence of the prop stiffness. The remaining properties were identical to Test 1. For this reason, the simulation of Test 4 followed predominantly the same input as with Test 1; only the prop stiffness was adjusted. The calculation of prop stiffness followed the scaling laws as was described in Section 3.2.3. For Test 1, a prop stiffness of $1.66kN/mm$ and for Test 4 a prop stiffness of $0.55kN/mm$ was reported by Lam (2010). The axial stiffness of prop for Test 4 with soft props is calculated by:

$$\left(\frac{EA}{L_{equivalent}} \right)_m = 0.55kN/mm \quad (5.6)$$

$$\left(\frac{EA}{L_{equivalent}} \right)_p = \left(\frac{EA_m}{L_{equivalent}} \right)_m * n = 0.55kN/mm * 60 = 33kN/mm \quad (5.7)$$

$$EA_p = \frac{100kN * L_{equivalent}}{mm} = \frac{33kN * 1m}{10^{-3}m} = 33000kN = 33E3kN, \quad (5.8)$$

where the $L_{spacing} = 5.4m$ and $L_{equivalent} = 1m$. Lam (2010) presented the lateral wall displacement and the vertical ground displacement in Figure 5.31. As illustrated, it is expected that both lateral wall displacement and vertical ground displacement will increase when using softer props with Test 4. The magnitude of the settlement obtained in the centrifuge tests shows significant influence due to the softer props. As seen in Figure 5.32 and Figure

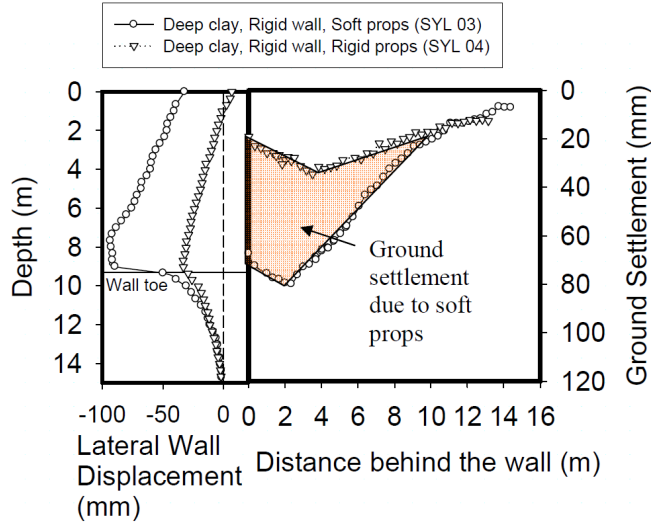


Figure 5.31: Lateral wall deflection and vertical ground displacement for Test 1 (SYL04) with stiff props and Test 4 (SYL03) with soft props (Lam, 2010).

5.33, both horizontal and vertical displacement showed a relatively small change due to softer props in PLAXIS. Test 1 and Test 4 from PLAXIS showed a small difference, and indicates that the difference of soft and stiff prop have a low influence. Additionally, Test 4 from centrifuge test was added in order to compare with the numerical calculations. Centrifuge Test 4 showed high values of vertical and horizontal displacement, and the position of the maximum vertical ground displacement moved towards the retaining wall. The difference between centrifuge Test 4 and PLAXIS Test 4 may be a combination of too stiff wall and props for the numerical model, that cause smaller vertical and horizontal displacements. The stiffness of soil might have an influence on the ground displacement. Note that both Test 1 and Test 4 is based on HSS10 soil model from Chapter 4. Another soil model, for instance HSS01, might provide another results, especially when the HSS01 gave larger vertical ground displacement and similar displacement shape than the HSS10.

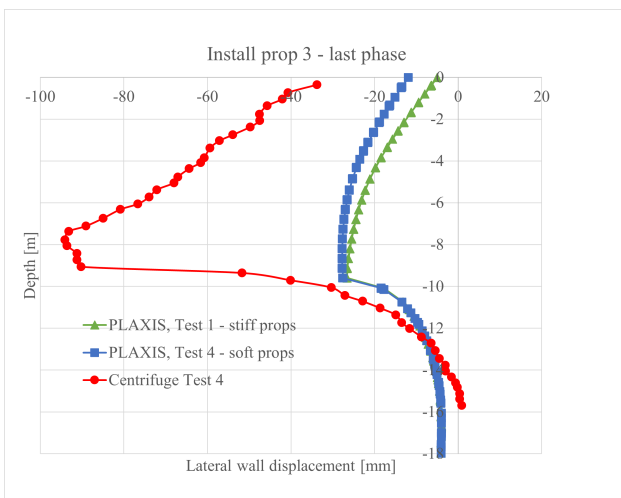


Figure 5.32: Lateral wall displacement of Test 1, Test 4 and centrifuge Test 4.

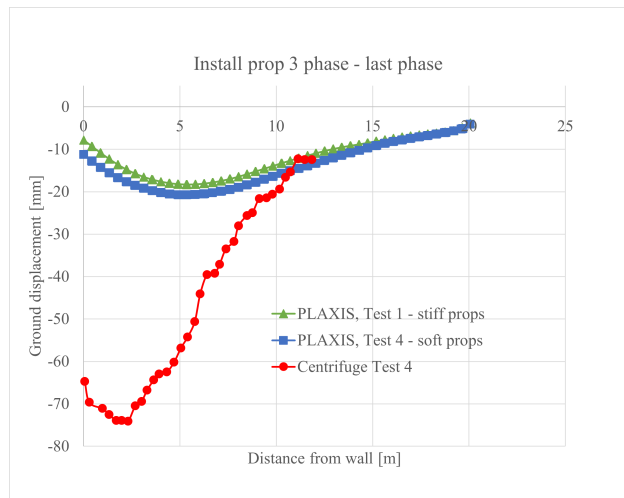


Figure 5.33: Vertical ground displacement of Test 1, Test 4 and centrifuge Test 4.

5.5.6 Test 2 with flexible wall

Test 2 (SYL05) performed by Lam (2010) focused on a floating flexible wall with stiff props. For this test, the retaining wall was modelled as a 2mm thick aluminium alloy representing a sheet pile wall with a stiffness EI of $10.4MNm^2/m$. The same scaling law procedure is accomplished for the SPW as for the DW in Section 3.2.2. The axial stiffness for the prototype scale is determined with the following equations:

$$EI_m = \frac{EI_p}{n^3} = \frac{10.4MNm^2/m}{60^3} = 0.048kNm^2/m \quad (5.9)$$

$$E_{rw} = \frac{EI_m}{I_{rw}} = \frac{0.048kNm^2/m}{\frac{(2mm/1000)^3}{12} * \frac{1}{1m}} = 72.2E6kN/m^2 = 72.222E3MPa \quad (5.10)$$

$$EA_m = E_{rw} * A_{rw} = 72.2E6kN/m^2 * \frac{2mm}{1000} * 1m * \frac{1}{1m} = 1.44E5kN/m \quad (5.11)$$

$$EA_p = EA_m * n = 1.44E5kN/m * 60 = 0.867E7kN/m \quad (5.12)$$

Specific weight is calculated by:

$$t_p = t_m * n = 2mm * 60 = 0.12m \quad (5.13)$$

$$m_p = \rho * V = 2700kg/m^3 * 0.12m * 1m * 1m = 324kg/(m * m) \quad (5.14)$$

$$F = m_p * g = 324kg/(m * m) * 9.81m/s^2 = 3178.44N/(m * m) = 3.17kN/(m * m) \quad (5.15)$$

The input parameters for the retaining wall of Test 2 are summarized in Table 5.11. The prop parameters and ground parameters remained identical to Test 1 (see Section 3.2). A slightly different excavation sequence was used for Test 2, and was adopted for the PLAXIS simulation.

Table 5.11: Prototype scale values calculation with model scale values for retaining wall parameters for Test 2.

Physical quantity parameter	Scaling factor	Model value	Prototype value
Flexural/bending stiffness pr. meter, EI	$1/n^3$	$0.048kNm^2/m$	$10.4E3kNm^2/m$
Axial stiffness, EA	$1/n$	$1.44E5kN/m$	$0.867E7kN/m$
Specific weight pr. meter, w	1	$3.17kN/m/m$	$3.17kN/m/m$
Poisson ratio, ν , [-]	1	0.32	0.32

Figure 5.34 shows the development of the vertical ground displacement and lateral wall displacement under construction stages. The last phase, *Install prop 3*, from the centrifuge test, was adopted in Figure 5.35 and Figure 5.36 in order to compare with the PLAXIS result. The result shows a similar horizontal wall displacement, but a rather considerable difference for the vertical ground displacements. The magnitudes for both vertical ground displacements and lateral wall deflection reveal very different values, as well as the maximum vertical ground displacement adjacent to the wall. The maximum vertical ground displacement and its position do not match for the centrifuge

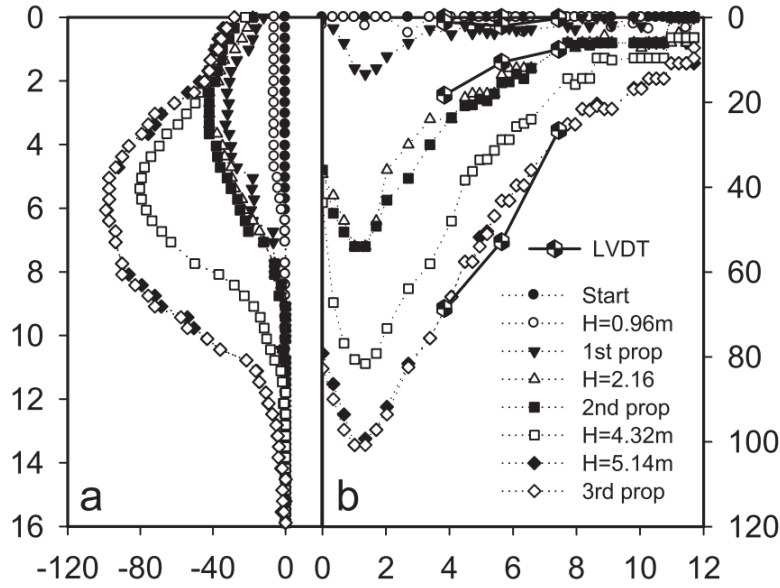


Figure 5.34: Lateral wall and vertical ground displacement for Test 2 (SYL05) (Lam, 2010).

test Test 2 and PLAXIS Test 2. The position of the horizontal maximum wall displacement do occur at the same

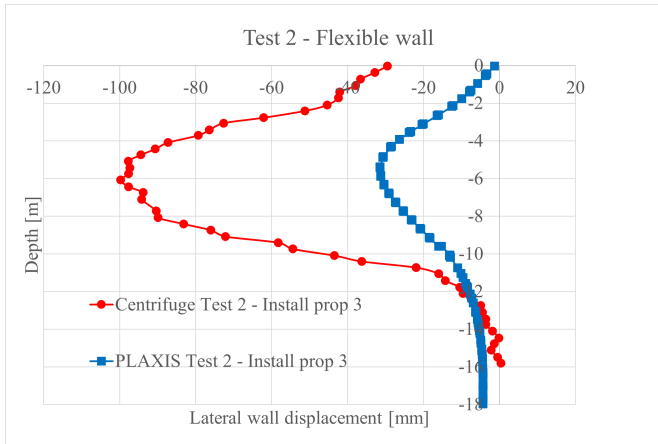


Figure 5.35: Lateral wall displacement of Test 2 with flexible wall.

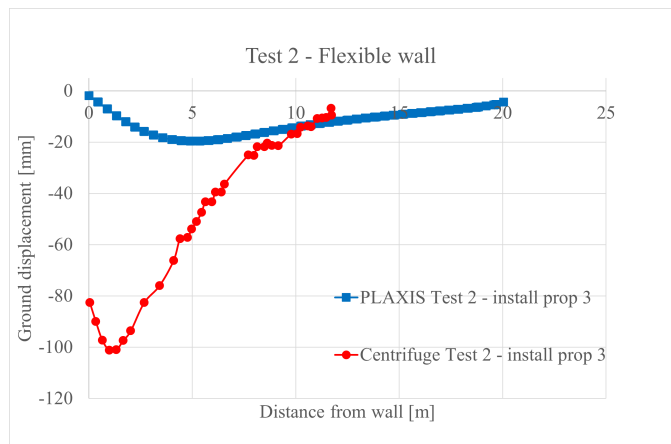


Figure 5.36: Vertical ground displacement of Test 2 with flexible wall.

depth, approximate around $5.4m$ depth, which is the final excavation depth. Overall, the comparison of centrifuge Test 2 and numerical model Test 2 shows a lack of similarity, despite some similar trends. This may be caused by too rigid wall and/or too stiff props in PLAXIS. Another factor, the magnitude of vertical and horizontal wall displacement from centrifuge test shows similar values as with centrifuge Test 4, and an explanation might therefore be softer soil model, for instance the HSS01.

5.5.7 Earth pressure

An aspect to carry out is to evaluate the earth pressure performance, in order examine the effect of input parameters in a deep excavation in soft clay. Although active and passive earth pressure theory are applicable in simple cases, multi-propped braced deep excavations tend to experience more complex earth pressures. Deep excavations require bracing if an economical design is to be achieved. The most common method for determine the soil pressure exerted on the retaining wall is Peck's apparent earth pressure diagrams (Hsu et al., 2014). Lam (2010) presented the earth pressure based on the apparent earth pressure calculation as follows:

$$K_a = 1 - m \left(\frac{4 * S_u}{\gamma * H} \right) = 1 - 0.4 \frac{4 * 27kPa}{16kN/m^3 * 5.4m} = 0.5 \quad (5.16)$$

$$\sigma_h^A = K_a * \gamma * H = 0.5 * 16kN/m^3 * 5.4m = 43.2kPa, \quad (5.17)$$

where $m = 0.4$. The apparent earth pressure from Test 1 (SYL04) and calculated from Peck's method is presented in Figure 5.37. SYL04 (i.e. rigid wall with rigid props) showed a much higher apparent earth pressure (see white dots in Figure 5.37). A simple total earth pressure is calculated based on active and passive earth pressure coefficients

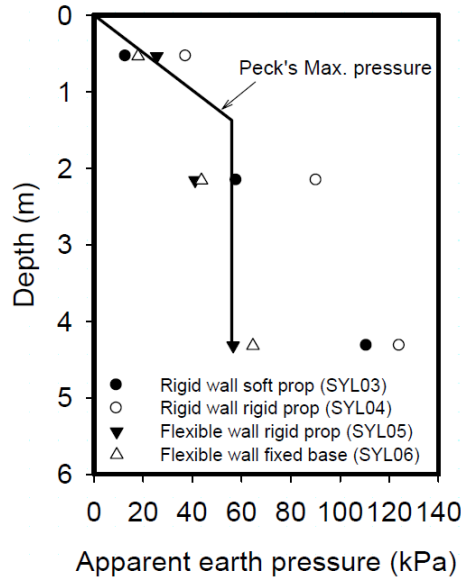


Figure 5.37: Apparent earth pressure of baseline Test 1 (SYL04) and Peck's maximum from estimation methods (Lam, 2010).

using Equation 3.28 in Section 3.3.2 with $\kappa = 2$ (when $r = 0$ and $f = 1$).

$$P_v = \gamma * z + q \quad (5.18)$$

$$P_{A/P} = p_v \mp \kappa_{A/P} * \frac{S_u}{F} = \gamma * z \mp \kappa_{A/P} * S_u \quad (5.19)$$

$$P_{A,z=0m} = -54kPa \quad P_{A,z=9,6m} = 99.6kPa \quad (5.20)$$

$$P_{P,z=5,4m} = 54kPa \quad P_{P,z=9,6m} = 121.2kPa \quad (5.21)$$

The obtained values consider only the last excavation stage and neglected soil-structure interaction effects by ignoring the retaining system stiffness. Therefore, these values give only an indication of the magnitude of the earth pressure. These values were also calculated by Lam (2010) and are represented by the stippled line in Figure 5.38.

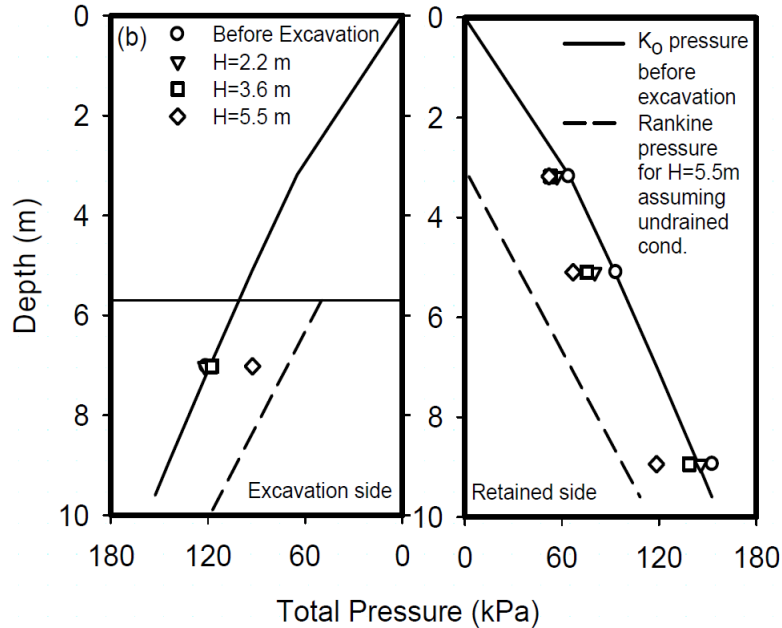


Figure 5.38: Total pressure for SYL05, (i.e Test 2 with floating, flexible wall with stiff props (Lam, 2010)).

The K_0 -line in Figure 5.38 represents the earth pressure coefficient at rest for all five centrifuge tests. The K_0 performance coincide with the assumed value from Section 3.3.2 with $K_0 > 1$ and in Chapter 5 SA with a $K_0 = 1.1$.

An interesting approach is the total earth pressure from the numerical calculations in PLAXIS and from the centrifuge test. The centrifuge test by Lam (2010) installed six earth pressure cells (EPC) on the retaining wall in the model setup, as illustrated in Figure 5.39. Four EPCs were positioned on the active side and two EPCs were installed on the passive side, which allows to calculate the total earth pressure to the wall.

Lam (2010) presented the total earth pressure from from EPC A1, EPC A2 and EPC A4 for Test 1 (SYL04) with different excavation depth, as seen in Figure 5.40. The total earth pressure at excavation depth at 5.4m is measured approximately as 34kPa for EPC A1, 74kPa for EPC A2 and 165kPa for EPC A4.

Basic hand calculation for earth pressure on active and passive side is earlier presented in Section 3.3.2, and represents the Rankine theory with $K_0 = 1.0$. Note that this calculation do not consider the wall or prop stiffness. From numerical calculations in PLAXIS and *total normal stresses* σ_N function, the total earth pressure can be calculated for active and passive side along the retaining wall. The PLAXIS output of earth pressure is presented in Appendix D. The total earth pressure from *install wall* phase can be compared with the total earth pressure K_0 -line before

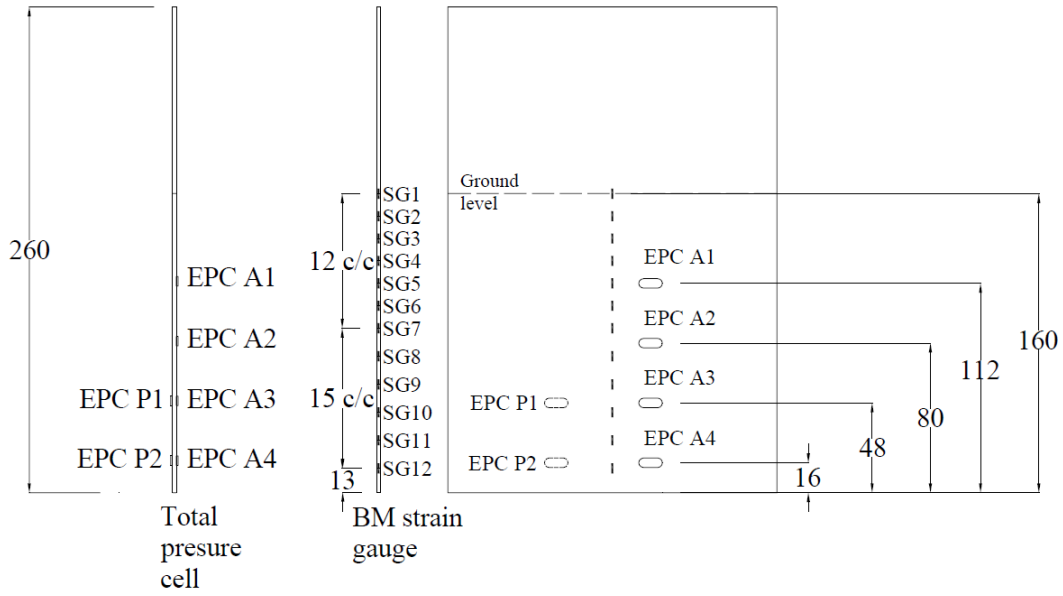


Figure 5.39: Position of EPC instruments in centrifuge model (Lam, 2010).

excavation. For the final excavation phase *install prop 3*, the total earth pressure from PLAXIS can be compared to the values from both Figure 5.38 and 5.40.

Test 1 Earth pressure

Earth pressure cells for Test 1 (rigid wall and stiff props) is installed and the total earth pressure is measured by Lam (2010). The centrifuge test measured the total earth pressure for EPC A1, EPC A2 and EPC A4 during the excavation process, as illustrated in Figure 5.40.

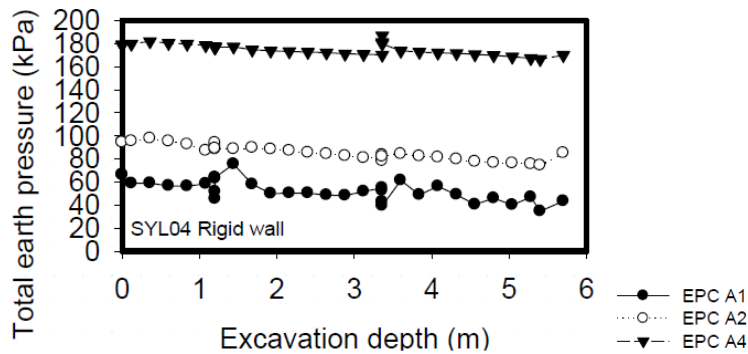


Figure 5.40: Test 1 (SYL04) - Total earth pressure with EPC A1, EPC A2 and EPC A4 measurement (Lam, 2010).

For Test 1, the centrifuge test only provided EPC values for the active side, not the passive side. Active and passive earth pressure presented in Figure 5.42 and Figure 5.41 show good and reasonable estimations for PLAXIS before and after excavation compared to classic Rankine theory. However, EPC measurements before and after excavation from the centrifuge test reveals higher earth pressure on the active side.

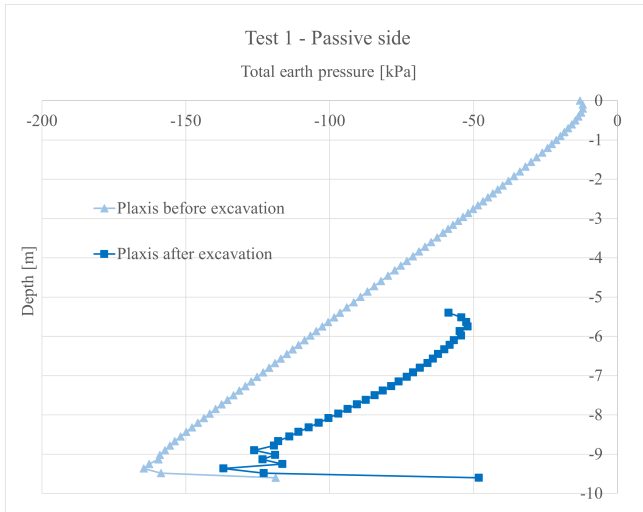


Figure 5.41: Test 1 - Total earth pressure of passive side.

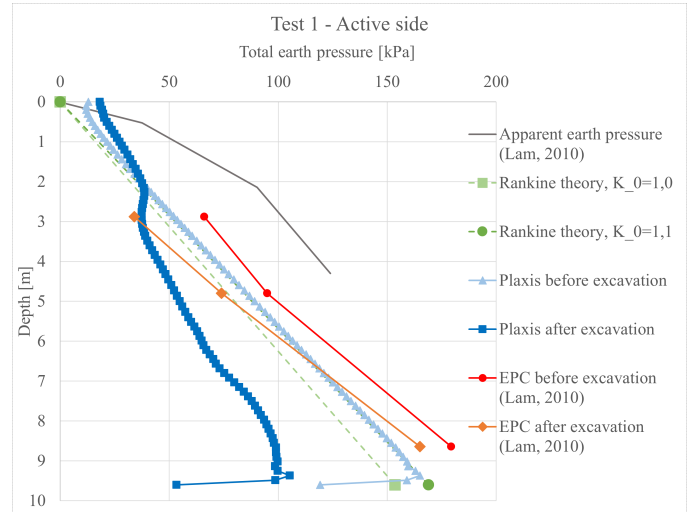


Figure 5.42: Test 1 - Total earth pressure of active side.

Test 2 Earth pressure

The EPC instruments for Test 2 obtained the following values: 153.6kPa for EPC A2, 67kPa for EPC A2 and 118kPa for EPC A4 at excavation depth 5.4m. Figure 5.44 and Figure 5.45 provides earth pressure calculations for the active

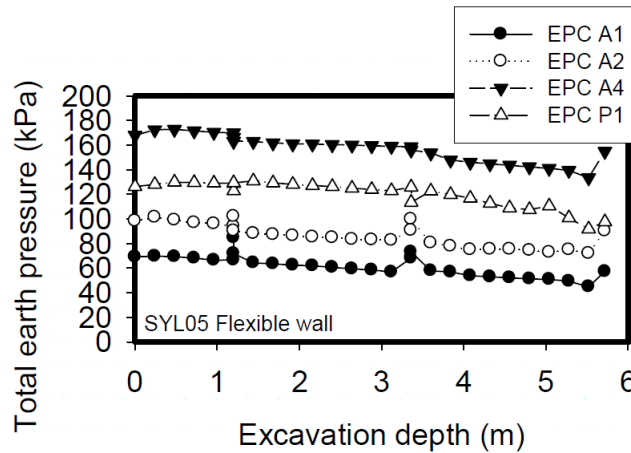


Figure 5.43: Test 2 (SYL05) - Apparent earth pressure (Lam, 2010).

and passive side before the excavation started. The Rankine theory $K_0 = 1.0$ -curve assumes isotropic consolidation, while Rankine theory $K_0 = 1.1$ -curve assumes anisotropic conditions. Additionally, the K_0 curve before and after excavation provided by Lam (2010) indicates a $K_0 = 1.1$ curve. Results from the PLAXIS earth pressure calculations are presented, as well as the EPC measured from Lam (2010). EPC measurements showed greater earth pressure compared to PLAXIS and Rankine theory.

Figure 5.46 and Figure 5.47 illustrates the passive and active earth pressure after excavation. Earth pressure calculations after the excavation was finalised show relatively good agreement between PLAXIS simulations and Rankine

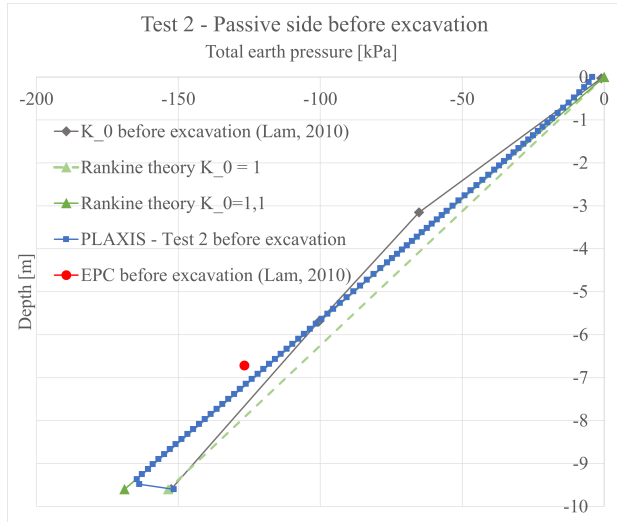


Figure 5.44: Test 2 - Total earth pressure on passive side before excavation.

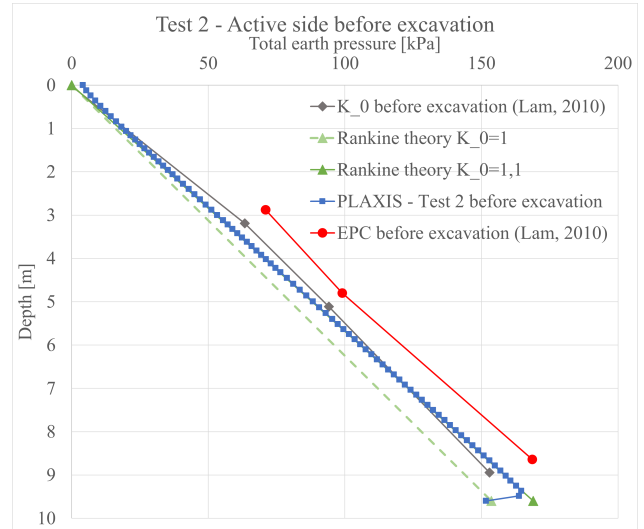


Figure 5.45: Test 2 - Total earth pressure on active side before excavation.

theory calculation for both passive and active side. Note that the Rankine theory and hand calculations on the active side show negative earth pressure at ground surface due to calculations without other factors, such as the prop stiffness. EPC measurements from Lam (2010) show slightly higher earth pressure values for both the passive and active side. On the active side, PLAXIS calculations shows good estimations, but differ in the higher depth due to the prop system.

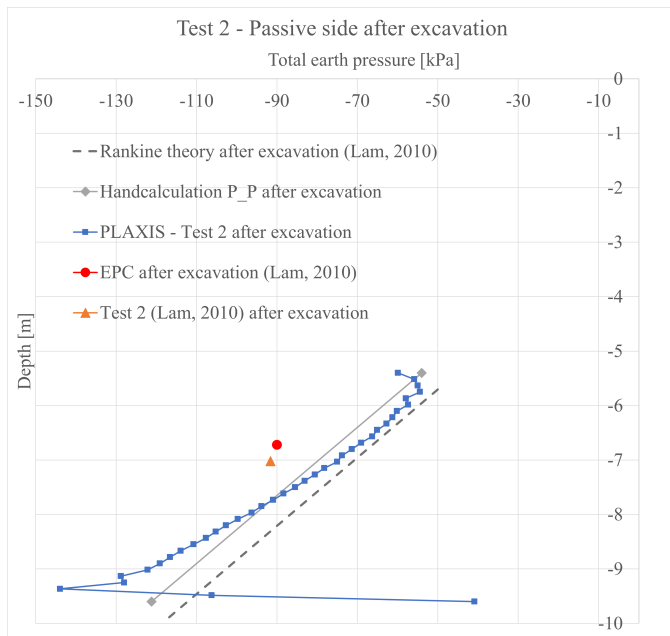


Figure 5.46: Test 2 - Total earth pressure on passive side after excavation.

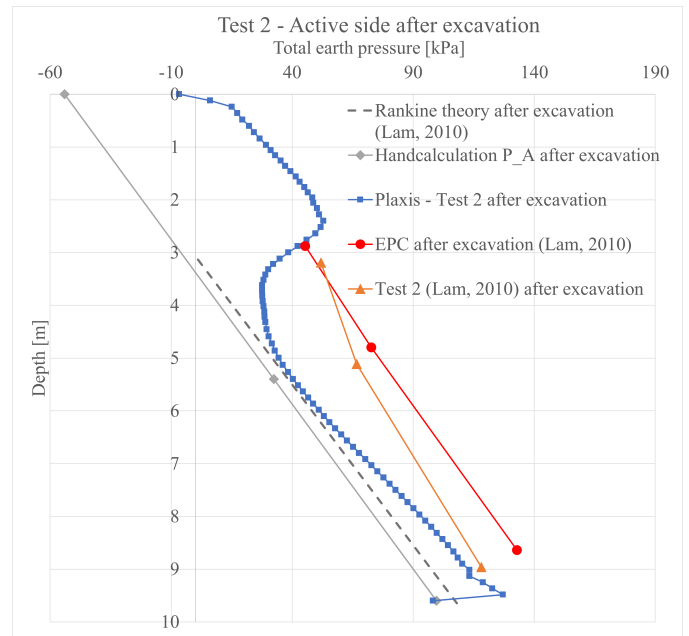


Figure 5.47: Test 2 - Total earth pressure on active side after excavation.

5.6 Validation of calibrated model

This chapter aims to investigate the soil behaviour in a deep excavation in soft clay based on the Hardening Soil Small model. Input parameters for the HSS model are based on the prominent model and scenario HSS10 from the sensitivity analyzes conducted in Chapter 5. By replicating characteristic soil response from the centrifuge test in a numerical model, a calibrated model can be developed in order to further investigate the influence of parameters of interest.

Vertical and horizontal ground displacements from the calibrated model are shown in Figure 5.48. The centrifuge test results are plotted for comparison. The comparison shows similar trends for the vertical ground displacement.

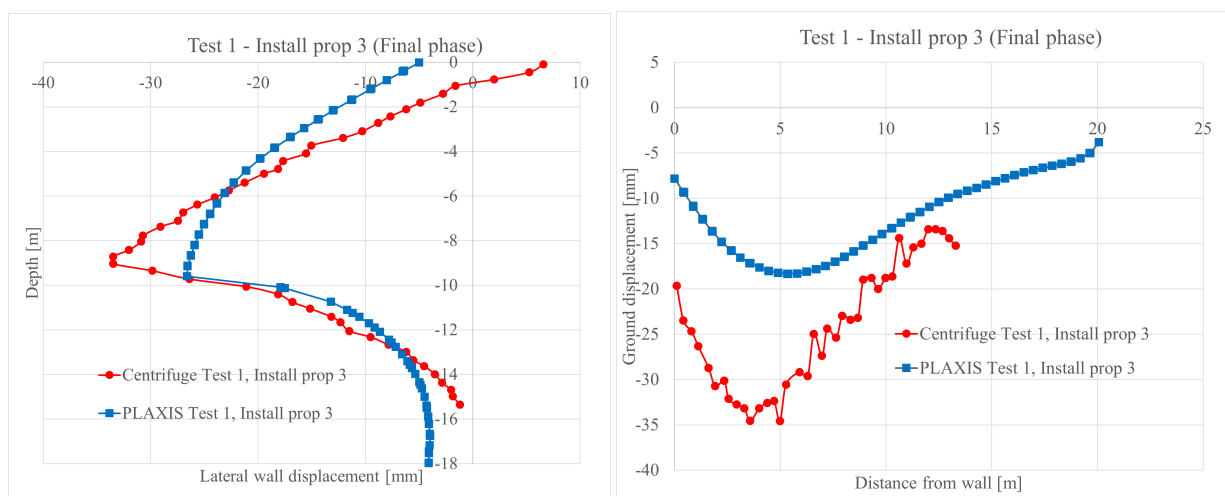


Figure 5.48: Test 1 a) Lateral wall displacement b) Vertical ground displacement

The maximum vertical displacement occurs at an approximate position from the wall and the shape of the ground displacement profile shows both a concave shape. However, the magnitude differs and may relate to the base heave in the excavation in PLAXIS. Additionally, the magnitude of the maximum vertical displacement adjacent to the wall is half the value of the centrifuge test. When it comes to the lateral wall displacement, it shows a more similar displacement magnitude. The maximum horizontal displacement has similar value, but the wall bending profile shows a less stiff wall than the centrifuge test. The wall deflection from the centrifuge test indicates either a stiffer bending stiffness for the wall or a stiffer axial stiffness for the props.

An analysis of the soil test where the shear strain and deviatoric stress is compared and fitted with the shear stress-strain curve provided from the triaxial test by Lam (2010). By adjusting parameters to replicate the measured stress-strain behaviour obtained in the triaxial test. Further, the construction stages for the HSS10 is presented in eight stages, and compared with the centrifuge test phases. The stages indicated a clear difference in the vertical ground displacement magnitude, but shows a rather similar trend in the vertical ground displacement profile and in the

lateral wall deflection.

Test 4 with soft props, however, shows a very different result in the displacement magnitude than the centrifuge test and indicates a lack of similarity, especially in the vertical ground displacements. Additionally, Test 2 with a flexible sheet pile wall is studied for both vertical and horizontal ground displacements. Similar trends as observed in Test 4 with a lack of ground displacement magnitude were found, but shows a corresponding vertical and lateral displacement profile and position of maximum vertical ground displacement.

Another aspect to evaluate the reliability of the numerical model, is to investigate the earth pressure acting on the retaining wall. In the centrifuge test, the earth pressure was measured by using EPCs, and provided data for the active and passive side before and after the excavation. Earth pressure measurements from the centrifuge tests revealed that Test 2 (i.e. flexible wall) causes a slightly increase in the earth pressure. However, Test 1 (i.e. baseline test) reveals a marginally lower earth pressure from PLAXIS compared to the centrifuge test. A closer investigation of total earth pressure for Test 1 and Test 2 is considered in this paper, and both tests with numerical calculations affirm relative good agreement with the centrifuge test.

The HSS10 model shows a lack of representing the other tests than Test 1. Based on vertical ground displacement and lateral wall deflection for Test 2 and Test 4, the HSS10 model represents an insufficient model. However, the HSS10 model indicates agreeable result compared to the centrifuge Test 1, such as imitating the stress strain curve from the centrifuge test and earth pressure profiles from EPC system.

5.6.1 PLAXIS model outputs

PLAXIS model outputs from calibrated model is presented in the Appendix B showing deformed mesh, total displacement and total deviatoric strain of soil. Additionally, total displacement, bending moment and shear force of the retaining wall is presented. Observations from PLAXIS output show significant base heave in the excavation from deformed mesh and is verified with high total displacement and deviatoric strain. The bending moment and shear force results indicates the influence of earth pressure and prop system resistance.

The validation of the calibrated model shows agreeable results with the centrifuge test and the PLAXIS outputs. The model will therefore be explored to investigate how the vertical ground displacements and lateral wall displacement change when considering the variation of uncertain parameters such as the bending stiffness, axial stiffness and specific weight under different uncertainties and assumptions. Further, the calibrated model will investigate the influence of uncertain parameters.

5.7 Summary

One of the research objectives is to develop a calibrated model that is able to estimate reliable ground displacement and investigate the influence of uncertain parameters. By replicating the soil behaviour from the centrifuge test in a numerical model in PLAXIS, a soil model may be considered as a calibrated model.

Although, the numerical modelling results which aimed to replicate Test 2 (flexible wall) and Test 4 (soft props) showed a considerable difference in ground displacements, the results of Test 1 indicated a reasonably good estimation. Additionally, Test 1 with HSS10 model shows an agreeable stress-strain curve and earth pressure. For this reason, the model HSS10 was considered to be adequate to be used for further studies that aimed to investigate how uncertain parameters influence the ground displacement. However, further work is recommended to better replicate the centrifuge test series by Lam (2010) in order to obtain a more reliable numerical model. This work should focus on investigating how the soil stiffness affects the vertical ground displacement and lateral wall deflection. Note that the numerical model is based on FEM that considers a plain strain scenario, while the centrifuge test is a laboratory test in model scale. The hence of replicating the soil behaviour and capture the characteristic soil response from an excavation is to develop a relative calibrated in order to estimate ground displacement, and is concluded to have been accomplished. Further, the HSS model with HSS10 soil properties represents the calibrated model with parameters presented in Table 5.12.

Table 5.12: Calibrated model: Input parameters for Test 1 with HSS10 model in PLAXIS.

Parameter	Value
Drainage type	Undrained (B)
Unit weight of soil, γ_s	$16kN/m^3$
Secant stiffness, E_{50}^{ref}	$4MPa$
Tangent stiffness, E_{oed}^{ref}	$4MPa$
Unloading/reloading stiffness, E_{ur}^{ref}	$16MPa$
Power, m	1
Undrained shear strength, S_u^{ref}	$27kPa$
Threshold shear strain, $\gamma_{0.7}$	0.0002
Shear modulus, G_0^{ref}	$22MPa$
Interface roughness, $R_{inter,soil}$	1.0
Interface roughness, $R_{inter,wall}$	0.5
Earth pressure coefficient at rest, K_0	1.1

Chapter 6

Effect of wall stiffness

This chapter contains of an evaluation of how sensitive the ground displacement and wall deflection is when varying different parameters with a calibrated model. The calibrated model is based on Test 1 from Lam (2010) and is conducted using the HSS10 (i.e. calibrated Hardening Soil Small model) in PLAXIS. Finally, this chapter will investigate how the ground displacement is influenced by varying uncertain parameter, such as the wall stiffness.

This chapter aims to distinguish the influence of an uncertain parameter of interest, the wall stiffness, by varying the parameters in a calibrated model. The calibrated model is based on the HSS model with Test 1 inputs and earlier sensitivity analysis. The result of the vertical ground displacement and wall deflection is based on the HSS10 with soil input parameter from Table 5.12, retaining wall input parameters from Table 3.2 and prop input parameters from Table 3.3. The HSS10 scenario will be specified as the calibrated model for further investigations.

Note that the term *uncertain* determines the parameters that will be conducted in the parameter variation analysis, in order to achieve a better understanding of the influence of the parameters when estimating the ground displacement.

6.1 Parameter variation analysis of wall stiffness

This section investigates how the ground displacement is influenced by varying the uncertain parameter of wall stiffness. A parameter variation (PV) will be conducted for investigating the sensitivity of varying the wall properties and its influence on the ground displacement and wall deflection. An evaluation of varying the wall stiffness properties will check the effect on the ground movement. The calibrated model is based on the centrifuge Test 1 of an aluminium alloy plate replicating a 0.36m thick diaphragm wall with bending stiffness $280.8MNm^2/m$, axial stiffness $6.60E7kN/m$ and specific weight $9.53kN/(m * m)$.

Due to the numerical calculations in PLAXIS with *plate-tool* as a retaining wall, the calculations assumes a rectangular cross section. A sheet pile wall will therefore not give reasonable values when calculating, especially for thickness and specific weight. However, a concrete diaphragm wall is applicable and gives reasonable values and will therefore be considered in this parameter variation. For a concrete diaphragm wall, a Young's modulus of $E = 30GPa$, a Poisson's ratio of $\nu = 0.15$ and a mass density of $\rho = 2400kg/m^3$ is defined (Manie and Chatterjee, 2015). Note that these material properteis will be adopted for the model PV - 0 (calibrated) and will be specified as fixed in this chapter, as presented in Table 6.1. This scenario is presented in order to represent a more realistic scenario compared to the centrifuge test which considers typical material properties of a diaphragm wall, rather an artificial wall of aluminium alloy.

Table 6.1: PV Calibrated CT and PV calibrated

Parameter	Model	
	PV Calibrated CT	PV - 0 (calibrated)
Model ID	Aluminium alloy	Concrete diaphragm wall
Material	Aluminium alloy	Concrete diaphragm wall
Poisson's ratio, ν	0.32	0.15
Young's modulus, E	$72.2E6kN/m^2$	$30E6kN/m^2$
Mass density, ρ	$2700kg/m^3$	$2400kg/m^3$

Table 6.1 shows two scenarios, where the first *PV Calibrated CT* is based on the calibrated centrifuge Test 1 developed from previous chapters, which is the HSS10 model presented in the previous chapters. The second scenario *PV - 0 (calibrated)* is based on the bending stiffness EI from centrifuge Test 1 and additional parameters such as axial stiffness EA and specific weight w are calculated based on the fixed bending stiffness and by using the material properties for the diaphragm wall as described above. The parameter variation includes in addition 4 scenarios: PV-1-DW, PV-2-DW, PV-3-DW and PV-4-DW as presented in Table 6.2. The PV-1-DW and PW-2-DW represent the higher estimates (HE) of the bending stiffness EI , while PV-3-DW and PV-4-DW consider lower estimates (LE) of the bending stiffness.

Table 6.2: Parametric variation analysis.

Parameter variation ID	Range	Wall stiffness calculations						
		EI [kNm^2/m]	I [m^4]	t [m]	A [m^2]	EA [kN/m]	m [$kg/(m * m)$]	w [$kN/(m * m)$]
PV Calibrated CT	-	$280.8E3$	$1.8E-8$	0.36	$6E-3$	$2.60E7$	972	9.53
PV - 0 (Calibrated)	-	$280.8E3$	$9.36E-3$	0.48	$4.82E-1$	$1.45E7$	1158	11.36
PV-1-DW	x2.0	$5.62E5$	$1.87E-2$	0.608	$6.08E-1$	$1.82E7$	1460	14.3
PV-2-DW	x4.0	$1.12E6$	$3.74E-2$	0.766	$7.66E-1$	$2.30E7$	1840	18
PV-3-DW	x0.5	$1.40E5$	$4.68E-3$	0.383	$3.83E-1$	$1.15E7$	919	9.02
PV-4-DW	x0.25	$7.02E4$	$2.34E-3$	0.304	$3.04E-1$	$9.12E6$	729	7.16

Notations: Calculations is based on a DW.

The first scenario PV Calibrated CT and the second scenario PV - 0 (calibrated) is based on the same bending stiffness EI . The two scenarios are illustrated in Figure 6.1, and show quite similar trends. Note that the calibrated curve conducted with centrifuge test (i.e. PV Calibrated CT) gives a good estimation with calibrated curve (i.e. PV - 0 (calibrated)) from the calculations described above. Both models indicates nearly identical ground displacement profiles and are reasonably well fit with the centrifuge test results as presented in Chapter 3. A parameter validation will therefore further be analysed based on the PV - 0 (calibrated) curve and calculations.

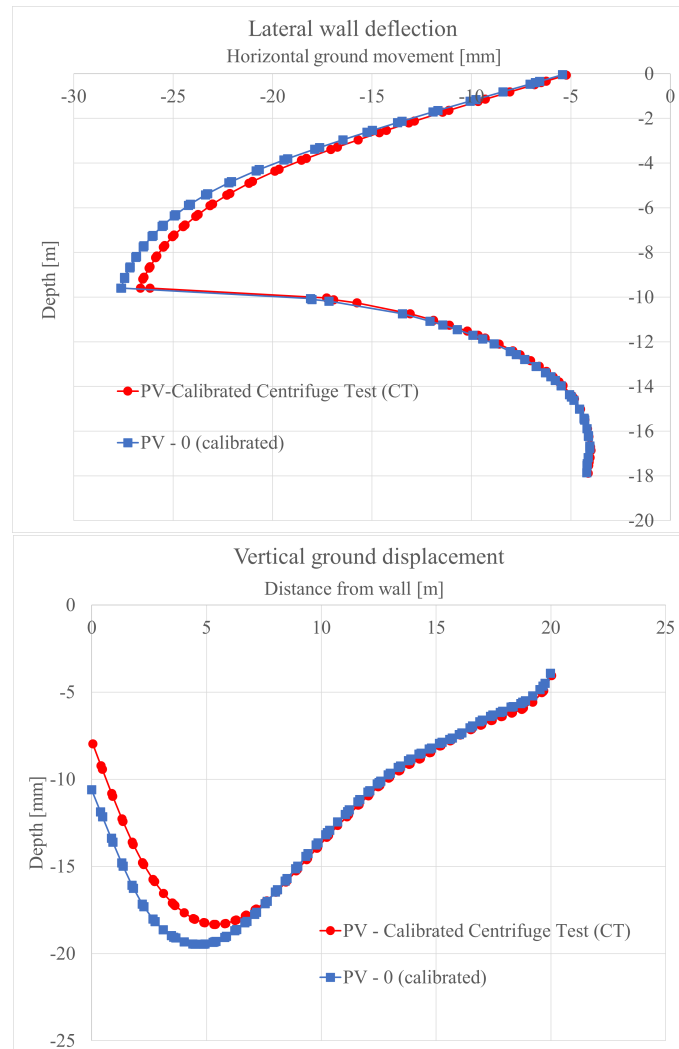


Figure 6.1: Lateral wall and vertical ground displacement profiles with *PV - Calibrated Centrifuge Test (CCT)* and *PV - 0 (Calibrated)*. FIKS BILDE med lateral wall

Further values from the different scenarios are presented in Table 6.2 and calculated with the following equations. Note that scenario PV-1-SPW to PV-4-DW follows the same calculation procedure as PV - 0 (calibrated). The bending stiffness EI from PV - Calibrated CT is multiplied with a factor of 2 and 4, and divided with a factor of 2 and 4, in order to create low estimate and high estimate. Consequently, provides the bending stiffness EI for all the sce-

narios. The following calculations is estimated for further calculations of all scenarios including PV - 0 (calibrated). First, the second moment of area I is calculated by:

$$I = \frac{EI_p}{E}, \quad I = \frac{t * h^3}{12}, \quad (6.1)$$

where E is the Young's modulus. The second moment of area I is used to calculate the thickness t of the retaining wall. The area A and axial stiffness EA are calculated by:

$$A = \frac{t}{1000} * 1m * \frac{1}{1m} \quad (6.2)$$

$$EA = E * A \quad (6.3)$$

The values for estimating the mass weight m and specific weight w were derived as follows:

$$m = \rho * V = \rho * t * 1m * 1m \quad (6.4)$$

$$w = m * g, \quad (6.5)$$

where g is the gravitational acceleration $9.81m/s^2$ and the mass density ρ is defined as $2400kg/m^3$ for a concrete diaphragm wall (Manie and Chatterjee, 2015).

The parameter validation contains of the following and the input values will be taken from Table 6.2:

- Vary the bending stiffness EI , and keep other parameters fixed as in the model PV - 0 (calibrated)
- Vary the axial stiffness EA , and keep other parameters fixed as in the model PV - 0 (calibrated)
- Vary both EI and EA (correspondingly), and keep other parameters fixed as in the model PV - 0 (calibrated)
- Vary EI , EA and w (correspondingly), and keep other parameters fixed as in the model PV - 0 (calibrated)

Analyzing certain parameters by variation and keep additional parameters fixed (e.g. varying only EI), in order to investigate the impact of single property only.

6.1.1 Vary only bending stiffness EI

By varying only the bending stiffness EI , it was obtained that higher value of stiffness result in lower displacements, as expected. The horizontal wall displacement shows a higher bending of the wall with lower level of stiffness. This indicates more bending for flexible walls rather than rigid walls. The vertical ground displacement increases when the bending stiffness decreases, and opposite. The position of the maximum vertical displacement tends to move forward against the retaining wall when bending stiffness decreases, and the maximum vertical displacement adjacent to the wall increase.

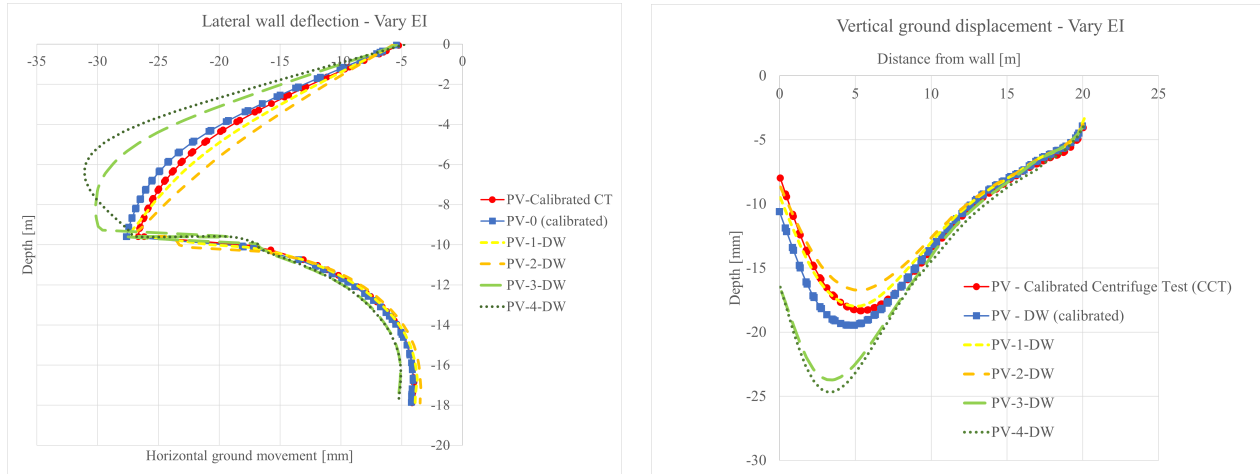


Figure 6.2: Parameters variation of bending stiffness EI .

6.1.2 Vary only the axial stiffness EA

The axial stiffness EA appears to have an insignificant influence on the vertical ground displacement and lateral wall deflection. This is due to no axial load other than the weight of the wall itself. Small changes in the magnitude of the displacement and displacement shape for all scenarios.

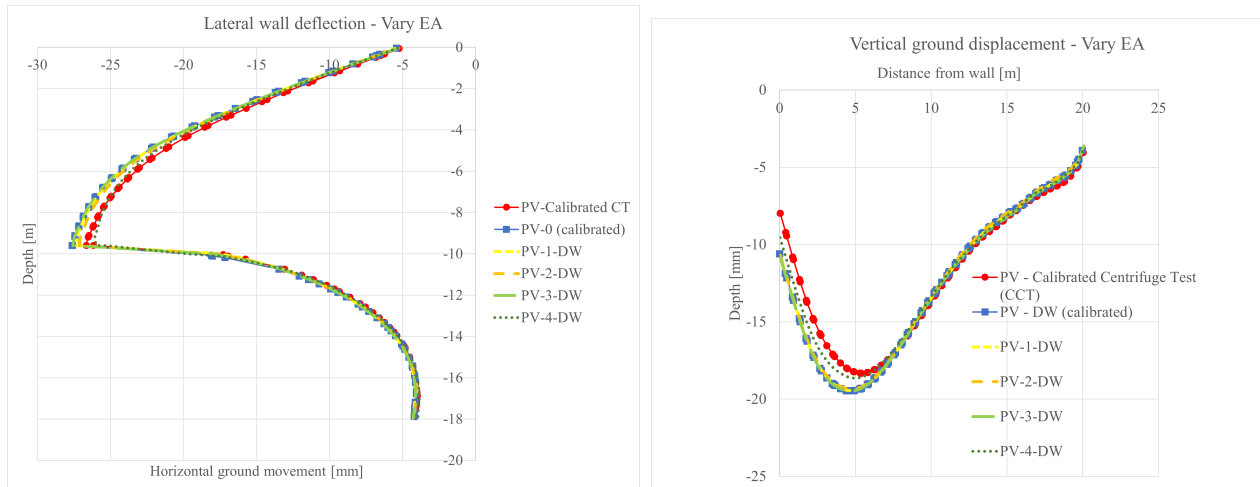


Figure 6.3: Parameter variation of axial stiffness EA .

6.1.3 Vary bending stiffness EI and axial stiffness EA

Varying both bending stiffness EI and axial stiffness EA , gives similar result when only varying the bending stiffness EI , as presented in Figure 6.2. This confirms that the influence of EA is insignificant and play a negligible role in the vertical ground displacement and lateral wall deflection. Similar conclusion of the bending stiffness is therefore already obtain when only varying the bending stiffness.

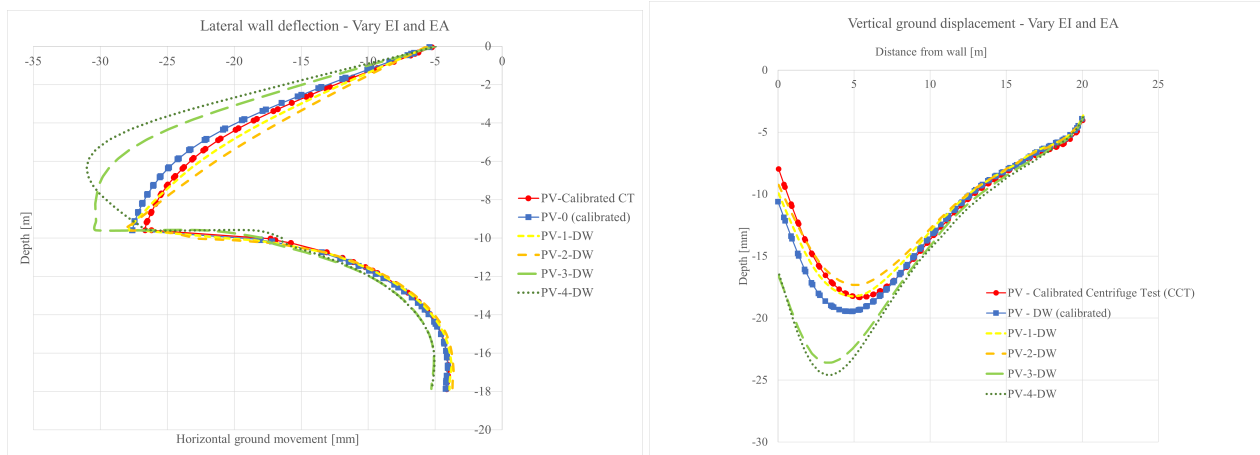


Figure 6.4: Parameter variation of bending stiffness EI and axial stiffness EA .

6.1.4 Vary bending stiffness EI , axial stiffness EA and specific weight w

By varying the bending stiffness EI , axial stiffness EA and specific weight w , the results reveals quite different displacements. For the vertical ground displacement, the PV-1-DW and PV-2-DW gives more vertical displacement and higher maximum displacement adjacent to the wall. Additionally, the vertical displacement shape changes from a concave to spandrel. This indicates a heavy wall with a high specific weight w that correspondingly drags the wall by gravity and the vertical displacement along the wall increase with the direction of the wall. The calculations of specific weight is based on thickness estimations from assumed bending stiffness EI .

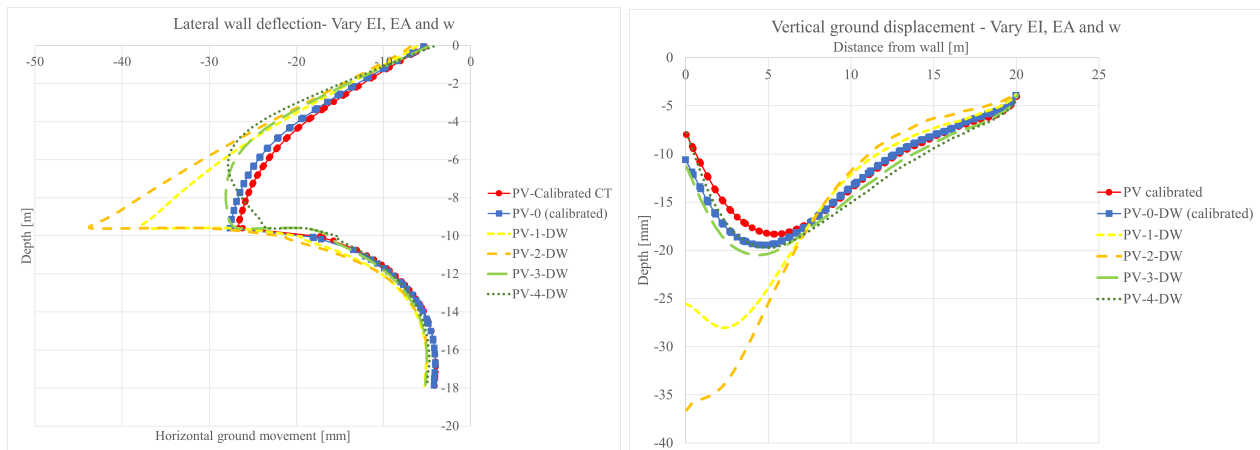


Figure 6.5: Parameter variation of bending stiffness EI , axial stiffness EA and specific weight w .

Overall, the results from the parameter variation of bending stiffness EI , axial stiffness EA and specific weight w show how the input parameters in PLAXIS influence the vertical ground displacement and horizontal wall displacement. Together these results provide important insights into their ability and importance of the wall stiffness properties. The results show that the axial stiffness EA has an insignificant influence on the ground displacement. Unlike the specific weight w and bending stiffness EI . The specific weight w is based on calculations of EI and

EA following Equations 6.5. The calculations gives large value of specific weight and consequently large vertical deformations. This may be a consequent of a too heavy wall on a too soft clay. Due to an insignificant influence of the axial stiffness EA and an unreasonable calculation of specific weight w for a DW when dealing with soft clay. A further investigation of varying only the bending stiffness EI , while keep specific weight w and axial stiffness EA fixed as the calibrated scenario PV - 0 (calibrated).

6.2 Parameter variation analysis of bending stiffness EI

A parameter variation for the bending stiffness EI is further conducted. All input parameters are fixed and follows PV - 0 (calibrated), except from the bending stiffness EI which follows Table 6.3. The bending stiffness EI is multiplied with factor of 10, 50 and 100 as higher estimates. Additionally, dividing the EI with 10, 50 and 100 accordingly, and represents the lower estimates.

Table 6.3: Parameter variation for bending stiffness EI .

Parameter variation ID	Range	EI , [MNm^2/m]
PV - Calibrated CT	–	280.8
PV - 0 (calibrated)	–	280.8
PV - 1	x10	2808.0
PV - 2	x50	14040.0
PV - 3	x100	28080.0
PV - 4	÷10	28.08
PV - 5	÷50	5.616
PV - 6	÷100	2.808

The scenarios PV-1, PV-2 and PV-3 represent lower estimates, while the scenarios PV-3, PV-4 and PV-5 represent higher estimates. All scenarios are obtained from PLAXIS and presented in Figure 6.6 for vertical ground displacements and in Figure 6.8 for lateral wall displacements. As was expected, the figures show that the vertical and horizontal displacements increase when the bending stiffness EI decreases. Additionally the magnitude of both vertical ground displacement and lateral wall displacement increases when the bending stiffness decrease.

6.2.1 Vertical ground displacement

The graphs in Figure 6.6 show a gradual increase in vertical ground displacement S_v for PV-4, PV-5 and PV-5 with lower bending stiffness EI . However, PV-5 and PV-6 shows nearly identical vertical displacement profile, magnitude and shape although PV-6 have two times lower bending stiffness value than PV-5. The distance of the maximum vertical displacement from the retaining wall increase when the bending stiffness increase, and moves towards the wall for lower bending stiffness scenarios. Additionally, the maximum vertical displacement adjacent to the wall decreases when the bending stiffness increases. From Figure 6.6, the position of the maximum vertical ground displacement tends to move towards the retaining wall at lower bending stiffness, and moves away from wall with higher bending stiffness values.

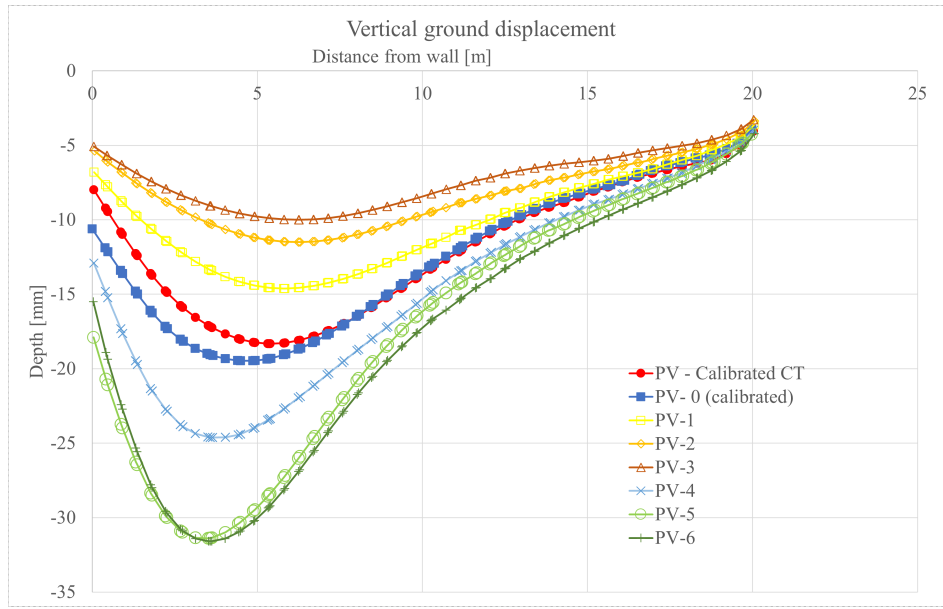


Figure 6.6: Vertical ground displacements when varying bending stiffness EI .

6.2.2 Horizontal ground displacement

Horizontal ground displacement S_h behind the retaining wall illustrated in Figure 6.7 shows smaller maximum displacement compared to the vertical ground displacement. The displacement reveals less magnitude of displacement, but shows similar concave displacement profile as the vertical ground displacement. The maximum horizontal ground displacement adjacent to wall remains at a certain value for all scenarios. The maximum horizontal ground displacement increase when the bending stiffness decrease, and decreases when the bending stiffness increases.

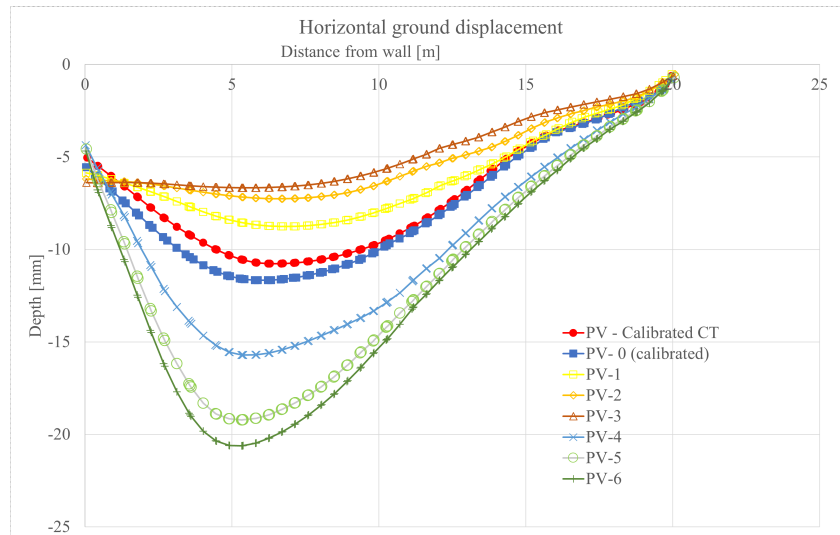


Figure 6.7: Horizontal ground displacements when varying bending stiffness EI .

6.2.3 Lateral wall deflection

The lateral wall displacement δ_w (i.e. horizontal ground displacements adjacent to the retaining wall) in Figure 6.8 shows the the of displacement shape differs with EI . There is a clear correlation between bending stiffness of wall and horizontal displacement profile, which can be seen in the displacement profile with different bending stiffness. Higher bending stiffness values generate more linear horizontal displacement profile due to the linear wall deflection, for instance the PV-1, PV-2 and PV-3. For high bending stiffness EI values, the wall can be defined as rigid and rotates towards the excavation without experiencing notable bending. The horizontal displacement deflects non-linear at lower levels of bending stiffness, as modelled in the scenarios PV-4, PV-5 and PV-6. The maximum horizontal displacement increases with lower levels of bending stiffness, and decreases at higher levels of bending stiffness. Note that the maximum ground displacement for softer bending stiffness occurs at the excavation depth, and at wall depth for stiffer bending stiffness. However, the maximum horizontal displacement at surface shows negligible changes when varying the bending stiffness. This may be caused by the influence of props and their stiffness.

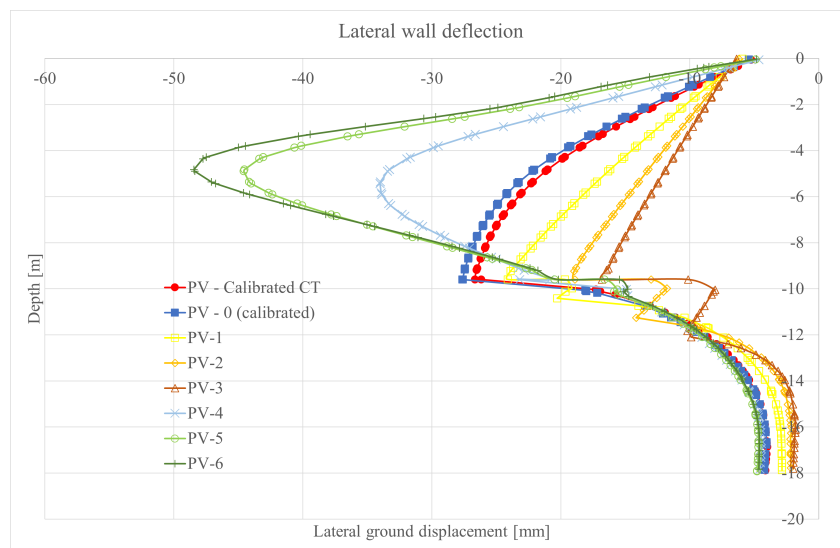


Figure 6.8: Lateral wall deflection (i.e. horizontal ground displacements adjacent to the retaining wall) when varying bending stiffness EI .

6.2.4 Maximum vertical ground displacement

The maximum vertical displacement $S_{v,max}$ is plotted against the bending stiffness in semi-logarithmic scale in Figure 6.9 to summarize the presented scenarios. The summary reveals a gradual decrease in maximum vertical displacement when the bending stiffness increases. The scenarios indicates a linear relation in a semi-logarithmic scale, and represents the trend line. With a trend line from a calibrated model, one may use the trend line and semi-logarithmic graph to determine the required bending stiffness for a certain maximum vertical ground displacement. For instance, with a bending stiffness EI of $10MNm^2/m$ will generate approximate $28mm$ of maxi-

imum vertical ground displacement. Note that the calibrated model is developed for a single ground condition, in this case, the HSS10 soil model.

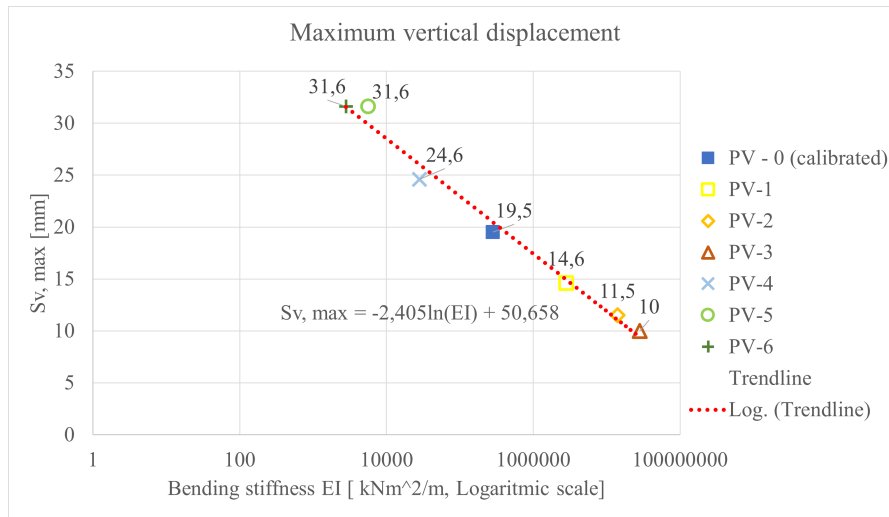


Figure 6.9: Maximum vertical ground displacement at soil surface versus bending stiffness EI .

6.2.5 Maximum horizontal ground displacement

The maximum horizontal ground displacement $S_{h,max}$ at ground surface indicates a linear relation in the semi-logarithmic scale, as presented as a trend line in Figure 6.11. A clear increase in the maximum horizontal ground displacement when the bending stiffness decreases. The linearly relation is similar to the maximum vertical displacement in Figure 6.9, but is located in a lower range of displacement values. The $S_{h,max}$ equation presented in the figure may be used to identify the maximum horizontal ground displacement for a certain bending stiffness.

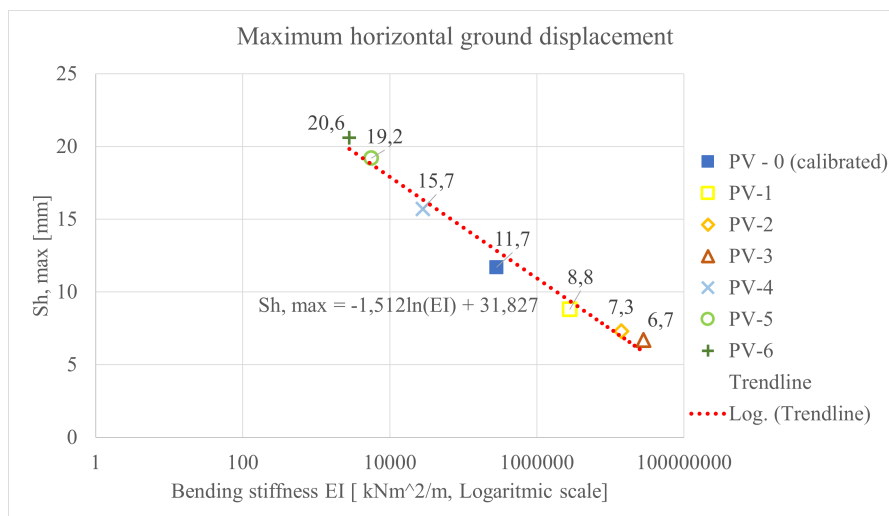


Figure 6.10: Maximum horizontal ground displacement versus bending stiffness EI .

6.2.6 Maximum lateral wall deflection

The maximum lateral wall deflection $\delta_{w,max}$ (i.e. horizontal displacement along the retaining wall with) with varied bending stiffness is presented in Figure 6.11. The result shows that the maximum lateral wall deflection increases when the bending stiffness decreases.

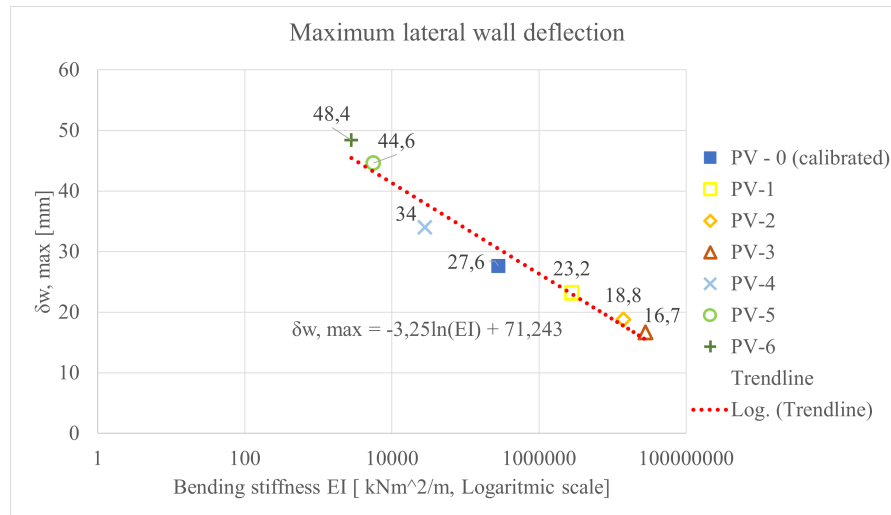


Figure 6.11: Maximum lateral wall deflection versus bending stiffness EI .

6.2.7 Maximum vertical ground displacement adjacent to wall

The maximum vertical ground displacement adjacent to the retaining wall is summarized in Figure 6.12 for different bending stiffness. The maximum vertical displacement adjacent to the wall decreases when the bending stiffness increases. The relation follows a linearly line in a semi-logarithmic scale, but PV-5 shows a slightly higher maximum vertical displacement compared to PV-6 with a greater bending stiffness.

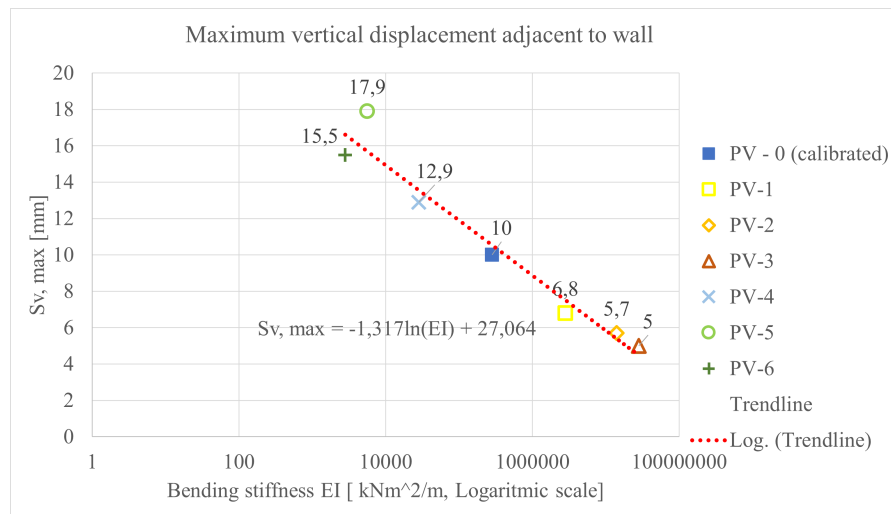


Figure 6.12: Maximum vertical ground displacement adjacent to retaining wall versus bending stiffness EI .

6.2.8 Maximum horizontal ground displacement adjacent to wall

For the maximum horizontal ground displacement adjacent to the wall at the ground surface increases when the bending stiffness increases, as illustrated in Figure 6.13. This can be describes as a result of the combination of cantilever wall deflection and prop system stiffness influence. Accordingly, the relation indicates a linearly trend line. An interesting finding is that maximum horizontal ground displacement adjacent to the wall increases when the bending stiffness increases, which the opposite of what the maximum vertical ground displacement revealed.

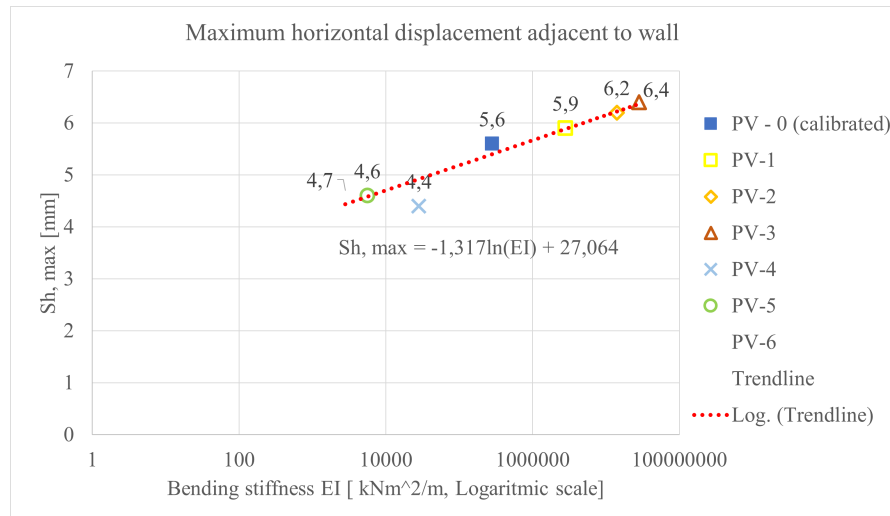


Figure 6.13: Maximum horizontal ground displacement adjacent to retaining wall versus bending stiffness EI .

6.2.9 Maximum lateral wall deflection at ground surface

The maximum lateral wall deflection at ground surface with varied bending stiffness is presented in Figure 6.14. The results indicate similar trends as the maximum horizontal ground displacement adjacent to the wall, with an increase in the displacement when the bending stiffness increases. The summary shows a linear correlation in a semi-logarithmic scale.

6.2.10 Position of maximum vertical ground displacement

The position of the maximum vertical displacement from the retaining wall shows an increase when the bending stiffness increase. This may result from an increase of the maximum vertical displacement accordingly. The relation shows a gradual increase in Figure 6.15. A roughly assumption, the plots indicates an almost double distance from the wall, with highest estimate PV-3 and lowest estimate PV-6. This contributes with relevant knowledge to the extent of the excavation-induced displacement field. The trend line may be used to define the position of the maximum vertical ground displacement with a certain bending stiffness with respect to adjacent constructions. This may indicate where the influence zone is affecting and give guidance in the design phase.

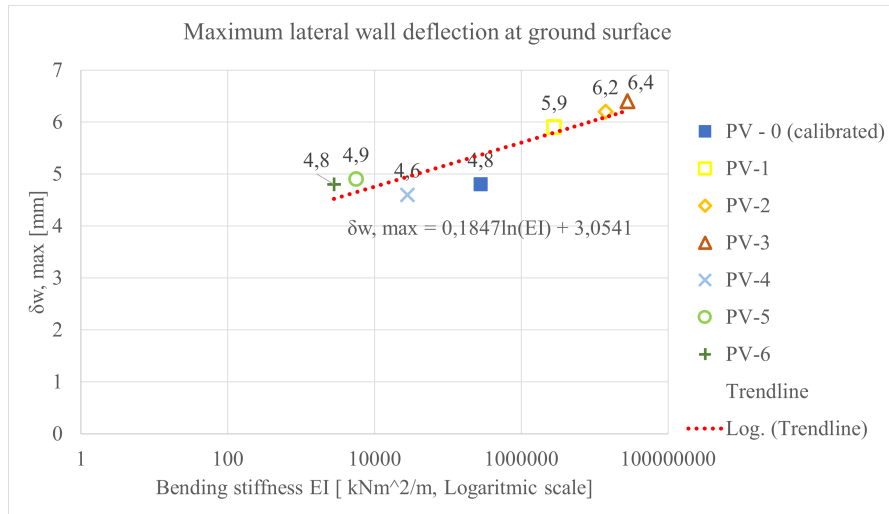


Figure 6.14: Maximum lateral wall deflection (i.e. horizontal ground displacement adjacent to the retaining wall) versus bending stiffness EI .

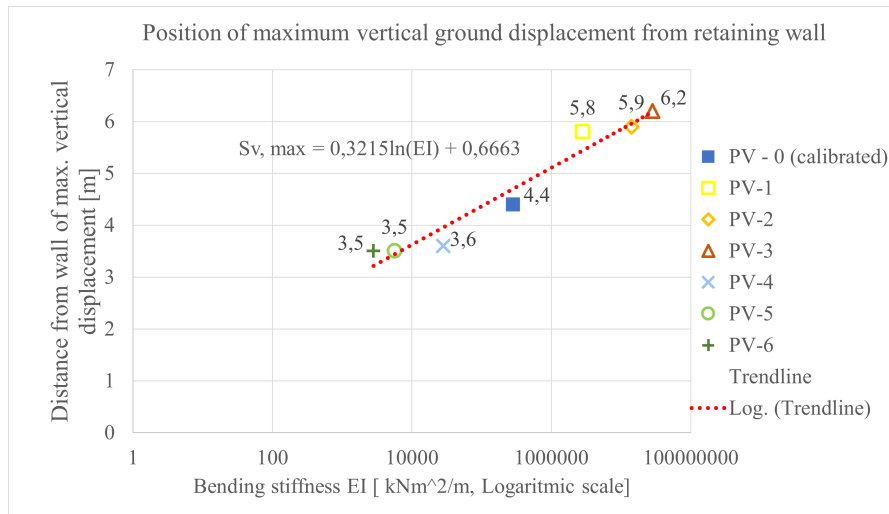


Figure 6.15: Position of maximum vertical ground displacement when varying bending stiffness EI .

6.2.11 Position of maximum horizontal ground displacement

The position of the maximum horizontal ground displacement at ground surface shows a rather different development of the displacement profile when varying the bending stiffness, which is illustrated in Figure 6.16. According to the calculations, the distance of the maximum horizontal ground displacement increases and moves away from the wall when the bending stiffness increases. However, the increase is rather slight compared to the other trend lines as presented and scenario PV-5 and PV-6 indicates that the position tend to move towards the wall when the bending stiffness increases.

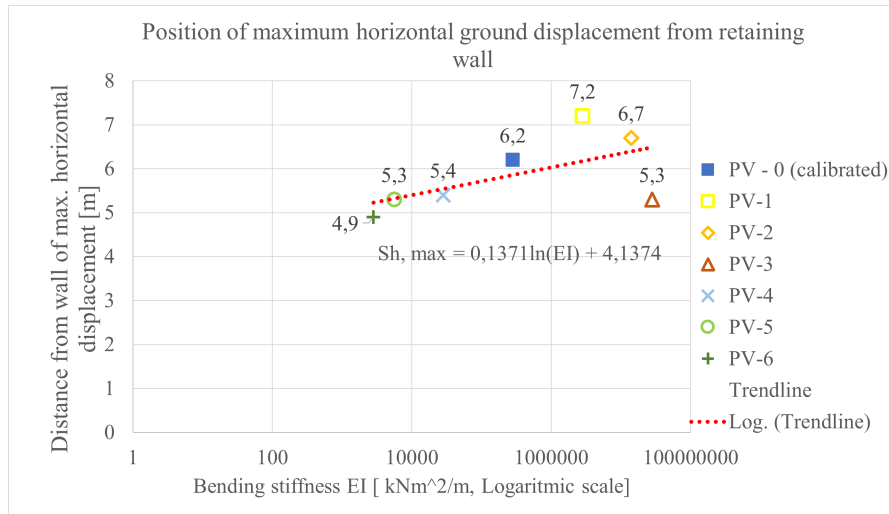


Figure 6.16: Position of maximum horizontal ground displacement at surface when varying bending stiffness EI.

6.3 Summary

The results in this chapter indicate that wall stiffness, more specific, the bending stiffness is a dominant parameter compared to the axial stiffness and specific weight when evaluating the ground displacement. The results from the parameter variation reveals typically linear relation in a semi-logarithmic scale between the lower estimates scenarios, higher estimates scenarios and the PV-calibrated scenario. The figures may be complemented with trend lines, in order to illustrate the relation between bending stiffness and the different ground displacement aspects as presented above. This could provide design guidance with respect to the bending stiffness for similar ground conditions. With respect to a certain bending stiffness, one may predict the ground displacement. For instance, for a particular bending stiffness, the position of the maximum vertical ground displacement could be determine. Note that the trend lines and graphs is based on the limitations of single ground condition for the HSS10 model and is therefore recommended do be conducted in design phases for other ground conditions with cautions. Overall, the result shows that the bending stiffness plays a vital role for the development of the vertical and horizontal ground movement. The next chapter, therefore, moves on to discuss the calculation process and result of this papers findings.

Chapter 7

Discussion

The aim of this chapter is to emphasize the presented work and distinguish the research objectives. Further, challenges with calibrated model will be evaluated and the results are discussed to clarify how uncertain parameters influence the short-term vertical and horizontal ground displacements.

This chapter contains of a more comprehensive discussion of the findings from the previous chapters, especially results presented in Chapter 5 and Chapter 6.

Calibrated model validation

This paper set out with the aim of assessing the importance of crucial parameters when estimating the ground displacement adjacent to a deep excavation in soft clay. In order to accomplish this objective, a calibrated model was developed by replicate soil behaviour and centrifuge test in a numerical model. The SA presented a prominent model for each constitutive model, and for the HSS model, the HSS10 was selected. Although the HSS10 indicated good agreement with the vertical ground displacement and wall deflection, the HSS01 revealed a significant better result. The HSS10 was chosen as the represented calibrated model mainly due to the stress-strain curve provided from the the soil test. The HSS01 as a calibrated model may have provided different result presented in the parameters variation in Chapter 6.

The second part of the model calibration work focused on an investigation of unidentified parameters. These parameters were not in detail provided in the description of the centrifuge tests, but were required for the numerical simulations. These parameters were throughout this paper termed as *unidentified* parameters. When evaluating these parameters in the SA, only the vertical ground displacement and maximum vertical ground displacement was considered, as well as the lateral wall deflection when comparing the different scenarios. Different result in the SA would have been provided if other parameters was conducted, for instance a partly drain-undrained Poisson Ratio

than $\nu_u = 0.5$. Additionally, the PSA was based on defined criteria presented in Table 5.7, and due to the complex PLAXIS simulations only three pairs of parameters were able to be compared at a time. A PSA which considered different criteria and parameters, may have provided other SensiScore than presented in Chapter 5.

Calibrated model result

The numerical model was not able to replicate the centrifuge test results in detail. This can for instance be seen with the vertical ground displacement and lateral wall deflection for Test 2 with flexible wall and Test 4 with soft props when evaluating. This shows a rather unexpected outcome in PLAXIS, when the Test 1 shows a quite good agreement with PLAXIS. An explanation is that the results are likely related to the difference of prototype model with numerical calculations and measurements in model scale laboratory experiments. A lack of detailed data provided in the centrifuge experiment which required certain assumptions in the input parameters of the numerical model such as soil stiffness parameters and interface strength factor R_{inter} .

The parameter variation analysis of uncertain parameters was obtained by using the calibrated model. The selected parameters for the analysis were the wall properties, such as the bending stiffness EI , the axial stiffness EA and the specific weight of wall w . The calculations of axial stiffness EA and specific weight w were expressed from the determined bending stiffness value. This may cause arbitrary wall properties. A strong evidence is illustrated when varying all three parameters EI , EA and w , it shows that the weight of the wall did not correspond with the strength of soil. The results showed a major axial deformation adjacent to the and downwards movement of the wall in Figure 6.5, which is not representative.

The calibrated model is based on certain assumptions and uncertainties, and may develop consequential errors when calculating. The PV analysis evaluated the ground displacement based on a calculated bending stiffness. This means that if the calibrated model is based on unreasonable parameters calculations, the model will provide inapplicable results. The result can be validated by evaluating calculated results from the calibrated model with presented results from the centrifuge test. For instance, how the vertical ground displacement develops with different bending stiffness. From PV analysis of flexible wall PV-5 and PV-6, with calculated bending stiffness from approximate $5.6MNm^2/m$ to $2.8MNm^2/m$. Additionally, the maximum vertical ground displacement did not increase more than approximate $30mm$ from PV-5 to PV-6. Compare these PV analyses to centrifuge Test 2 with flexible wall with bending stiffness $10.4MNm^2/m$, a significant increase of approximate $100mm$ in the vertical ground displacement was presented in Figure 5.34. Note that the PV-5 and PV-6 should not directly be compared with Test 2 with respect to different axial stiffness, specific weight and Poisson ratio, but gives an indication of how different parameters can overrule consequential results.

Undrained condition

The Hardening Soil Small model is a numerical model mainly developed for a drained $a-\phi$ condition. However, as mentioned in the literature review of the constitutive models in Chapter 4, the HS and HSS models only provides *Undrained (A)* and *Undrained (B)* for the undrained drainage type, unlike the MC model that additionally consists of the *Undrained (C)*. The *Undrained (C)* defines the stiffness and strength in terms of undrained properties. Unlike the *Undrained (A)* which defines the stiffness and strength in terms of effective properties. This paper has conducted the HSS model based on the *Undrained (B)* that defines the stiffness in terms of the effective properties and the strength in terms of the undrained shear strength. This causes a lower failure criterion when reaching the failure envelope, and represents a more realistic behaviour of the stress path of soil, as presented in Figure 4.5. Note that the model then uses a fixed input of undrained shear strength value, which defines the failure criterion and is not calculated by effective input parameters.

The HSS parameter calibration indicates that the back-calculated drained condition are needed for undrained materials in PLAXIS analysis when considering other aspects (e.g. pore pressure, consolidation etc.), due to non-representative soil behaviour for soft clay. Therefore, it is recommended that a detailed process of parameter calibration is carried out in order to obtain realistic prediction of undrained behaviour of clay when using PLAXIS (Surarak et al., 2012). The HSS model is therefore limited in simulating undrained soil behaviour and provides unrealistic ground displacements next to a deep excavation, as observed in this work. For this reason, the sensitivity analysis and parameter variation carried out in this thesis should be interpreted with caution. Further work should focus on a soil model that is able to represent a more realistic soil behaviour.

An undrained situation is traditionally analyzed with a total stress approach and undrained shear strength. This may be recommended in practical situations. However, it is an advantage to adopt the effective stresses when analyzing for undrained loading and consider the undrained excess pore pressure that develop during rapid loading. According to Nordal (2020), it is considered that the effective stress approach is fundamental in order to simulate how the undrained condition continuously develop into a drained condition. In order to simplify complex modelling in this research, some simplification, such as undrained condition, have to be determined.

Input parameters

The reviewed constitutive models demand certain input parameters as presented in Table 4.1, Table 4.2 and Table 4.3. When evaluating the calibrated model as the second objective, the HSS10 model scenario from Table 5.6 emphasize good agreement with the centrifuge baseline Test 1. The concave shape of ground displacement profile and the position of the maximum vertical displacements from PLAXIS agree with the centrifuge Test 1. However, the results revealed inadequacies for the maximum horizontal ground displacements and in the magnitude of the horizontal ground displacement. HSS10 indicated similar horizontal ground displacement shape and maximum

horizontal displacement at ground surface. The discrepancies could be attributed to unidentified parameters that is either based on default values, assumed from relevant research or calculated.

Laboratory experiments vs. Numerical model

The centrifuge test is a plain strain laboratory experiment modelled in a 3D small scale model, while PLAXIS is a numerical 2D model based on the finite element method in plain strain. Both centrifuge test and PLAXIS involves accordingly deformation in x- and z-direction. Directions of deformation plays a role when calculating the ground displacement, and differences may cause a considerable difference between the total volume of vertical ground displacement for the centrifuge test and PLAXIS. The volume of horizontal ground displacement of the wall should correspond to the volume of vertical displacement, which is accomplished in the centrifuge test. Additionally, PLAXIS shows base heave in the excavation, which is likely the difference between the total volume of vertical ground displacement. The base heave is illustrated in Appendix B. However, Figure 3.7 indicates no base heave according to the volume difference between the vertical and lateral ground displacement. Additionally, Lam (2010) presented the base heave with vectors, and the result shows very good agreement with PLAXIS. Note that the numerical model conducted the incremental displacement vectors by Lam (2010) may use another soil model than the HSS model, and other model settings, such as drained condition.

Numerical models is based on complex mathematical calculations, while the centrifuge test is a laboratory test. It is therefore not expected to achieve identical result when replicating the centrifuge test in a numerical model, but rather similar trends. PLAXIS output of stress-strain curve from Soil Test with scenario HSS10, demonstrate agreeable result compared to the stress-strain curve obtained from triaxial test conducted by Lam (2010). The result from Soil Test with scenario HSS10 was manipulated in order to fit the stress-strain curve obtained from a hyperbolic power-law idealization. Scenario HSS01 indicated a better ground displacement fit, but showed a very different stress-strain curve compared to the centrifuge test. Unlike the HSS01, the HSS10 showed a better stress-strain curve and less fitted ground displacement result. Additionally, PLAXIS Test 2 and Test 4 indicated smaller ground displacement compared to centrifuge Test 2 and Test 4. This may be explained by an overestimating of soil stiffness in PLAXIS.

Another notable aspect is the earth pressure calculations conducted for Test 1 and Test 2 from the centrifuge tests. The observed correlation of the earth pressure between the centrifuge tests and PLAXIS reveals similar calculations and result before excavation process. The result from basic earth pressure hand calculations correspond with the earth pressure values measured in the centrifuge tests and with the PLAXIS results. However, the earth pressure values after excavation showed rather contradictory results. The basic hand calculation of earth pressure corresponded with the earth pressure from PLAXIS. The contradiction may be explained by the influence of prop system, which was excluded in the hand calculation. However, the earth pressure measured from the EPC from the

centrifuge test provides a rather higher value. This is expected and may be explained by the different calculation and measurement method, and is presented in Figure 7.1. It is expected that the results from the numerical calculation, net Rankine theory and apparent earth pressure calculation method or earth pressure cells from centrifuge test are within about 10% of each other. Although the in-situ bracing system may locally change the pattern of a load distribution on the wall, the total load imposed by earth pressure changes very little (Boone and Westland, 2006).

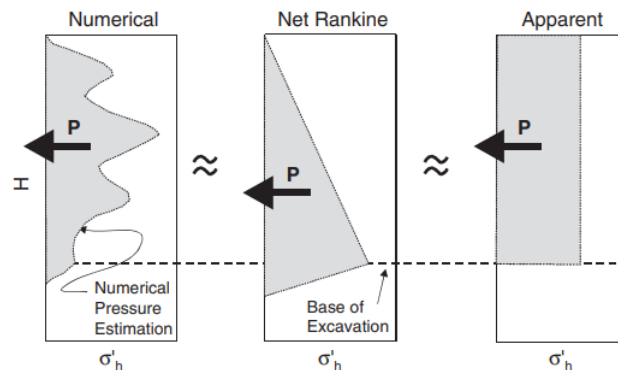


Figure 7.1: Illustration of total net active loads on flexible retaining structure (Boone and Westland, 2006).

Limitations

Deep excavation are characterised by complicated soil-structure interaction mechanisms, and a significant number of parameters influence their performance. A major limitation of this study is the fact that many parameters are not considered, assumed or is based on default values in PLAXIS. These factors could prove to be more relevant when estimating the vertical and horizontal displacement. The sensitivity analysis considered exclusively the uncertain parameters that could not directly be derived from the centrifuge tests. Additionally, the parametric study considered only the wall stiffness properties. In order to be able to conduct the problem it is necessary to simplify the problem by neglecting certain/various factors (e.g. workmanship, adjacent constructions, installation activities, consolidation, creep) and assume a limited/specific soil condition (i.e. undrained conditions). Regarding the complexity behind soil movement in undrained soft clay due to a deep excavation, some assumptions and limitations were required. Characterizing the isolated effects of the various factors by consider only the vital parameters, requires a significant amount of well documented and controlled case studies in order to obtain a calibrated model.

This paper focuses on the soil parameters when conducting the sensitivity analysis manually and with PLAXIS application, while focuses on the wall properties/parameters in the parameter variation analysis. However, PLAXIS sensitivity analysis and parameter variation application is able to consider also the input parameters of structural elements such as the retaining wall. It is possible that the wall stiffness is more important than the soil parameters when determining ground displacement. Furthermore, the influence of prop stiffness were not considered in the

sensitivity analysis nor in the parameter variation, while it is included in many prediction methods. The long-term condition of soft clay and its effect with consolidation and creep was not considered in the study, but may play an important role in the accuracy of the prediction of ground displacement.

Chapter 8

Conclusion and Further Research

This chapter sums up the main findings from this study, provides a conclusion to the research objectives and contribute with recommendations for further work.

8.1 Summary of main findings

The primary objectives of this research are: (1) to develop a calibrated model by replicating a centrifuge experiment in a numerical model in PLAXIS, and (2) to examine the uncertain parameters in a deep excavation and investigate how the parameters influence the vertical and horizontal ground displacements. With respect to these objectives, the main findings are as follows:

- An overview of how the different constitutive models capture the soil response in a deep excavation and accentuate their ability to replicate the centrifuge experimental results.
- A calibrated model based on the HSS model with input parameters from scenario HSS10, which provided good estimations.
- Soil stiffness revealed to be a vital input parameter and have a significant influence on the ground displacement, based on sensitivity analysis.
- The bending stiffness plays a crucial role for the ground displacement, and an increase in the bending stiffness decreases the ground displacement calculated from parameter variation analysis.
- The relation between bending stiffness and vertical and horizontal ground displacement tends to show a linearly correlation in a semi-logarithmic scale.

8.2 Conclusion

The aim of the current thesis is to determine how uncertain parameters influence the vertical and horizontal ground displacement with a calibrated model. For this purpose, a well-defined centrifuge test is examined in order to replicate in PLAXIS. The calibrated model will be adopted to study the influence of uncertain parameters. Based on the main findings above, this dissertation has provided: (1) an better insight into the complexity of the constitutive models and the models requirement of comprehensive input parameters, (2) a increased knowledge of the sensitivity of soil parameters and their ability to affect vertical and horizontal ground displacement (3) a deeper understanding of how the wall stiffness influences the vertical and horizontal ground displacement, and how the wall deflection develops.

Deep excavation induced soil displacements are complex in many aspects, and examining the soil behaviour is complicated. To determine the effect of uncertain parameters in the soil displacement, a comprehensive analysis is necessary to be conducted. This thesis has focused on a few of those factors, such as the bending stiffness, axial stiffness and specific weight, in order to give an indication on how they impact the ground displacements. The sensitivity analysis results obtained for the HSS model indicated that the tangent and unloading/reloading stiffness did not impact the result significantly. The sensitivity analysis indicated that the most important parameters were the secant stiffness parameter and the earth pressure coefficient. The results also showed a clear difference in the threshold shear strain between the manual sensitivity analysis and PLAXIS sensitivity analysis, where it showed a high SensiScore but a rather low influence in the ground displacement for the manual sensitivity analysis. Furthermore, the wall properties in the parameter variation analysis indicated a significant influence on the ground displacements, especially the bending stiffness. The analysis confirmed that by increasing the bending stiffness, the magnitude and the maximum vertical and horizontal ground displacement decreases. By contrast, decreasing the bending stiffness caused on increase of the vertical and horizontal displacements. The position of the maximum vertical displacements moved towards the retaining wall when reducing the bending stiffness. Another important conclusion from the analysis is that the maximum vertical displacement adjacent to the wall increases when the bending stiffness increase. The analysis has also shown that the maximum horizontal displacement at the ground surface remains approximate at the same position, and may be explained by the fixed prop system stiffness. However, the shape of the vertical ground displacement remained concave when varying only the bending stiffness, but may change to a spandrel shape when increasing the specific weight of wall. The horizontal displacement adjacent to the wall shape changed significantly by varying the bending stiffness. Overall, this study strengthens the idea that by increase the bending stiffness, a decrease in the ground displacement will be obtained. The presented semi-logarithmic charts of bending stiffness and ground displacement, such as maximum vertical ground displacement and its position, provides guidance when estimating ground displacement based on a certain bending stiffness value. This may contribute as a guidance tool in the design phase.

Another important conclusion is that there are uncertainty if blindly using back-calculated calibrated model to evaluate the influence of the uncertain input parameters. Another approach is to rely on the results from a sensitivity analysis to identify which input parameters that are the most vital to evaluate. However, it is common to assess based on geotechnical knowledge, and identify which parameters that are well-known in the field and which are uncertain due to limited measurement by engineering judgement.

8.3 Recommendations for further research

This master thesis is restricted by certain limitations such as that a single soil type was considered in the explored centrifuge test series. Consequently, the developed numerical model and obtained results should only be applied for similar ground conditions. A natural progression of this work would be to consider the effect of a wider range of ground conditions such as different soil types and soil layers.

However, the method using a sensitivity analysis to identify vital parameters that can be repeated on numerous models in similar problems is an important achievement. As mentioned earlier, other crucial parameters, such as the prop system stiffness, may be studied more comprehensively. Furthermore, the variations of the different parameters should be within realistic limits and provide reasonable results. Although these results obtained in this study cannot be applied to other areas, due to different soil conditions, the same methodology could be used to study the effectiveness of the constitutive model in different areas. However, for further research it is recommended to determine an applicable constitutive model for the particular problem. The NGI-ADP model is based on undrained soft clay conditions and takes account for the active and passive undrained shear strength, which is optimal for a deep excavation situation. Further research might explore how the calibrated model can be adopted for a real case study and further findings about the impact of uncertain parameters can be used to inform design predictions.

Perhaps the most interesting knowledge obtained from the research is the vital importance of accessing the correct input parameters. Appropriate ground investigations and laboratory experiments are crucial to a numerical model. Without proper input parameters, the results of a PLAXIS analysis are arguably irrelevant, even as a calibrated model. However, with a well-defined calibrated model, a parameter variation reveals the influence of the vital parameters. Moreover, this importance of influence may contribute as guidance in design phases when predicting the ground displacement in a deep excavation in soft clay.

Appendix A

Acronyms

EPC - Earth Pressure Cell

CM - Constitutive model

CL - Center line

CT - Centrifuge Test

DW - Diaphragm Wall

DSS - Direct Simple Shear

EM - Empirical methods

FE - Finite Element

FEM - Finite Element Method

GSA - Global Sensitivity Analysis

HE - Higher estimate

HS - Hardening Soil

HSM - Hardening Soil Model

HSS - Hardening Soil Small

HSSM - Hardening Soil Small Model

KC - Kaolin Clay

LE - Lower Estimate

MC - Mohr-Coulomb

MCM - Mohr-Coulomb Model

MSA - Manual Sensitivity Analysis

NGI - Norwegian Geotechnical Institute

NGI-ADP - NGI Active Direct Simple Shear Passive

NC - Normal Consolidated

NTNU - Norwegian University of Science and Technology

OC - Over-Consolidated

OCR - Over-Consolidated Ratio

PLEP - Perfect linear elasto-plastic

PSA - Plaxis Sensitivity Analysis

PV - Parameter Variation

SA - Sensitivity Analysis

SYL03 - Centrifuge Test 4

SYL04 - Centrifuge Test 1

SYL05 - Centrifuge Test 2

SYL06 - Centrifuge Test 3

SYL07 - Centrifuge Test 5

SPW - Sheet Pile Wall

TC - Triaxial Compression

TE - Triaxial Extension

Appendix B

PLAXIS Calculations

PLAXIS output from calibrated model - HSS10

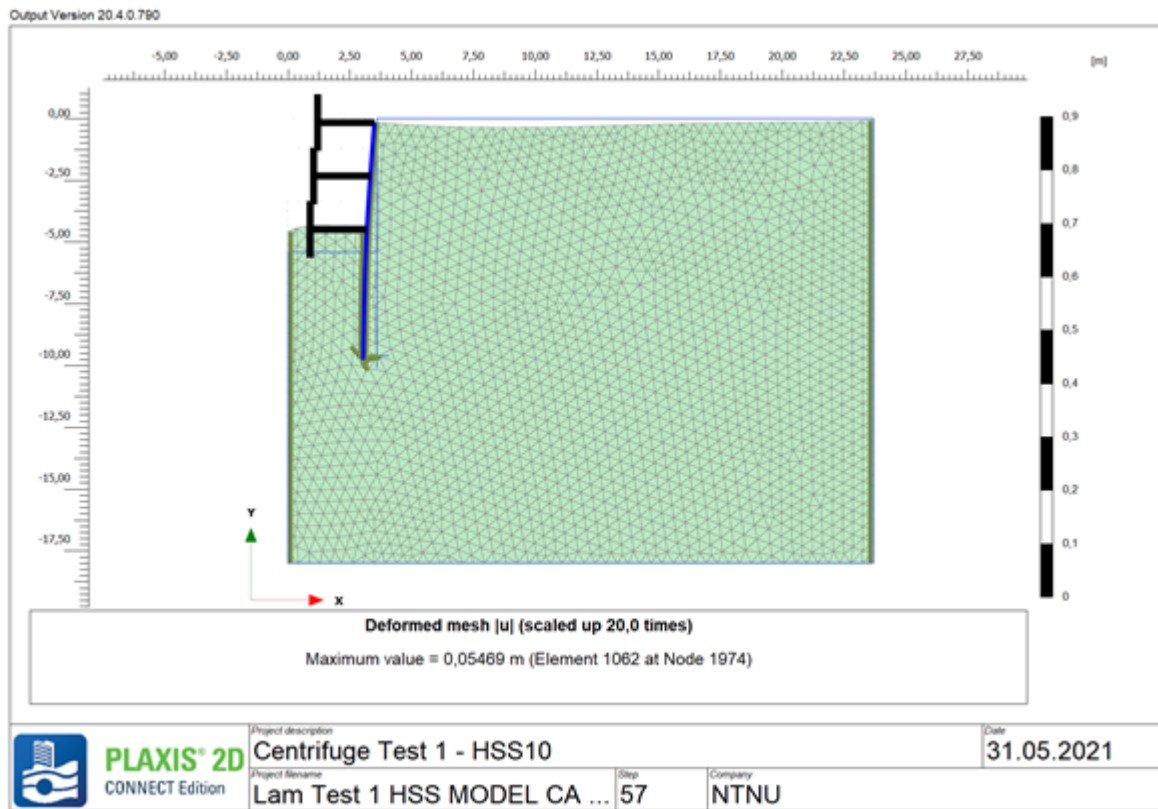


Figure B.1: PLAXIS Test 1 - Final phase: Deformed mesh [u].

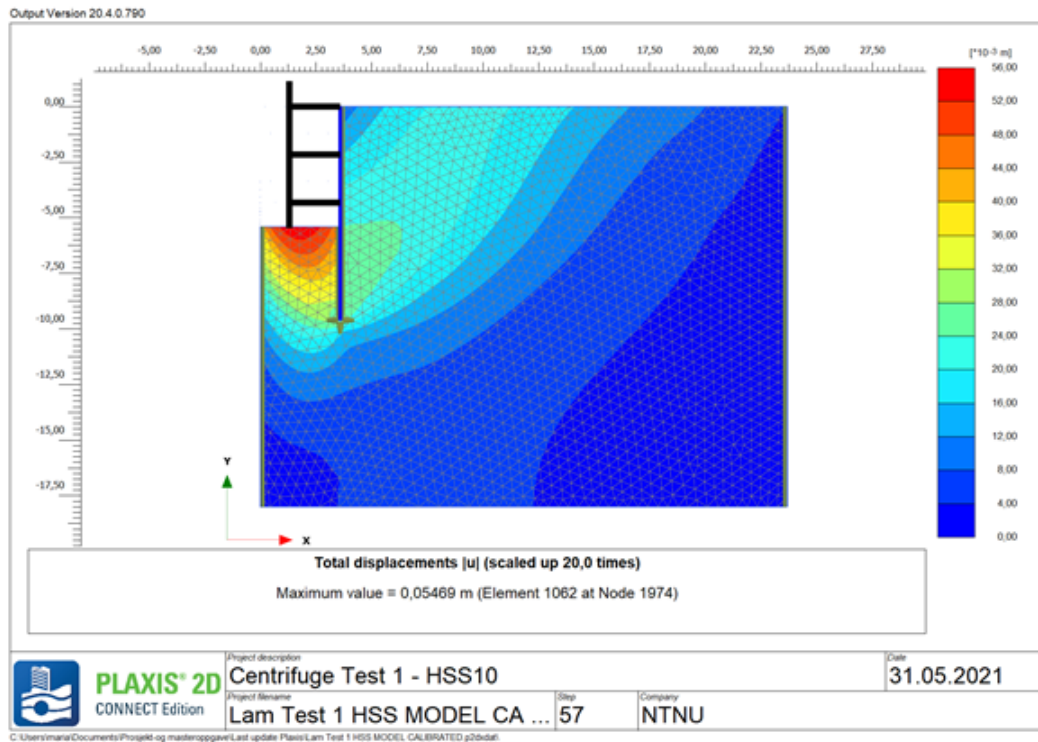


Figure B.2: PLAXIS Test 1 - Final phase: Total displacement $|u|$.

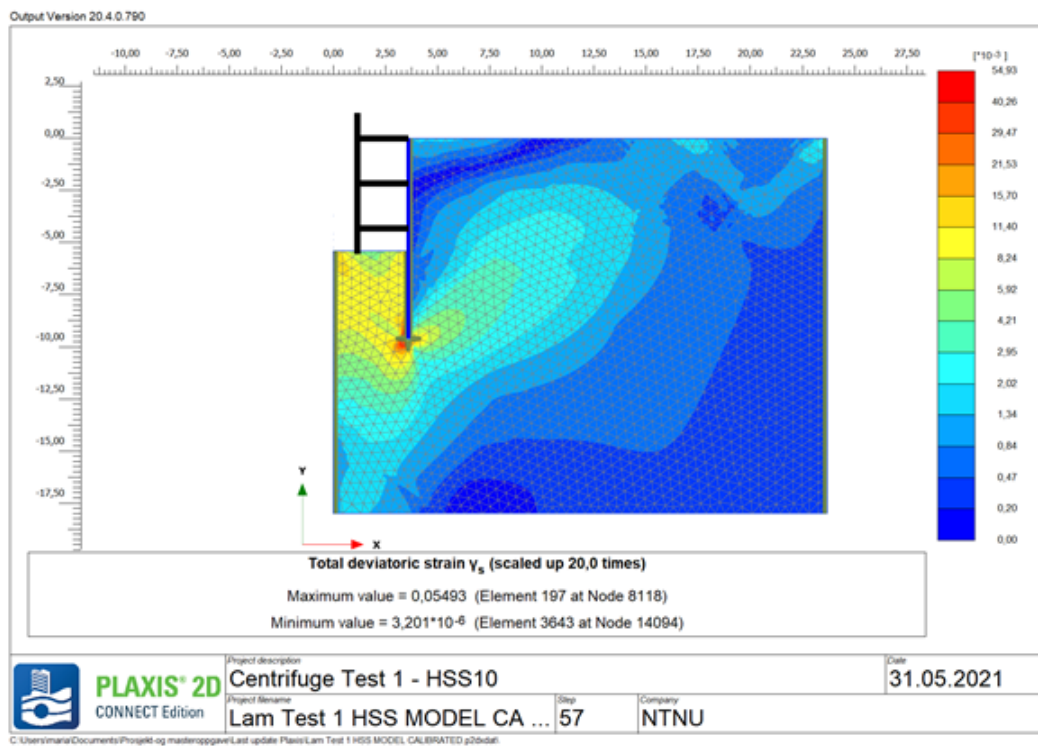


Figure B.3: PLAXIS Test 1 - Final phase: Total deviatoric strain γ_s .

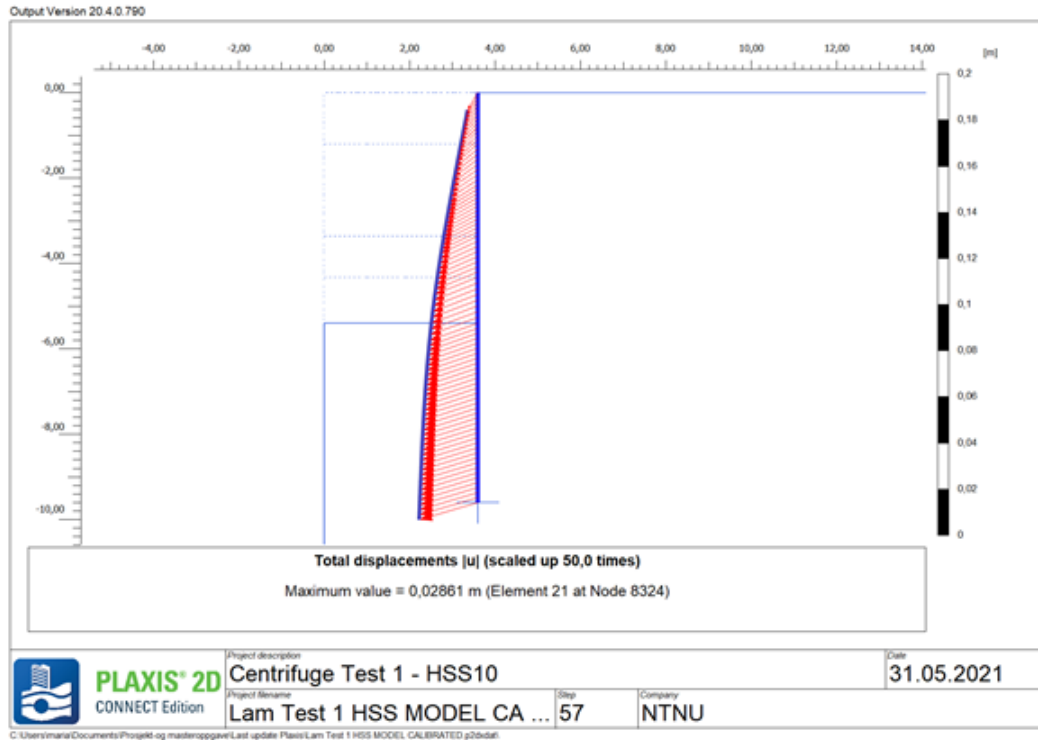


Figure B.4: PLAXIS Test 1 - Final phase: Total wall displacement [u].

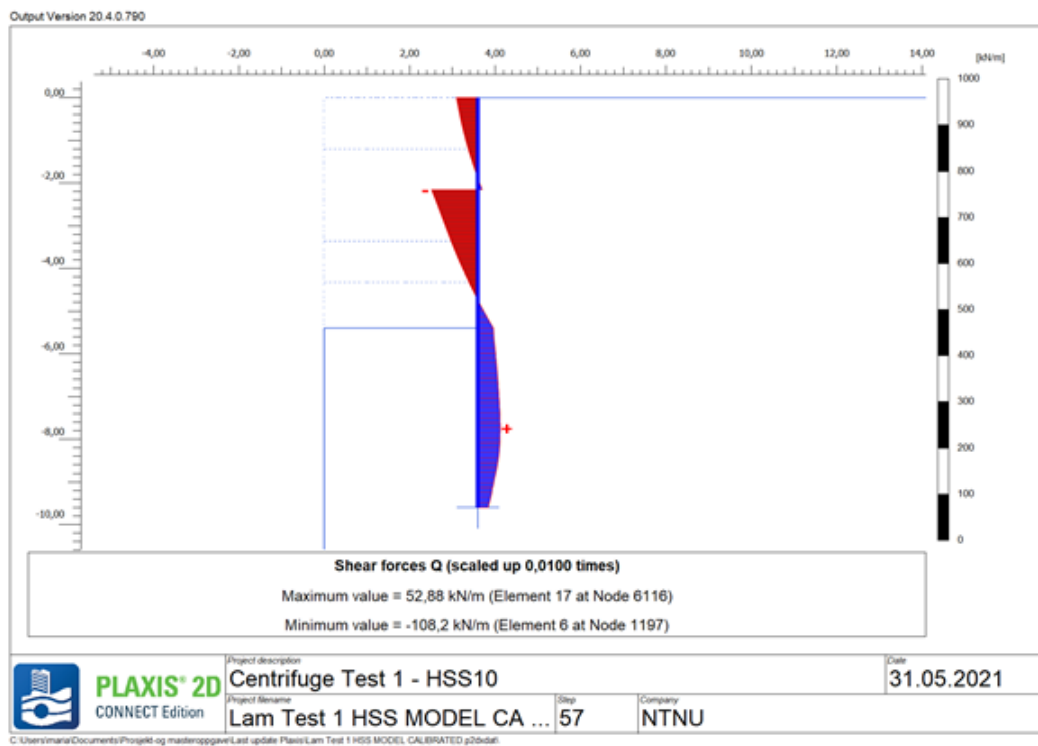


Figure B.5: PLAXIS Test 1 - Final phase: Total shear forces.

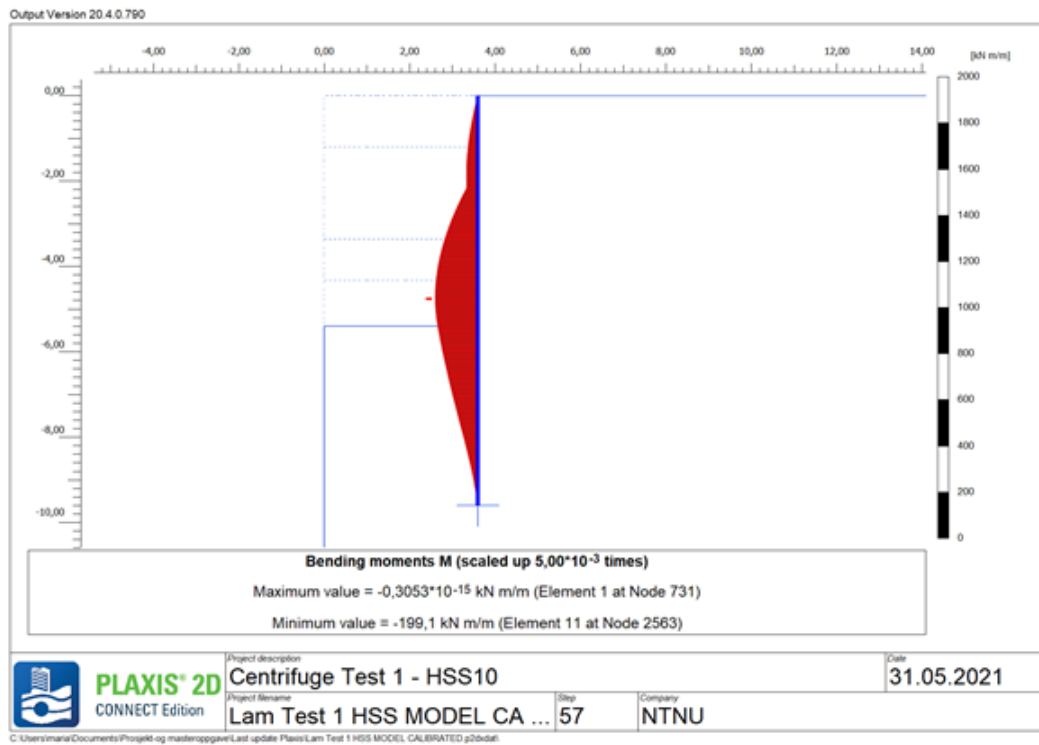


Figure B.6: PLAXIS Test 1 - Final phase: Total bending moment.

Appendix C

Sensitivity Analysis

Table C.1: Sensitivity analysis for Hardening Soil Small model.

Parameter	Description	Range	Sensitivity analysis ID									
			HSS01	HSS02	HSS03	HSS04	HSS05	HSS06	HSS07	HSS08	HSS09	HSS10
E_{50}^{ref}	Secant stiffness	1 – 25MPa	1	25	10	4	4	4	4	4	4	4
E_{oed}^{ref}	Tangent stiffness	1 – 25MPa	1	25	10	4	4	4	4	4	4	4
E_{ur}^{ref}	Unloading /reloading stiffness	3 – 50MPa	3	50	30	12	16	16	16	16	16	16
$\gamma_{0.7}$	Threshold shear strain, ($G_s = 0.722G_0$)	0.00015– 0.00025	0.0002	0.0002	0.0002	0.0002	0.0002	0.00015	0.00025	0.0002	0.0002	0.0002
K_0	Earth pressure coefficient	0.65 – 1.8	1.0	1.0	1.0	1.0	1.0	1.0	1.0	0.65	1.8	1.1
Results from centrifuge test [mm]			Results from PLAXIS in [mm]									
Max. wall deflection, $u_x = 33.3$			44.4	8	14.9	26	32	34	30	7.9	26.6	27.4
Max.lateral displacement, $u_x = 33.3$			42.2	8	14.8	25.3	31.2	33	29.3	7.8	25.9	26.6
Max. ground displacement, $u_y = 34.4$			27.9	5.2	10	17.1	18.9	20	18.3	7.1	17.8	18.3
Max. ground displacement adjacent to wall, $u_y = 19.5$			18.3	2.6	4.5	8.5	7.8	5	7.4	7.7	9	7.8

Notations: For clay a range between 3 to 5 times E_{50}^{ref} is assumed for E_{ur}^{ref} . Different values is therefore also considered.

Table C.2: PLAXIS Sensitivity analysis for Hardening Soil Small model.

Parameter	Ref	Range $\pm 10\%$	SensiScore [%]								
			PSA-HSS1	PSA-HSS2	PSA-HSS3	PSA-HSS4	PSA-HSS5	PSA-HSS6	PSA-HSS7	PSA-HSS	PSA-HSS
Criterion:			1	2	1,2,3	1	2	1,2,3	1	2	1,2,3
E_{50}^{ref}	4MPa	3.6 – 4.4MPa	89	94	91	51	53	52	26	36	31
E_{oed}^{ref}	4MPa	3.6 – 4.4MPa	0	0	0	–	–	–	–	–	–
E_{ur}^{ref}	16MPa	14.4 – 17.6MPa	11	6	9	7	3	5	4	2	3
$\gamma_{0.7}$	0.0002	0.00018 – 0.00022	–	–	–	42	44	43	–	–	–
K_0	1.1	0.99 – 1.21	–	–	–	–	–	–	70	62	66

Notations: The result is from PLAXIS SA tool and is based on the last construction stage: Installation of prop 3 with a 10% of the Ref-value that is determined from MSA.

Appendix D

PLAXIS Earth pressure

Test 1 - Earth pressure before excavation

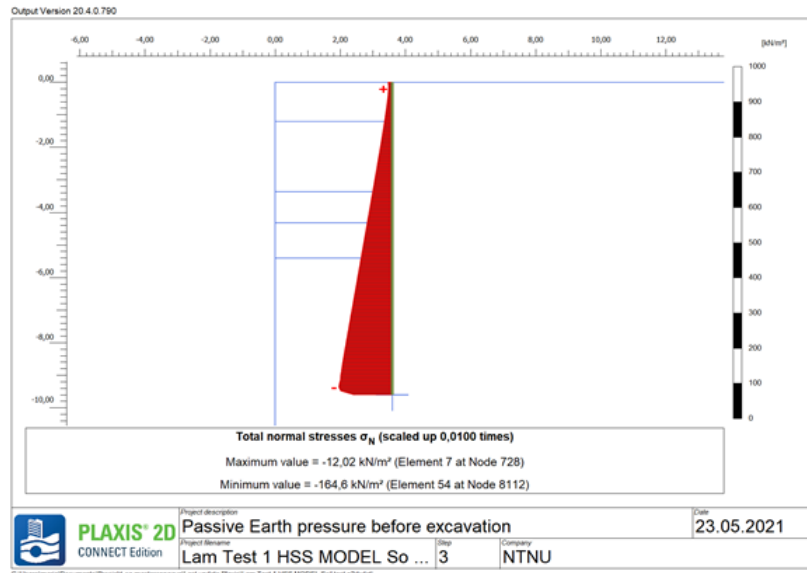


Figure D.1: PLAXIS Test 1 - Passive earth pressure before excavation.

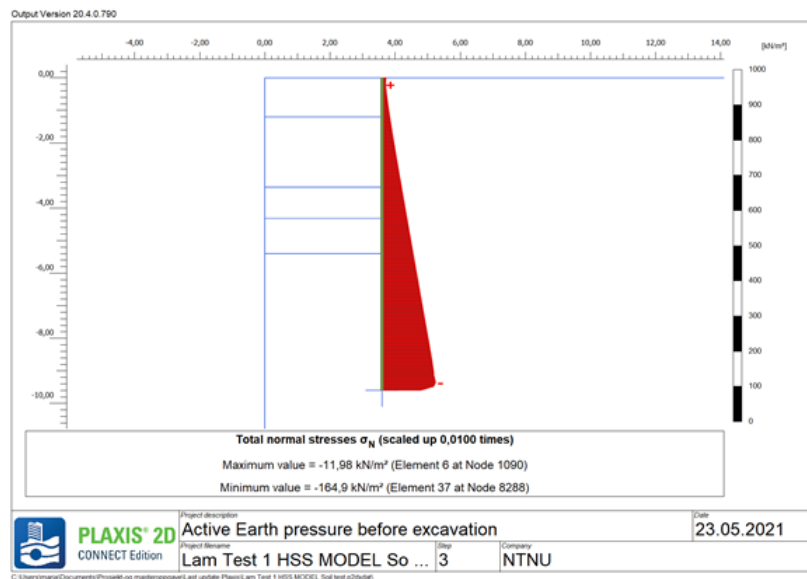


Figure D.2: PLAXIS Test 1 - Active earth pressure before excavation.

Test 1 - Earth pressure after excavation

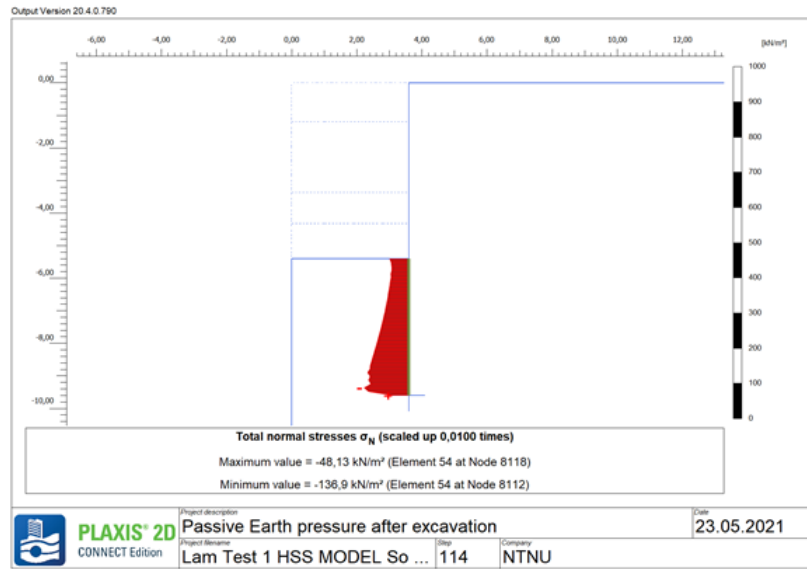


Figure D.3: PLAXIS Test 1 - Passive earth pressure after excavation.

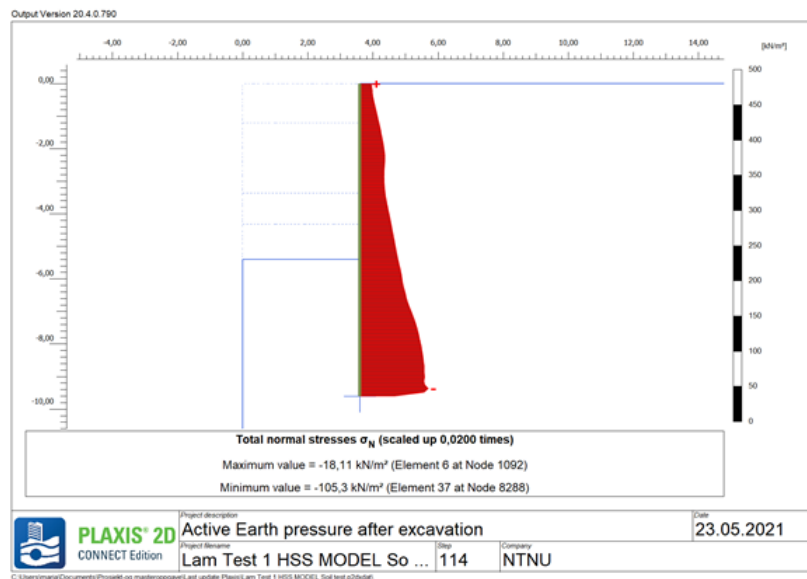


Figure D.4: PLAXIS Test 1 - Active earth pressure after excavation.

Test 2 - Earth pressure before excavation

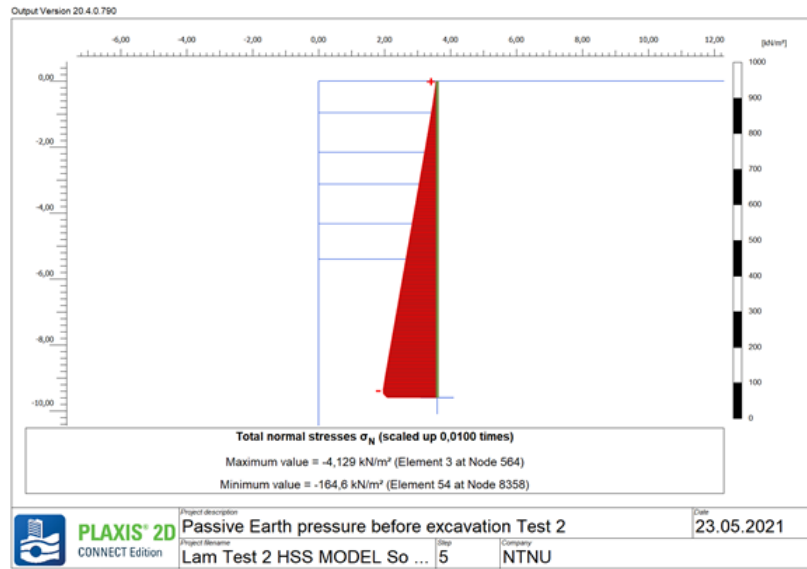


Figure D.5: PLAXIS Test 2 - Passive earth pressure before excavation.

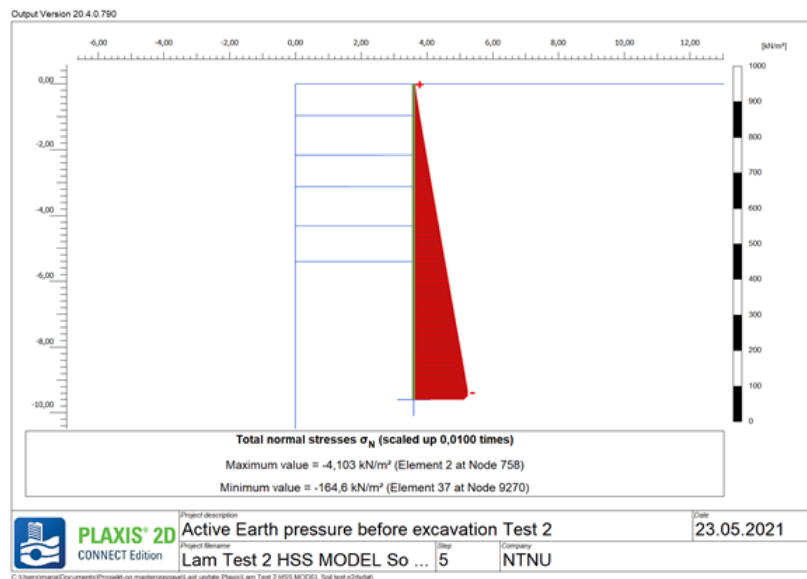


Figure D.6: PLAXIS Test 2 - Active earth pressure before excavation.

Test 2 - Earth pressure after excavation

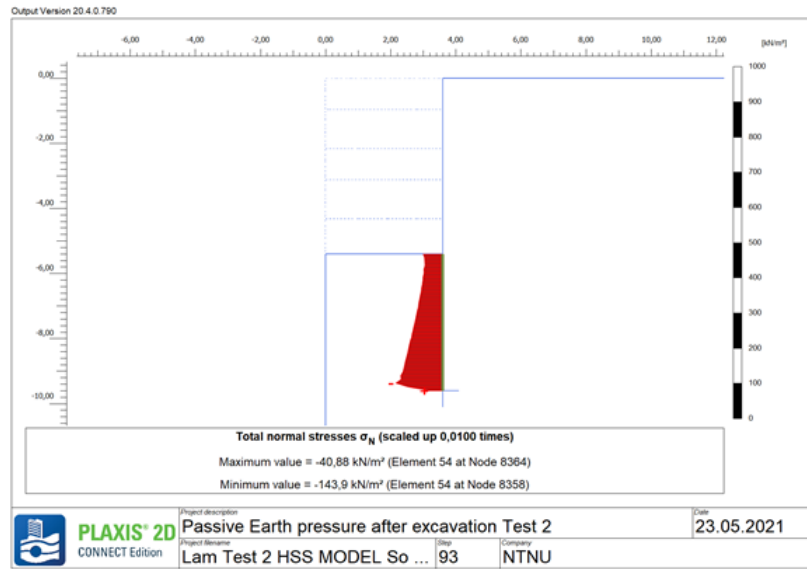


Figure D.7: PLAXIS Test 2 - Passive earth pressure after excavation.

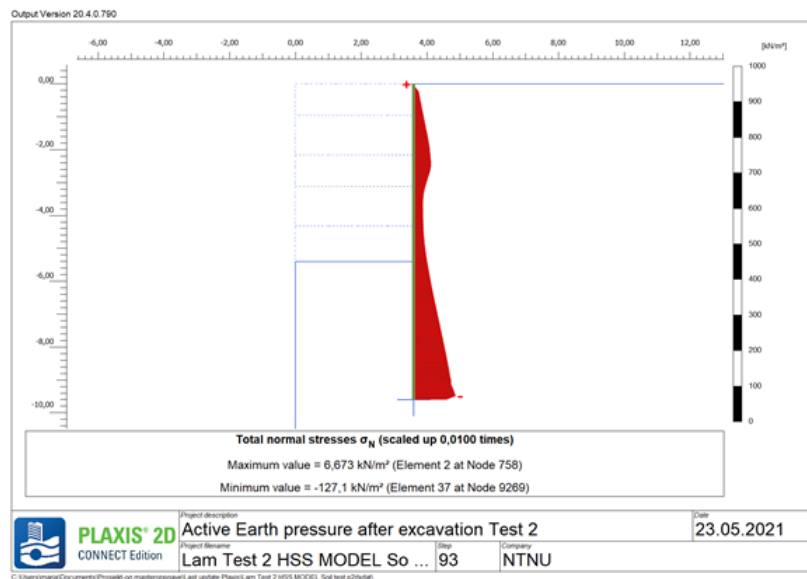


Figure D.8: PLAXIS Test 2 - Active earth pressure after excavation.

Bibliography

- Z. Z. Aye, D. Karki, and C. Schulz. Ground movement prediction and building damage riskassessment for the deep excavations and tunneling works in bangkok subsoil. In *International Symposium on Underground Excavation and Tunelling. Urban Tunnel Construction for Protection of Environment* . SEAFCO Public Company, Bangkok., 2006.
- S. Boone and J. Westland. Design of excavation support using apparent earth pressure diagrams: consistent design or consistent problem? In *International Society for Soil Mechanics and Geotechnical Engineering*. Online Library of the International Society for Soil Mechanics and Geotechnical Engineering (ISSMGE)., 2006. URL <https://www.issmge.org/publications/online-library>. (Accessed:16.04.2021).
- R. B. Brinkgreve, E. Engin, and W. M. Swolfs. Plaxis 2d manuals. In *CRC Press, Inc.* Rotterdam, Netherlands, Balkema., 2017.
- P. Castaldo, M. Calvello, and B. Palazzo. Probabilistic analysis of excavation-induced damages to existing structures. In *Computers Geotechnics*. Elsevier. Department of Civil Engineering University of Salerno, Italy., 2013.
- A. Emdal, L. Grande, S. Nordal, E. Hjeldnes, K. Senneset, and S. Skotheim. Tba 5100 theoretical soil mechanics. In *Geotechnical Division*. Norwegian University of Science and Technology, Norway., 2019.
- C. Fartaria. Soil-structure interaction in integral abutment bridges. In *Soil Structure II*. Semantic Scholar., 2012.
- G. Grimstad, L. Andresen, and H. Jostad. Ngi-adp: Anisotropic shear strength model for clay. In *International Journal for Numerical and Analytical Methods in Geomechanics*. John Wiley Sons, Ltd. Wiley Online Library by Norwegian Geotechnical Institute (NGI), Oslo., 2011.
- P. G. Hsieh and C. Y. Ou. Shape of the ground surface settlement profiles caused by excavation. Canada Geotechnical, 1998.
- S. Hsu, P. Huang, and T. Cheng. Earth pressure distribution for deep excavations in gravel formation. In *Earthwork Project Management, Slope Stability Analysis, and Wave-Based*. ASCE by University of California, San Diego., 2014.

- K. B. Huat, J. Noorzaei, and M. S. Jaafar. A review of basic soil constitutive models for geotechnical application. In *Electronic Journal of Geotechnical Engineering*. Department of Civil Engineering, University Putra Malaysia, 2009.
- K. Karlsrud. Some aspects of design and construction of deep supported excavations. In *Discussion leader's contribution to XIVth International Conference on Soil Mechanics and Foundation Engineering, Hamburg, Germany*. Norwegian Geotechnical Institute. Oslo, Norway., 1998.
- A. Kullingsjö. Effects of deep excavations in soft clay on the immediate surroundings. In *Analysis of the possibility to predict deformations and reactions against the retaining system*. Chalmers University of Technology, Department of Civil and Environmental Engineering, Geotechnical Engineering., 2007. ISBN 978-91-7385-002-5. doi: 10.1061/(ASCE)1090-0241(2007)133_6(731).
- G. Kung, C. H. Juang, E. C. L. Hsiao, and Y. M. A. Hashash. Simplified model for wall deflection and ground-surface settlement caused by braced excavation in clays. In *Journal of Geotechnical and Geoenvironmental Engineering*, pages 731–747. J. Geotech. Geoenviron. Eng., 2007. doi: 10.1061/(ASCE)1090-0241(2007)133_6(731).
- S. Lam. Ground movements due to excavation in clay: Physical and analytical models. In *A dissertation submitted for the degree of Doctor of Philosophy, University of Cambridge*. Churchill College., 2010.
- S. Y. Lam, S. K. Haigh, M. Z. E. B. Elshafie, and M. D. Bolton. A new apparatus for modelling excavations. In *International Journal of Physical Modelling in Geotechnics*. ICE - Institution of Civil Engineering., 2012.
- S. Y. Lam, S. H. Haigh, and M. D. Bolton. Understanding ground deformation mechanisms for multi-propped excavation in soft clay. In *Soils and Foundations*, pages 296–312. The Japanese Geotechnical Society, Department of Engineering, University of Cambridge, UK., 2014.
- S. J. Lee, T. W. Song, Y. S. Lee, Y. H. Song, and J. K. Kim. A case study of building damage risk assessment due to the multi-propped deep excavation in deep soft soil. In *Soft Soil Engineering - Chan Law*, pages 281–289. Taylor Francis Group, London., 2007. ISBN 13 978-0-415-42280-2.
- A. Locat, H. Jostad, and S. Leroueil. Numerical modeling of progressive failure and its implications for spreads in sensitive clays. In *NRC, Research Press*. Canadian Geotechnical Journal. University of Connecticut., 2013.
- J. Manie and P. Chatterjee. Diaphragm wall properties. In *Geotechnical Analysis*. TNO DIANA BV, 2015. URL <https://dianafea.com/manuals/d96/GeoTech/node192.html>. (Accessed:26.05.2021).
- F. Meng, R. Chen, S. Liu, and H. Wu. Centrifuge modeling of ground and tunnel responses to nearby excavation in soft clay. In *J. Geotechnical Geoenvironmental Engineering*. ASCE, American Society of Civil Engineering., 2020.
- S. Nordal. Undrained condition. In *TBA4116 Geotechnical Engineering Advanced Course*. Norwegian University of Science and Technology Geotechnical Engineering Group., 2020.

- N. Phien-Wej, M. Humza, and Z. Zaw Aye. Numerical modeling of diaphragm wall behavior in bangkok soil using hardening soil model. In *Geotechnical Aspects of Underground Construction in Soft Ground*. ISSMGE. Taylor Francis Group, London., 2012.
- M. Schuster, G. C. Kung, H. Juang, and Y. Hashash. Simplified model for evaluating damage potential of buildings adjacent to a braced excavation. In *Journal of Geotechnical and Geoenvironmental Engineering*. Cambridge University., 2009.
- N. Sivasithamparam and J. Castro. An anisotropic elastoplastic model for soft clay based on logarithmic contractancy. In *International journal for numerical and analytical methods in Geomechanics*. Wiley Online Library., 2015.
- M. Sloop. Material properties and material database. In *PLAXIS 2D-Reference Manual. CONNECT Edition 20.04*. Bentley Communities., 2020a.
- M. Sloop. The hardening soil model. In *Material Models Manual. CONNECT Edition V20.04*. Bentley Communities., 2020b.
- B. Stojanovic, M. Bukvic, and I. Epler. Application of aluminum and aluminum alloys in engineering. In *Applied Engineering Letters Journal of Engineering and Applied Sciences*. University of Kragujevac, Serbia., 2018.
- C. Surarak, S. Likitlersuang, D. Wanatowski, A. Balasubramaniam, E. Oh, and H. Guan. Stiffness and strength parameters for hardening soil model of soft and stiff bangkok clays. In *Soils and Foundations*. Elsevier, Tokyo., 2012. doi: 10.1016/j.sandf.2012.07.009.
- J. Takemura, M. Kondoh, T. Esaki, M. Kouda, and O. Kusakabe. Centrifuge model tests on double propped wall excavation in soft clay. In *Soils and Foundations* 39. Japanese Geotechnical Society., 1999.
- P. Teo and K. Wong. Application of the hardening soil model in deep excavation analysis. In *The IES Journal Part A: Civil Structural Engineering*. Taylor Francis Group., 2012.
- M. Tran. Characterisation of excavation-induced soil displacement. In *Project Thesis*. Department of Civil and Transport Engineering, Norwegian University of Science and Technology (NTNU)., 2020.
- B. Ukritchon and T. Boonyatee. Soil parameter optimization of the ngi-adp constitutive model for bangkok soft clay. In *Geotechnical Engineering Journal of the SEAGS AGSSEA*. ResearchGate by Department of Civil Engineering, Chulalongkorn University, Bangkok Thailand., 2015.
- J. Wesseling, J. Kroes, T. C. Oliveira, and F. Damiano. The impact of sensitivity and uncertainty of soil physical parameters on the terms of the water balance: Some case studies with default r packages. part i: Theory, methods and case descriptions. In *Computers and Electronics in Agriculture*. Elsevier., 2020.

- W. Zhang, A. Goh, and F. Xuan. A simple prediction model for wall deflection caused by braced excavation in clays. In *Technical Communication. Computers and Geotechnics*. Elsevier by School of Civil and Environmental Engineering, Nanyang Technological University, Singapore., 2015.
- C. Zhao, A. Lavasan, T. Barciaga, V. Zarev, M. Datcheva, and T. Schanz. Model validation and calibration via back analysis for mechanized tunnel simulations – the western scheldt tunnel case. In *Computers and Geotechnics*. Elsevier by Ruhr-Universität Bochum, Soil and Rock Mechanics, Germany., 2015.

